University of West Bohemia in Pilsen
Faculty of Applied Sciences

AUTOMATED INFARCTION CORE DELINEATION

Ing. Petr Maule

doctoral thesis
in fulfillment of the requirements for the degree of
Doctor of Philosophy
in the specialization of
Computer Science and Engineering

Supervisor: Doc. Dr. Ing. Jana Klečková
Department of Computer Science and Engineering

Pilsen 2012

Západočeská univerzita v Plzni
Fakulta aplikovaných věd

AUTOMATICKÁ DETEKCE NEKROTICKÉ TKÁNĚ

Ing. Petr Maule

disertační práce
k získání akademického titulu
doktor
v oboru Informatika a výpočetní technika

Školitel: Doc. Dr. Ing. Jana Klečková
Katedra Informatiky a výpočetní techniky

Plzeň 2012

Declaration

I do hereby declare that this doctoral thesis is a result of my own work and that it has been completed by myself. Where appropriate, I have made acknowledgement of others' work.

Pilsen, April, 2012

.....
Petr Maule

Acknowledgements

I wish to express my thanks to my supervisor Mrs. Jana Klečková and colleagues from the University Hospital in Pilsen for their valuable advices, comments and also for their patience. I would like to thank also to my partner Eliška Tomanová for her support and optimism and also to my entire family for understanding during my studies.

Abstract

This thesis deals with methods that could provide additional information for physicians when deciding about the most appropriate treatment for patients with ischemic strokes. The thesis proposes a method for automated infarction core delineation based on combination of angiography and non contract computed tomography examinations. Such perfused blood volume mapping has advantage in whole brain coverage. The volume of the infarction core area is the crucial factor for thrombolytic treatment indication. Such information is not yet available for physicians. Patients who exceed certain level of the infarction core volume should not be indicated for thrombolytic treatment because of high risk of further bleeding.

Keywords: automated infarction core delineation, perfused blood volume mapping, computed tomography, infarction core volume, ischemic strokes

Abstrakt

Tato práce se zabývá návrhem metody, která by mohla lékařům poskytnout dodatečné informace při rozhodování o nejvhodnější léčbě pro pacienty s ischemickou cévní mozkovou příhodou. Navrhovaná metoda je automatická a dokáže označit nekrotickou tkáň na snímcích, které vznikly kombinací angiografického a nekontrastního vyšetření počítačovou tomografií. Tato kombinace dokáže pokrýt oblast celého mozku. Objem nekrotické tkáně je kritickým faktorem pro aplikaci trombolytické léčby. Takový parametr nemají lékaři v současné době k dispozici. Lidem, kteří přesáhnou určitou hodnotu objemu nekrotické tkáně, by neměla být aplikována trombolytická léčba, neboť je vysoké riziko dalšího krvácení.

Klíčová slova: automatická detekce nekrotické tkáně, perfúzní objemové mapy, počítačová tomografie, objem nekrotické tkáně, ischemické cévní mozkové příhody

The research was supported by a grant of the Grant Agency of the Czech Republic - Microstructure oriented hierarchical modeling of brain perfusion for CT based cerebral blood flow evaluation, no. 106/09/0740

Contents

List of Figures

List of Tables

List of Acronyms

AUC Area Under Curve

CBF Cerebral Blood Flow

CBV Cerebral Blood Volume

CT Computed Tomography

CTA Computed Tomography Angiography

CTP Computed Tomography Perfusion

DICOM Digital Imaging and Communication in Medicine

HU Hounsfield units

MIP Maximum Intensity Projection

MR Magnetic Resonance

MTT Mean Transmit Time

NCCT Non-Contrast Computed Tomography

PET Positron Emission Tomography

PBV Perfused Blood Volume

PCA Picture Archiving and Communication System

PCA Principal Component Analysis

PCT Perfusion Computed Tomography

RMS Root Mean Square

ROC Receiver Operating Characteristic

TTP Time To Peak

VRT Volumetric Reconstruction Technique

Chapter 1

Introduction

A healthy man has a thousand wishes, a sick man only one.
Indian saying

Human health is for everyone very important. We often realize this just after we get sick or when some accident happens to us. Hand by hand with the time there come improvements of the quality of the health care. Technological development brings new instruments with more possibilities and better precisions. Nowadays instruments provide such information that its correct evaluation and understanding is challenge of current research.

1.1 Motivation

Acute ischemic strokes are the third leading cause of death [43] and the first leading cause of disability in population over 60 years old. Early patient diagnosis significantly improves the prognosis. Thrombolytical treatment can be applied only to patients who did not exceed certain level of the necrotic tissue volume. There is still no satisfactory method which is able to evaluate this volume. This work introduces automated method for this purpose using commonly performed examinations. The proposed method can become as another factor which can help physicians with treatment decisions.

1.2 Declaration

This work was created in cooperation with The University Hospital in Pilsen.

1.3 Thesis structure

This document is divided into several chapters. The Chapter 2 mentions basic description of strokes, possible instruments for their investigation and it also summarizes the generally performed examination using the computed tomography. Next are described studies dealing with the examination results processing and the method of perfusion blood volume mapping is introduced. Next follows description of possible image processing methods while some of them are used in the further chapters. The Chapter 3 specifies the objective of the thesis and Chapter 4 describes the available material and its features. There are presented also methods used for obtaining manual delineation patterns provided by two physicians. The Chapter 5 is dedicated to segmentation adjustment step which prepares the source images for further processing. The Chapter 6 uses several methods for infarction core detection and it also evaluates the matches according to physicians' patterns. It also shows that these methods are not strong enough to provide satisfactory results using the perfused blood volume maps. The Chapter 7 proposes a method which is aimed for the perfused blood volume maps and it is able to delineate the infarction core. In the Chapter 8 the optimization process for the proposed method is described and the optimal parameters are found. Results evaluation is presented and compared to other methods and also to the mutual match between two physicians. In conclusion chapter (Chapter 9) is summarized the proposed method and its advantages and disadvantages are presented. Appendix A presents detailed tables covering individual matches of different methods according to specific anonymized patients of the used material. There are presented different characteristics like settings of the methods, match descriptions in a form of sensitivity, specificity and Matthews correlation coefficient, delineated volumes, its maximal values, etc. Appendix B contains figures depicting the individual matches of different methods according to the two physicians' manual delineations individually.

Chapter 2

State of the art

2.1 Strokes

Stokes mean disorder of blood flow in brain. We can dived strokes into ischemic and hemorrhagic. Ischemic strokes are caused by an obstacle which blocks the common blood supply. Hemorrhagic strokes are caused by rupture of any of the brain vessels. The ischemic strokes mean reduction of the blood flow, the hemorrhagic strokes mean leakage of the blood. This work deals with the ischemic strokes.

2.2 Investigation instruments

There are several instruments which can be used for stroke diagnosis. There are Computed Tomography (CT), Magnetic Resonance (MR) or Positron Emission Tomography (PET). They all are imaging modalities providing images where value of each point of the image corresponds to the tissue characteristic at the corresponding place. Only computed tomography will be further used in this work.

2.2.1 Computed Tomography

Computed Tomography is radiological diagnostic method. It is provided by an instrument called CT scanner. It is based on X-ray which comes out of the X-ray tube and it is absorbed by a detectors. Number and position of the X-ray tubes and detectors depend on the device. The most widely used, the spiral CT type, combine rotation of the X-ray sources and detectors with moving of the table. The amount of the absorbed radiation by detectors is connected with the density of tissue which it went through. Complex mathematical calculations reconstruct final 2D images which all together give 3D volume.

Final images contain information about density in Hounsfield's units [HU]. Further more it contains also information like number of rows, number of columns, bits per one

Object	**Density [HU]**
Water	0
Gas	-1000
Bones, iron	+1000 till +2000
Calcification	60
Muscles	+35 till +50
Gray matter	+30 till +40
White matter	+25 till +32

Table 2.1: Objects and their densities [HU] ([6])

sample of the density, position of the table, dimensions of one voxel, etc. DICOM format allows to store all of these information together with the image.

Table 2.1 shows list of some materials and their densities [6].

2.2.2 Magnetic Resonance

Magnetic Resonance is currently considered to be the best imaging method. Its history starts in 1952 and it has been clinically used since 1973. The principal is different from computed tomography. Magnetic resonance monitors changes in behavior of nuclei of atoms when they are exposed to magnetic field and activated by a high-frequency pulses. There is measured voltage induced by radiofrequency coil. Detailed principle can be found in [6]. There are acquired two relaxation times - T1 and T2. According to the preferred relaxation time we distinguish between T1 and T2 weighted images. Final images contain grayscale voxels. There is no exact mapping between voxel intensities and specific tissue types. The intensity expresses ratio between water and fat. Magnetic resonance has good distinction of soft tissues even without need of using contrast material. Also there is not used any radiation and magnetic filed has not yet been proven to be harmful for human being. Disadvantages of magnetic resonance is its high operating costs and limitation in weight of patient, claustrophobia or longer acquisition time [6].

2.2.3 Contrast medium

CT examination uses injection of the contrast material when tracking of the blood-vessels is intended. After injection of the contrast material the contrast medium is spread through the blood-vessels. Acquired images indicate density change at the places with the contrast material. This change depends on the type and the amount of the used contrast material.

Figure 2.1: CT image sample

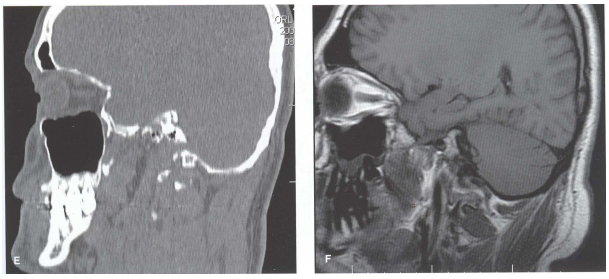

Figure 2.2: Comparison of CT and MR images [6]

There can be used positive or negative contrast medias. The negative ones absorb less x-ray radiation and the positive ones absorb more. Thus the change on the acquired images is positive or negative. There are widely used only positive non-ionized contrast material causing the positive enhancement of the measured density. Application of the contrast media requires to use correct amount, concentration and flow and the acquisition to be initiated at the right moment. All these factors reflect slope, duration of the increased density and also the rate of the increase.

2.2.4 Partial Volume Effect

Some CT images can seem to contain incorrectly measured values. We call it artifacts and it can be caused for example by movement of the patient, presence of metal objects, wrong instrument settings, etc. We can minimize presence of some artifacts but with some of them we must count. Partial volume effect is one the always present artifact. It is caused by the limited resolution of the instrument. Every voxel of the image corresponds to area which has some dimensions. Tissue inside this area can vary but the instrument can store it just as one scalar value. It stores the density as an average density of the area. This effect is most obvious on borders between two different density tissue types where the density change is rapid and steep (like bones and soft tissues).

2.2.5 DICOM

DICOM means *Digital Imaging and Communication in Medicine*. It is an international standard focused to medical area. It covers several domains like definition of communication between instruments and other systems like PACS *Picture Archiving and Communication System*, definition of data formats, security, etc.

Medical institution which uses the DICOM standard has advantages in new devices incorporating. DICOM standard also supports visit planning which means that the instrument get a list of planned patients, clinician just selects the correct one from the list and the instrument automatically stores images to the correct person with no need of manual identification filling which is often source of mistakes.

There are defined specifications how to exchange imaging documentation. DICOM images can be stored to different medias and it has the same format for all modality types. The format consists of attributes and values associated with the attributes. All possible attributes and their grouping is specified in [24]. Attributes describe patient, institution, modality and its settings and of course the acquired data.

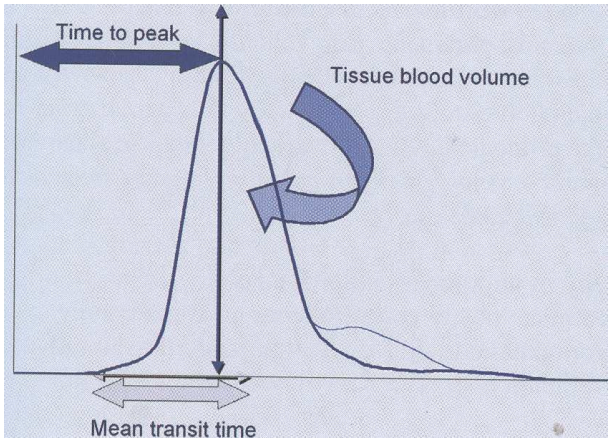

Figure 2.3: Intensity changes of a voxel on a perfusion CT [10]

2.3 Stroke investigation

2.3.1 Generally performed examination types

There are generally performed three types of examinations when a patient is admitted into the hospital with the stroke suspicion. All of them are CT examinations.

Non Contrast CT - NCCT

It is acquired very quickly and it provides the prime information about the stroke location and its extent. It covers area from the skull-base to the vertex. It contains generally about 30 images with 5 mm thickness.

Perfusion CT - CTP

The most precise tissue state information can be gained by the Perfusion CT examination type. It uses a contrast material. There is repeatedly acquired the same area monitoring the inflow of the contrast material, its spreading and outflow. Presence of the contrast material causes proportional increase of the acquired intensities. For every voxel there can be depicted the intensity curve mapping changes of intensity in time (Figure 2.3). This type of examination provides large number of images and their further processing follows. As an outcome of the perfusion examination there are volumetric maps mapping characteristics like Cerebral Blood Volume (CBV), Cerebral Blood Flow (CBF), Time To Peak (TTP), Mean Transmit Time (MTT), etc. The disadvantage of this examination type is limited width of the scanned area depending on the instruments capabilities. Generally only around 4 different slices can be acquired at one time. Recently there starts to appear instruments which are capable of acquiring the whole brain area.

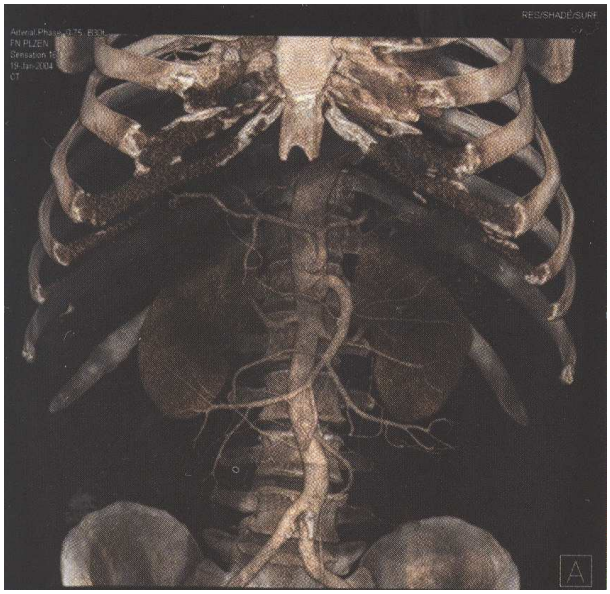

Figure 2.4: Volumetric Reconstruction Technique (VRT) [10]

CT Angiography - CTA

This kind of examination is acquired after the perfusion one. There is also used contrast material but instead of the perfusion one there is acquired whole brain area when the contrast material is saturated in the brain. There are acquired images of around 1 mm thickness from the vertex to the aortic arch. This type of examination is used for detection of the blood barriers. The vessels located behind the barrier has a lack of contrast material, so the intensities remain around the same as without using the contrast material. Images of the CTA are often displayed as 3D reconstructions using Volume Rendering Technique (VRT) where the vessels behind blood barrier are not shown at all and thus they are easily visible for the physicians.

Volumetric reconstructions (Figure 2.4) are created on request of the physician respecting all settings like position, viewing angle, etc. Some other parameters specify resulting image features. You can define density intervals and corresponding colors and transparency in the resulting image. The user have to define what is desired to be shown - bone structures, organs, vessel trees, etc. Lighting and shadowing can be also used for the final image. Depending on the workstation user can further process resulting images - crop area, subtract different structures, etc.

2.3.2 Changes of brain tissue during ischemic strokes

Acute ischemic strokes mean disturbance in blood supply to the brain. The change of the blood supply affects the brain tissue. According to severity of the blood supply change we can classify affected brain tissue into the three following categories [10].

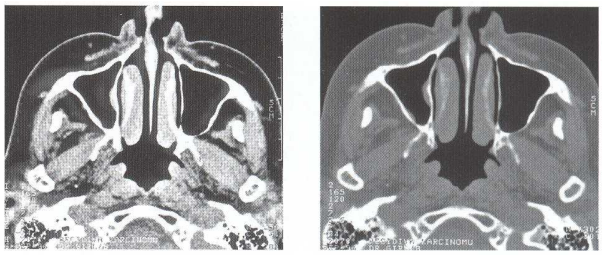

Figure 2.5: Comparison of the soft tissue window and the bone window [6]

- Oligemia - Reduced blood supply but the tissue still keeps its neuronal function.
- Penumbra - Savable tissue if the blood supply is restored. Neuronal function is temporarily lost.
- Infarction Core - Necrotic tissue.

Penumbra and Infarction Core are two categories with the most valuable information for the physicians. Using this information they can make decisions of the best suitable treatment.

Correct identification of the categories for an ischemic stroke patient is a task for medical imaging.

2.3.3 Windowing

CT images can contain different types of tissues having different range of Hounsfield's units (see Table 2.1). Common CT stores density in 12 bits format. It means about 4000 possible densities. Human eye is capable to recognize only 20 different levels of gray color [6]. Windowing is displaying method allowing user to focus on the limited gray range interval while displaying it using the full gray scale (from black to white). User must specify Window Center - the center density of the interest. And the Window Width - this range around the Center will be displayed using the full gray scale. Densities out of this window will be displayed as black or white. Interactive windowing is a tool for physicians allowing effective CT images interpretation. Complete description of the windowing method can be found in [24].

For example for displaying bones we use wider windows with width about +1200 to 3000 HU. For soft tissues we must use thinner window like 150 - 500 HU.

2.3.4 Penumbra and Infarction Core identification using Computed Tomography

In [19] is defined CT protocol for Acute Stroke with tips and tricks for general radiologists. There are discussed different types of examinations separately. NCCT images should be

reviewed twice, first with the window (Section 2.3.3) width and level settings approximately 40/20 HU and the second 20/32 HU. CTA images should be reviewed with various window width and level settings around 25/35 HU but with respecting differences between different CT scanners and patients. CTP maps can be used for marking penumbra and infarction core regions using parameters MTT, CBF and CBV parameters. By [39] infarction core can be marked as combination of elevated MTT, markedly decreased CBF, markedly decreased CBV (< 2.0 ml·100g^{-1}). However penumbra can be recognized as elevated MTT ($> 145\%$), decreased CBF and normal or mildly increased CBV. [19] also mentions that there is no report analyzing usefulness and reliability of these maps in clinical setting.

Other studies [39], [23] evaluate group of patients for finding optimal thresholds and specifies the most valuable perfusion parameters. [39] contains 130 patients with suspected acute stroke. NCCT, CTP, CTA and follow-up NCCT and MRI examinations were performed. Examinations were co-registered to each other and also interpolated to have the same matrix size. MRI images were manually traced for the final infarct volume. ROC analysis was evaluated for a set of threshold values on MTT maps, relative MTT, absolute TTP, realitve TTP, absolute CBF, relative CBF, absolute CBV and relative CBV maps. Relative maps are maps in percentage of the values in the contralateral normal hemisphere. [39] concludes that infarction core and penumbra is optimally differentiated by combination of relative MTT and absolute CBV parameters. Infarction core is described as absolute CBV < 2 ml·100g^{-1} and penumbra is described as mismatch between absolute CBV 2.0 ml·100g^{-1} and relative MTT with a threshold at 145%. [39] also says that the larger infarction core (80 ml of the infarct volume) the higher is the absolute CBV threshold (2.3 ml x 100g^{-1}).

[23] investigated group of 30 patients. They acquired admission NCCT, CTA and CTP and follow-up NCCT. There were manually outlined infarct ROI on follow-up NCCT and superimposed on admission CTP images and also outlined contralateral area. Statistical analysis was performed with following results. CBF in infarction core 13.3±3.75 ml·100g^{-1}·min^{-1}, in penumbra 25.0±3.82 ml·100g^{-1}·min^{-1}. CBV in infarction core 1.12±0.37 ml·100g^{-1}, CBV in penumbra 2.14±0.43 ml·100g^{-1} and CBV in contralateral area 1.78±0.30 ml·100g^{-1}. [23] shows that CBF and CBV maps can be used for detection of the infarction core.

2.4 Perfused Blood Volume Mapping

CTP technique is often limited by the instrument in the extent of the scanned area thus perfusion maps show parameters only for the preselected locations of the brain. Subtraction of NCCT from CTA source image provides information about local enhancement. This enhancement caused by contrast material depends on the actual cerebral blood volume and on quantity of the contrast material that reaches the tissue. That is why resulting maps are called perfused blood volume maps (PBV) [33]. The CBV maps of the CTP ex-

amination are constructed from a serie of source images tracking the spreading of the contrast material while the PBV maps use only two values - density with and without the contrast material.

Construction of the perfusion blood volume maps of the brain was introduced in [15] on white rabbits. There were acquired NCCT and CTA images and their subtraction was performed. Equation 2.1 defines formula for computing fractional voxel blood volume which can be converted into absolute volume [ml·100g^{-1}] by Equation 2.2.

$$\%CBV = 100 \cdot \frac{\Delta HU_{brain}}{\Delta HU_{blood}} \tag{2.1}$$

$$CBV = \frac{\Delta HU_{brain}}{\Delta HU_{blood}} \cdot V_{voxel} \cdot N \tag{2.2}$$

For correct evaluation of the equations 2.1 and 2.2 we need to define ΔHU_{brain}, ΔHU_{blood}, V_{voxel} and N. Major intracranial vessels were carefully outlined and only inside of this ROI was mean ΔHU calculated referring as ΔHU_{blood}. Evaluation of the perfusion blood volume maps is based on a voxel by voxel basis. Density change of the voxel which belongs to the brain tissue and does not belong to any major intracranial vessel is referred as ΔHU_{brain}. Voxel volume of 1.05 g·ml^{-1} was used and N is number expresses count of voxels in 100 g of the tissue.

Some commercial softwares (like *Siemens - syngo Neuro PBV*) are able to calculate perfused blood volume maps. Study [40] on a group of 48 patients with acute ischemic stroke evaluates the predictive value of perfused blood volume maps for finding perfusion abnormalities. Perfusion blood volume maps abnormalities were visually found and manually marked. CTP examination was also performed. On TTP maps was manually outlined area of perfusion abnormalities and only this area was used in CBV maps for infarction core delineation based on thresholds of study [39] (2.0 ml·100g^{-1}). Study [40] found a strong correlation between the extent of the perfusion abnormalities in perfusion blood volume maps and the infarct core of CBV maps. Follow-up examination were not assessed.

Study [17] can be classified also as a perfused blood volume mapping since all measurements are based on analysis of NCCT and CTA examinations. On the follow-up examinations of group of 28 thrombolysed patients were manually outlined infarcted areas. These areas were transferred to the NCCT and CTA examinations and the boundaries parrallel to the follow-up NCCT infarction area in the distance of 5 mm were drawn resulting in three boundaries - core infarction, inner and outer boundary. Areas of the infarct core and the inner band were also reflected about the midline to the contralateral nonischemic hemisphere. Contrast enhancement between NCCT and CTA was reported in each area and it was expressed as a percentage of ischemic enhancement according to the contralateral enhancement referring as normalized pCBV. Statistical analysis shown following values: $24.5\% \pm 2.3$ (infarction core), $36.3\% \pm 2.4$ (inner band), and $72.1\% \pm 2.4$ (outer band).

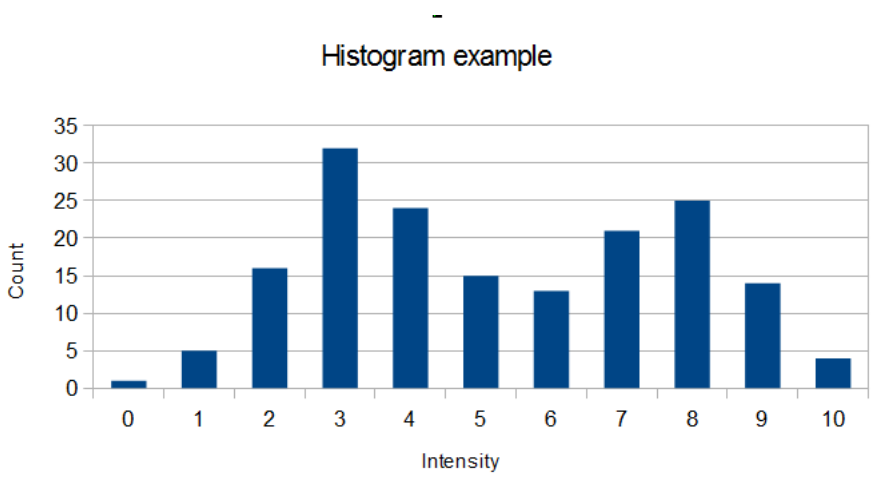

Figure 2.6: Example of a histogram

2.5 Image processing

Medical images acquired on a CT device are stored as a raster images using mostly DICOM format. One examination consists of many 2D source images were also descriptive features of the examination are stored. Whole examination can be considered as a 3-dimensional matrix with predefined origin, axes orientations and a spacing definition. Dimensions of the matrix depend on the instrument capabilities. Typical dimensions of one 2D image are 512x512 and the third dimension depends on the examination type and instrument settings. There are typically stored gray-scale values using 12 bit depth.

Image processing deals with processing of images in order to satisfy specific purpose. Depends on the purpose and input images we can choose suitable methods for the processing.

2.5.1 Histogram

One of the basic image processing method is a histogram calculation. The histogram of the image expresses frequencies of intensities in the image. It is often depicted in a chart where the horizontal axis means intensity and the vertical axis means frequency (counts). We can define the histogram as a vector of the frequencies of the corresponding intensities. We can display histogram for example as shown in the Figure 2.6.

2.5.2 Thresholding

Thresholding is another basic method identifying the image intensities according to a threshold value. Depends on our needs we can be interested only in intensities lower than a threshold or upper than a threshold value. Combining these two approaches we can also identify intensities between two threshold values. If i is an intensity of the image and T

$$\begin{pmatrix} -1 & -1 & -1 \\ 0 & 0 & 0 \\ 1 & 1 & 1 \end{pmatrix}$$

Figure 2.7: Prewitt's operator

is a threshold value then the thresholding can be described by Equation 2.3 [42] where L means values equal or below the threshold and H means higher values.

$$i' = \begin{cases} L, & \text{when } i < T \\ H, & \text{when } i \geq T \end{cases} \tag{2.3}$$

2.5.3 Convolution

Convolution is a special combination of two functions. We can define image as a function $I(x)$. Another function $h(x)$ is a convolution kernel and the convolution is expressed as $I_{i,j} * h_{i,j}$. We can consider just a discrete way of convolution since the image is divided into pixels (or voxels) which is not a continuous signal. The goal of the convolution is to take the convolution kernel, move it step by step over all pixels (or voxels) of the image and evaluate resulting value for every pixel (voxel) as a sum of multiplications of all the corresponding pixels (or voxels) of the image with the corresponding kernel function value as shows Equation 2.4 [42].

$$I'_{i,j} = I_{i,j} * h_{i,j} = \sum_{x=-k}^{k} \sum_{y=-k}^{k} I_{i+x,j+y} h_{i+x,j+y} \tag{2.4}$$

The example of a convolution kernel can be Prewitt's operator (Figure 2.5.3) for edge detection. It evaluates derivation in a vertical direction. Edge is defined as a high value of the derivation.

2.5.4 Noise reduction

Images often contain some level of noise which makes the image processing more difficult. Such noise can be characterized by sudden intensity change and it can be interpreted by different kind of methods incorrectly like edges. The noise reduction methods are often used for pre-processing the images in order to reduce the noise and prepare the image for the following processing.

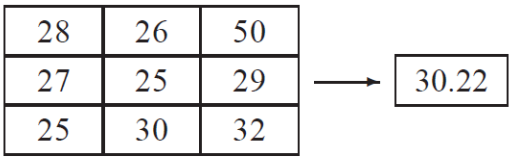

Figure 2.8: The example of mean smoothing, evaluation of the mean value from the neighborhood. [18]

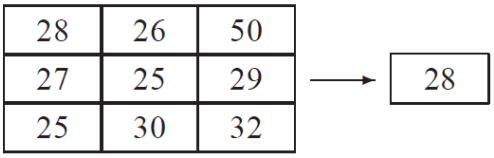

Figure 2.9: The example of median smoothing, evaluation of the median value from the neighborhood. [18]

Mean filtering

Mean filtering reduces the noise which can be characterized by sudden change of intensity by using average value of its neighborhood. For this method we must define the dimensions of the neighborhood and then on a voxel by voxel basis we can evaluate the average value of the neighborhood for all voxels and consider these mean values as a resulting image with the reduced noise.

Median filtering

Median filtering is a method for noise reduction similar to the Mean filtering. It also uses the neighborhood voxels but instead of evaluating the mean values it looks for the median values. The advantage of this approach is that it is not sensitive to extreme values which could influence the mean values.

The disadvantage of the median filtering is that with growing dimensions of the neighborhood it grows also the processing time because of the required sorting of the neighborhood values for each voxel.

Gaussian filtering

Gaussian filtering in opposite of previous methods tends to prioritize the nearer voxels. The method uses again the local neighborhood but all of the voxels in the local neighborhood gets a weight. The closer the voxel is to the central voxel the higher weight it has. The exact weight mapping is given by the Gaussian function which with the mean value μ=0 and optional variance σ^2 looks like:

$$f(x) = \frac{1}{\sigma\sqrt{2\pi}} e^{-\frac{x^2}{2\sigma^2}} \tag{2.5}$$

The size of the required nearest neighborhood is proportional to the used variance σ^2 and for the implementation purposes it can be reduced by setting maximum kernel width. This kind of smoothing can be also performed using the convolution method.

Edge preserving smoothing

All previous methods are based on processing of the local neighborhood and the resulting (smoothed) values are computed as mean, median or using the gaussian function weighted values. All these methods are not edge preserving because when the edge is present, these methods make the edge thinner or thicker because the steep change of the intensity at the edge is blurred. Using the meaning method this significant change is averaged with the normal neighborhood values.

Another approach was introduced by Perona and Malik in [26]. Anisotropic diffusion is connected with the heat equation which single slice solution is Gaussian smoothed image while the original image is taken as the initial condition [18]. The heat equation looks like [18].

$$\frac{\partial g(x,y,t)}{\partial t} = \nabla \cdot \nabla g(x,y,t) \tag{2.6}$$

The original image to be denoised is expressed by $g(x,y,0)$ and the $g(x,y,t)$ is a convolution of the original image with the gaussian function with the standard deviation $\sigma = \sqrt{2 \cdot t}$.

The anisotropic diffusion introduces *conductance* (function $c(\mathbf{x})$) which limits the changes at edges by reducing the smoothing influence on the high gradient magnitudes.

$$\nabla \cdot \nabla g(x,y,t) = \nabla \cdot c(|\nabla g(x,y,t)|)\nabla g(x,y,t) \tag{2.7}$$

Method called *Gradient Anisotropic Diffusion* defines the conductance as [18]:

$$c(\mathbf{x}) = e^{-(\frac{||\nabla U(\mathbf{X})||}{K})^2} \tag{2.8}$$

This equation reduces the smoothing at places with the higher magnitude of the gradient at each voxel which can be adjusted by the parameter K.

The numerical solution of the differential equation requires three parameters: conductance, time step and number of iterations. Typical values differ for 2D and 3D images. For 2D images - time step: 0.25, number of iterations: 5. And for 3D images - time step: 0.125, number of iterations: 5. The conductance parameter has typically values between 0.5 and 2.0. The lower the parameter is the stronger edges are preserved and vice versa.

In [18] we can find another similar method called *Curvature Anisotropic Diffusion* which we can express as:

$$\nabla \cdot \nabla g(x,y,t) = |\nabla g(x,y,t)| \nabla \cdot c(|\nabla g(x,y,t)|) \frac{\nabla g(x,y,t)}{|\nabla g(x,y,t)|} \tag{2.9}$$

The gradient anisotropic diffusion could in some cases even enhance the edges (negative diffusion). The advantage of the curvature anisotropic diffusion is that it provides only the positive diffusion and the conductance parameter influences only the strength of the diffusion. Usually used parameters for the curvature anisotropic diffusion are by [18] for 2D images - time step: 0.125, number of iterations: 5, conductance: 3.0. And for 3D images - time step: 0.0625, number of iterations: 5, conductance: 3.0.

2.6 Registration methods

Medical images are provided by different modalities like CT, MR, PET, etc. Each modality is based on different technology and acquired images differ in meaning of contained information. Images can differ in spatial resolution, color or bit depth and other features. Each modality has its advantages against the others and of course also disadvantages against the others. Registration methods allow fusion of different examination gaining some added value. For example MR is very good at displaying soft tissue and CT is better in bones mapping. By fusion of CT and MR we can get such images which have both of these advantages. For the fusion the registration process is necessary.

Another fusion example can be taken from Section 2.4. There is described study [15] processing CTA and NCCT examination. There must be taken into account only corresponding voxels. This correspondence can be achieved by the process of registration of both examinations.

The process of registration deals with finding the best fit of one image over the other. In the other words registration process finds the best transformation which transforms coordination system of one examination into the other maximizing correspondence of transformed voxels. Registration process can be also understand as finding of the common coordination system of both examinations.

Registration methods can be described by following criteria [1].

1. Dimensionality

   - 2D-2D - e.g. registration of single CT images
   - 2D-3D - e.g. x-ray image with CT examination
   - 3D-3D - e.g. CT with MR

   We can also register a time serie images, like source perfusion CT images which track the spreading of the contrast material. There is repeatedly scanned the same place during time. Each time serie can be also described as 2D or 3D.

2. Nature of registration basis
    - Extrinsic – based on artificial objects simplifying the registration process.
        - Invasive.
        - Non-invasive.
    - Intrinsic – no artificial objects, registration is based only on the acquired images.
        - Landmark-based – there is often required user interaction. It uses locating of the morphological points, geometrical features, etc.
        - Segmentation-based – the registration process is based on anatomical features which are segmented from the original images (bones, skin, etc.).
        - Voxel property based – methods like Principal Component Analysis (PCA) when coordination system is found only using the voxels property.
    - Non-image-based registration – requires calibrated instruments.
3. Nature of the transformation
    - Rigid – only rotations and translation.
    - Affine – preserves parallelism.
    - Projective – preserves lines.
    - Curved – transforms lines to curves.
4. Domain of the transformation
    - Global – one transformation for entire image.
    - Local – image is divided into parts where each part can have own transformation.
5. Interaction
    - Automatic – no user interaction required.
    - Semi-Automatic – user interaction is required.
    - Interactive – registration is made by the user.
6. Optimization procedure
    - Parameters computed – like PCA method, by mathematical formulas we get the final registration parameters.
    - Parameters are searched for – like finding extremes of a cost-function.
7. Modalities involved
    - Monomodal – CT-CT, MR-MR, etc.
    - Multimodal – CT-MR, CT-PET, etc.

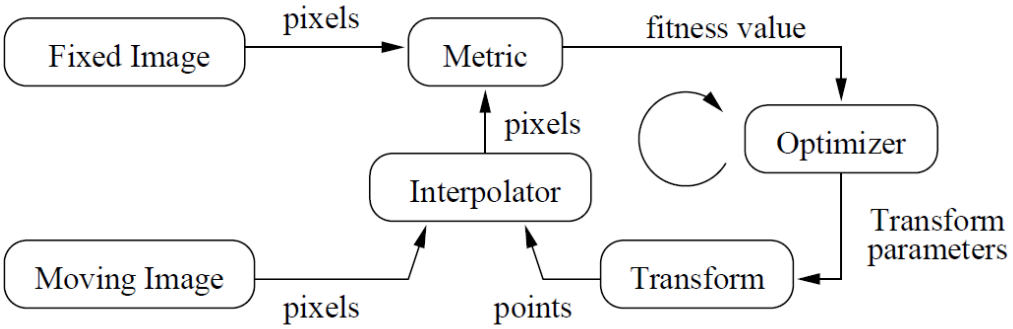

Figure 2.10: Typical registration framework [18]

- Modality to model – registration with mathematical model.
- Patient to modality – manipulate the patient for a modality.

8. Subject

   - Intrasubject – involved examinations belong to one subject.
   - Intersubject – involved examinations belong to different patient.
   - Atlas – registration of an examination according to an atlas.

9. Object

   - Head.
   - Thorax.
   - Abdomen.
   - Pelvis and perineum.
   - Limbs.
   - Spine and vertebrae.

2.6.1 Registration framework

Typical registration framework is shown in the Figure 2.10. It consists of the source images called Fixed and Moving image. The fixed image is during the registration process without any change. The moving image is transformed by a transform function using a set of parameters and interpolated. Resulting image is compared with the Fixed image and the accuracy is evaluated using a metric. Optimizer is responsible for choosing next iteration parameters.

2.6.2 Registration methods assessment

Registration methods assessment is not simple. It always depends on the method and its accuracy criteria. Mostly used registration methods are based on minimization of cost-function. The cost-function is responsible for evaluation of the precision. As the final transformation parameters are chosen those which belong to the best cost-function results. We can not find the only recipe how to globally compare accuracy of the registration methods.

Study [3] summarizes the methods for registration accuracy measurements. As a first example we can mention a method measuring the degree of imprecision using metrical units like millimeters. We can evaluate such values using Root Mean Square (RMS) method where the distances of the incorrectly registered voxels are measured. Registration methods capable of such accuracy measuring are for example based on Chamfer Matching principle [4]. Study [3] mentions that accuracy of 2 mm is generally supposed to be sufficient but it always depends on a purpose of the registration which can require higher or lower accuracy.

Simple form of registration accuracy measurement can be visual evaluation by a human eye. [3] mentions that human eye is able to detect imprecision of translation from 2 mm and imprecision of rotations from 2 degrees. It takes a short time for a human to make such evaluation.

RMS methods can be used also for registration accuracy measurement based on significant points. These points must be easily detectable on both registered images. RMS method can evaluate the degree of imprecision in absolute values.

Registration methods can be assessed also by a sensitivity for initial parameters which express the first estimate of the transformation parameters. The other criteria can be a noise sensitivity.

2.6.3 Maximization of the mutual information metric

The metric method of maximization of the mutual information is capable of multi-modal registration. The resulting transformation provides the maximal mutual information. Evaluation of the mutual information is based on information theory and it processes density histograms of both images.

Lets denote fixed image (reference) as r and moving image as f (floating volume). Then $r(t)$ and $f(s)$ express the density at the coordinations t and s. The aim of the registration is to find the parameters α^* of the transformation T:

$$\alpha^* = arg \max_{\alpha} M(f(s), r(T_\alpha s)) \tag{2.10}$$

where M expresses the rate of the mutual information which can be expressed as:

$$I(A, B) \equiv h(A) + h(B) - h(A, B) \tag{2.11}$$

$h(A)$ and $h(B)$ are entropies A and B and $h(A,B)$ is the mutual entropy. Entropy is defined as:

$$h(A) = -\int p(a) ln\ p(a)\ da \tag{2.12}$$

$$h(B) = -\int p(b) ln\ p(b)\ db \tag{2.13}$$

$$h(A,B) = -\int p(a,b) ln\ p(a,b)\ da\ db \tag{2.14}$$

The formula for the mutual information can be for discrete cases expressed as:

$$I(A,B) = \sum_{a,b} p(a,b) * log \frac{p(a,b)}{p(a)p(b)} \tag{2.15}$$

To evaluate the rate of probability of density a or b, we must make the density histogram of both images. $p(a)$ and $p(b)$ correspond to the occurrence probability of the density a or b in the image A or B. The mutual probability of $p(a,b)$ correspond to the density a occurrence probability in image A while at the transformed position in the image B is located the density b.

2.6.4 Optimization

Duration of the registration process depends on several factors. One of the main factors is the optimization process. When we use iterative registration methods, like minimization of a cost-function, we must go through all possible combinations of transformation parameters to find the best one. Optimization can limit this space of all possible combination by algorithms choosing combination for the next iteration. Such methods uses first or second order derivative or other geometrical features. Well known optimization methods are for example methods of the gradient descent. Other methods like Powell's method [27] can be also used.

2.7 ROC Analysis

ROC analysis is a method allowing to visualize and tune the classifier performance. The task of a general classifier is to process input information and make decision on which class the input belongs to. Classifiers often rely on parameters which have to be carefully set to make the classifier working correctly. For tuning the parameters we often have a set of learning data where we exactly know which input should belong to which output class. Using this set of learning data we can find the most suitable parameters which have the best precision in classifying. Unfortunately there is often no possibility to set the classifier parameters to ensure that all learning data will correspond to their class. Since we are aware that the classifier will not be ideal we must choose those parameters with the best possible results on the learning set. If we consider the only two-class classifier (yes/no), we can define confusion matrix and a set of equations as shown in Figure 2.11.

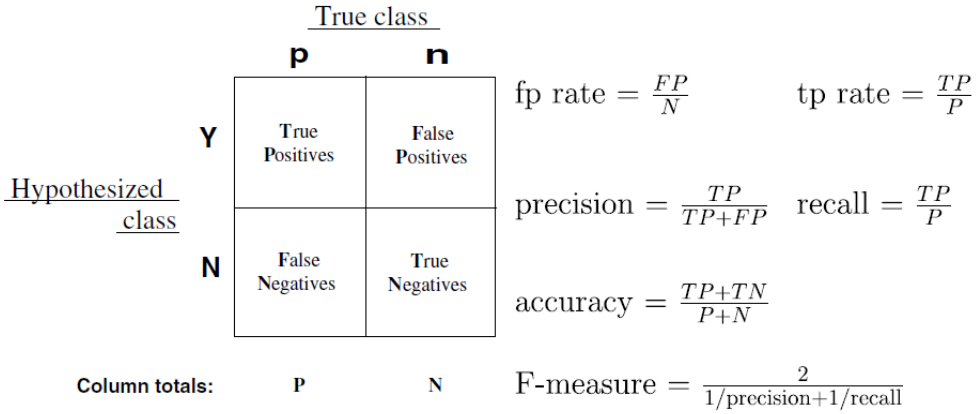

Figure 2.11: Confusion matrix and metrics definitions [9]

Confusion matrix is formed by the learning-set and results of the classifier with the actual set of parameters. One confusion matrix is per one set of parameters. The matrix expresses counts of:

- True positive (TP) - classified correctly as positives.
- True negative (TN) - classified correctly as negative.
- False positive (FP) - classified incorrectly as positive.
- False negative (FN) - classified incorrectly as negative.

Using the counts of TP, TN, FP and FN we can define sensitivity, specificity and also Matthews correlation coefficient:

$$\text{sensitivity} = \text{tp rate} = \frac{TP}{TP + FN} \tag{2.16}$$

$$\text{fp rate} = \frac{FP}{TN + FP} \tag{2.17}$$

$$\text{specificity} = 1 - fprate = \frac{TN}{TN + FP} \tag{2.18}$$

$$\text{Matthews correlation coefficient} = \frac{(TP \cdot TN) - (FP \cdot FN)}{\sqrt{(TP + FP)(TP + TN)(TN + FP)(TN + FN)}} \tag{2.19}$$

ROC graph is a graph where y-axis is a true positive rate (sensitivity) and x-axis is a false positive rate. ROC graph expresses the performance of the classifier. If we want to find the best settings for the classifier we have to evaluate tp-rate and fp-rate for different parameters. If we plot tp-rates and fp-rates for a set of parameters, we can get ROC graph for example like in Figure 2.12.

When the ROC graph is available for a set of parameters, we can choose the best one as the best for classifier. The choice should express balance between the tp-rate and

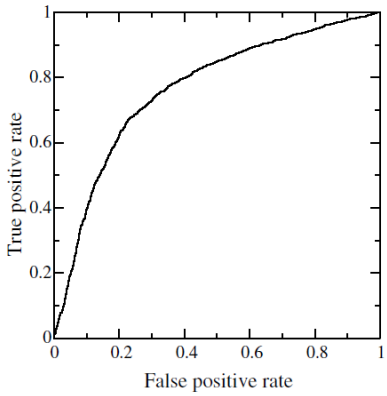

Figure 2.12: Example of ROC graph [18]

the fp-rate (in other words the balance between sensitivity and specificity). The decision always depends on use of the classifier. There must be taken into account consequences of false positives and also consequences of false negatives.

Another criteria how to assess classifier performance is the Area Under Curve (AUC). This value can be calculated from the ROC graph and the value is always between 0.0 and 1.0. More details about ROC analysis can be found in [9].

Matthews correlation coefficient is a correlation coefficient evaluating a performance between two classifications. The advantage of this coefficient is that it uses all four numbers TP, TN, FP, FN providing a better summary of performance than other coefficients like sensitivity, specificity or Hamming and L^P distances which are based only on two from the four numbers.

2.8 Automatization of ischemic stroke detection

Study [36] introduces an automated method for ischemic stroke detection in NCCT images. The presumption is that the stroke region is a complex but smooth 3D shape. [36] deals with processing of 7 people's NCCT of the head containing 16 slices of 8 mm slice thickness and dimensions 512x512. The whole process of the method presented in [36] can be described in following points.

- CT image pre-processing - selection of gray levels containing useful information, removal of "non-interesting" parts
- Investigation of local means and standard deviations, shown in Figure 2.13. There was used sliding window of 21x21 pixels. Depicted numeric labels are divided by 100.
- Definition of lower and upper limits of the mean and standard deviation aiming to define stroke areas.

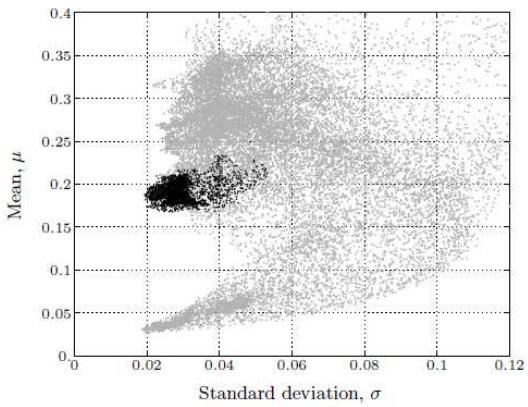

Figure 2.13: Local means and variations occurrences in NCCT image by [36], black color indicates stroke region [36]

- Post-processing - selection of the largest continuous area, forming a 3D shape of the stroke.

The algorithm described in [36] searches for the ischemic stroke areas slice by slice separately. The value ranges of means and variances are found for each slice separately and on each slice are selected areas satisfying the limits. Some of these areas are false positive and the rule that the true stroke area comes through several adjacent slices is used. Another feature is used. Lower and upper limits for each slice are approximated through all slices by polynomial approximation of the 3rd degree.

Study [14] presents a method for finding symmetry plane in NCCT images and [13] uses the symmetry plane in combination with the [36] method for the ischemic stroke detection and it describes the optimization of the whole process.

Recently there was also introduced semi-automated program for stroke-analysis [8] with the first results on 5 stroke patients [11]. The program processes CBF, CBV and MTT CT perfusion maps and on a voxel by voxel basis divides the voxels into 4 categories.

- N-Match - normal tissue.
- D-Match - necrotic tissue (dead).
- Mismatch - area of penumbra.
- Undefined - used criteria is not able to assign category above.

The program uses thresholds which can be adjusted by neurologists. There were used thresholds for CBF 20 ml·100g^{-1}·min^{-1} ($\pm$10), CBV 2.5 ml·100g^{-1} ($\pm$1.5) and for MTT 7.5 sec ($\pm$4.5).

Based on these thresholds were counted voxels belonging to the previously mentioned group. The program calculates percentage of the areas as division of the count of voxels in

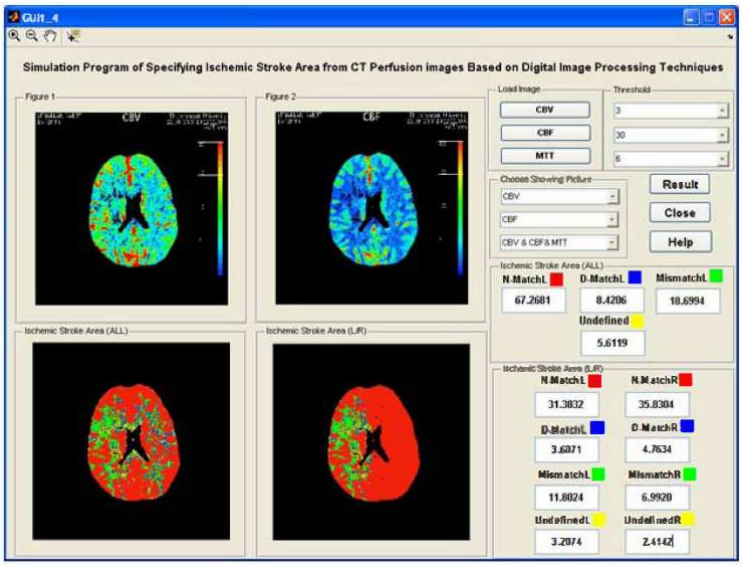

Figure 2.14: Interface of the simulation program for specifying ischemic stroke area [11]

the area and count of voxels in the whole brain. There are also compared counts of voxels in the left and right hemisphere and the one with the more N-Match voxels is considered as normal and the second one is considered as the side with the ischemic stroke area. The program interface shows Figure 2.14.

Chapter 3

Objective of the thesis

3.1 Infarction core delineation

Acute ischemic strokes are world-wide spread and are one of the leading cause of death and disability in population over 60 years old (Section 1.1). Thrombolytical treatment is not applicable for all patients since it depends on the volume of the infarction core in the whole brain. The objective of the thesis is to find an automated way of the infarction core delineation to allow measuring of the volume and to serve as another tool for physicians helping them with the thrombolytical treatment indication decisions.

Perfused blood volume mapping technique (Section 2.4) is used because it combines CTA and NCCT examinations (both generally performed and with the whole-brain coverage). The CTP examinations with the generated volumetric maps give detailed information about the tissue state but the coverage area is often limited.

3.2 Objective discussion

Detection of the infarction core is in most cases based on study [39] where the optimal CBV threshold was found as 2 ml·100g^{-1} using only CBV maps of the CTP examination. There was also mentioned that the larger infarction core has higher threshold (2.3 ml·100g^{-1}). Study [23] on a set of 30 patients found the mean values of infarction core areas 1.12±0.37 ml·100g^{-1}. Lower values than in [39] are discussed as caused by exclusion of voxels with specific properties by used algorithm. Anyway let me cite one sentence from [7] (page 431):

> Several studies developed different definitions of infarct core based on PCT with CBV thresholds and the "gold standard" for the identification of the infarct core in acute ischemic stroke is still a matter of debate.

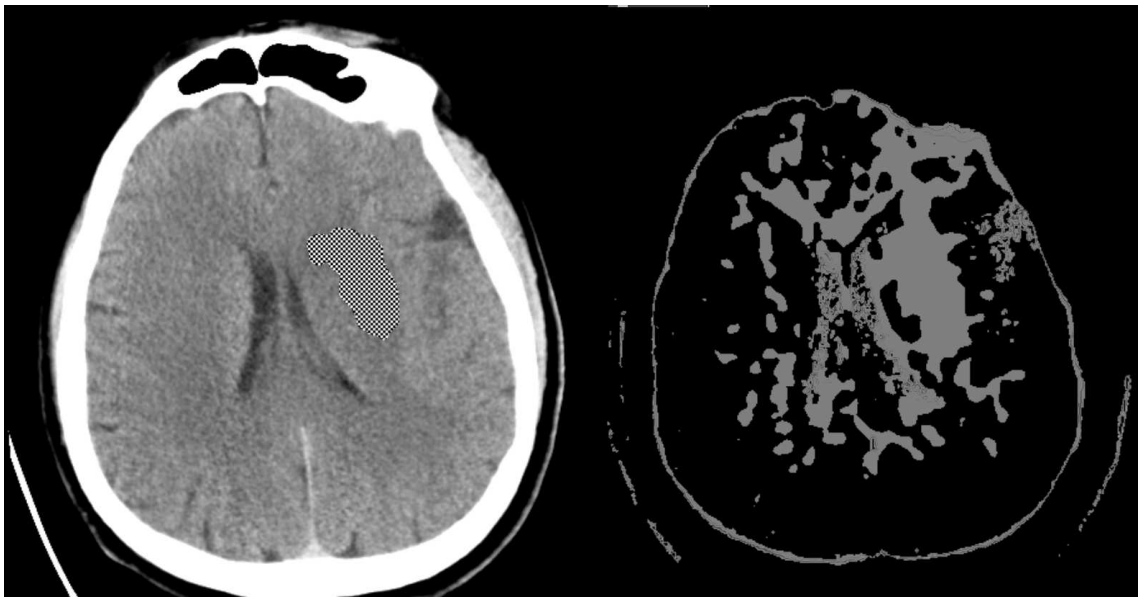

Figure 3.1: Marked infarction core on follow-up NCCT (left), simple thresholding on a source PBV image with 2 ml·100g^{-1} (right).

The citation is from article from year 2002 and there already exist some newer studies with the leading [39] containing probably the largest group of 130 patients. However semiautomated software presented by [8], [11] show requirements of adjusting threshold values by physicians since the threshold vary from patient to patient.

Recent studies confirm that CBV maps are suitable for infarction core detection. Most of the studies are based on manual tracking of ischemic area on follow-up images, superimposing this area to the source maps (CBV, PBV) and evaluating thresholds or mean values only inside this area. Figure 3.1 shows follow-up NCCT with marked infarction core (on the left) and simple thresholding of the corresponding admission PBV map showing only areas below or equal to threshold 2 ml·100g^{-1} (on the right). We can see that simple thresholding can depict the infarction core but together with it also portion of non infarction core area superimposed to the real core and also elsewhere. Using simple thresholding for evaluation of the infarction core volume by counting the thresholded voxels over whole examination and multiplying it by one voxel volume would lead to increasing the real infarction core volume by those false positive voxels. May be this can be the reason why several studies are concerned only to manually tracked areas identified on follow-up examination or why the semi-automated software [11] still requires the physician's adjustment of thresholds.

We would like to find a fully automated method capable of infarction core delineation while delineating only the infarction core area and minimizing the presence of false-positive areas.

Chapter 4

Method introduction

4.1 Presumptions

This work is based on several presumptions.

1. The infarction-core is a continuous area.
2. There is only one infarction-core area in the brain.
3. The values inside the infarction core areas are supposed to be low and it can vary from patient to patient with consideration of the generally accepted threshold 2 ml·100g^{-1}.

4.2 Verification

Since the automated method of the infarction core delineation is to be developed, there must be clearly verified findings of the proposed automated method according to some independent expert opinion. For this reason we asked two physicians to manually mark which areas should the method in ideal case delineate, in other words which areas are by their best opinion the real infarction core.

4.3 Material

In the cooperation with the University Hospital in Pilsen and after anonymisation process we had available admission CT examinations of 12 patients. Since the proposed method is supposed to process PBV maps which should be in a way analogous to CBV maps of the CTP examination, we received also the CBV perfusion maps for these 12 patients. All examinations were aquisited on dual-source CT (Somatom Definition, Siemens Healthcare, Forchheim, Germany). Since the cooperation with the University Hospital allowed also to obtain perfusion blood volume maps of these 12 patients we did not have to process

Map type	Units	Resolution	Thickness [mm]	Spacing [mm]
PBV	$ml \cdot l^{-1}$	1024x1024	5	3
CBV	$ml \cdot l^{-1}$	512x512	5	3

Table 4.1: Source images properties

admission NCCT and CTA to produce the perfusion blood volume maps and instead we could use those generated by the commercial software Siemens syngo Neuro PBV. All maps are stored in a series of DICOM files. PBV and CBV maps contain 44 source images and stored values are in ml·l^{-1} units. We can use formula 4.1 to convert [ml·l^{-1}] into [ml·100g^{-1}] using the density of the brain tissue 1.05 g·ml^{-1} [31].

$$x\ [ml \cdot l^{-1}]\ =\ (10,5\ *\ x)\ [ml \cdot 100g^{-1}] \tag{4.1}$$

To sum up in this study we used anonymised source images of 12 patients of following CT perfusion map types:

- PBV
- CBV

4.4 Image Representation

All images were available in DICOM format. Each map consists of a series of 2D axial source images as displayed in Figure 4.1. Indexation can be introduced, the first image at the top-left corner has image index 0, the next one on the right has image index 1 and the last image at the bottom-right of the Figure 4.1 has the maximum image index number. Both map types store voxel values as 12 bit integer and other features are shown in Table 4.1.

4.5 Image orientation

Map consists of serie of 2D images. Figure 4.3 shows commonly used kind of views of the map. 2D source images are the axial ones. Sagittal and coronal views are created by using all the 2D images using only specific voxels.

The map consists of voxels. For indexing them we can use three coordinations x, y, z. The coordinations x and y are used for positionoing in axial images where the x coordination corresponds to the horizontal axis and the y coordination corresponds to the vertical axis. The origin [0,0] is in the upper-left corner. The z coordination is used for indexing the axial slices. The axial image with $z = 0$ corresponds to the most bottom

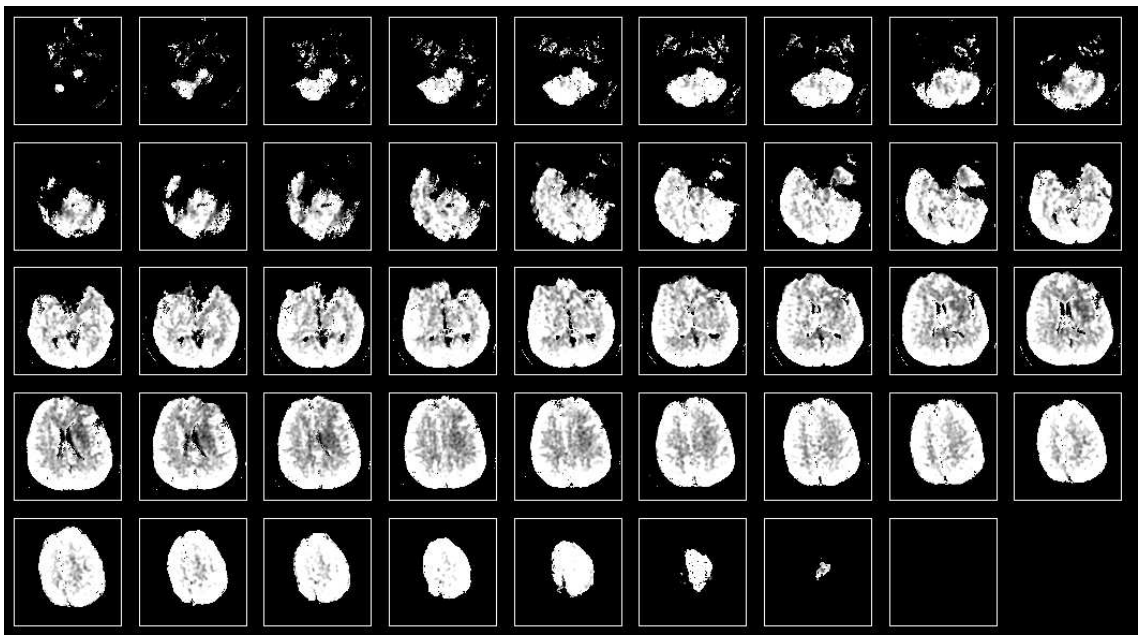

Figure 4.1: Example of serie of 2D axial source images (image generated by [29]).

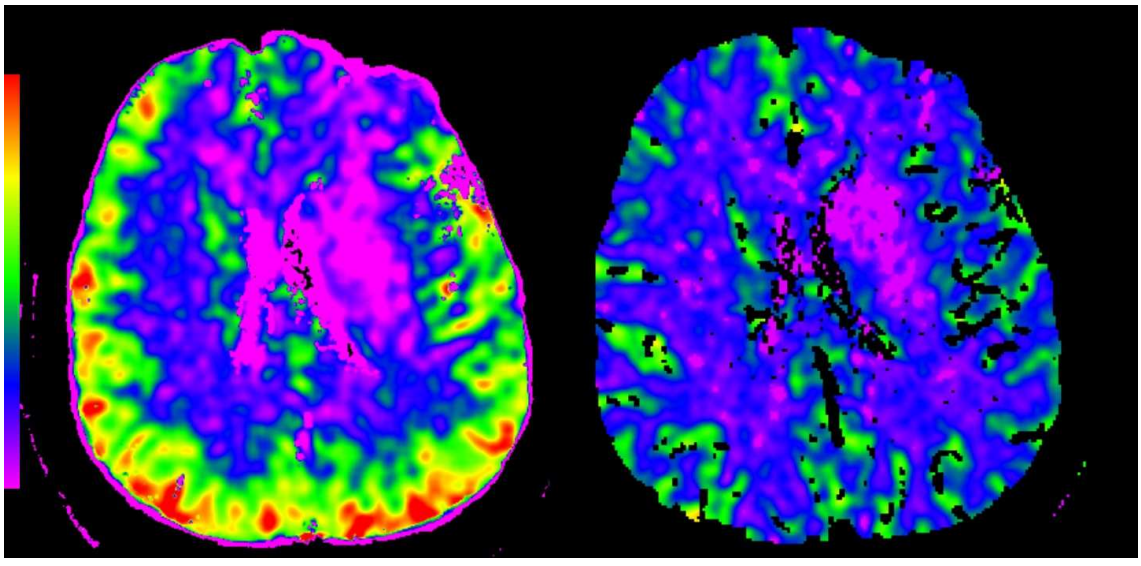

Figure 4.2: PBV (left) and CBV (right) source images displayed in a color scale using windowing technique with the center 6.5 and width 14 ml·100g^{-1}.

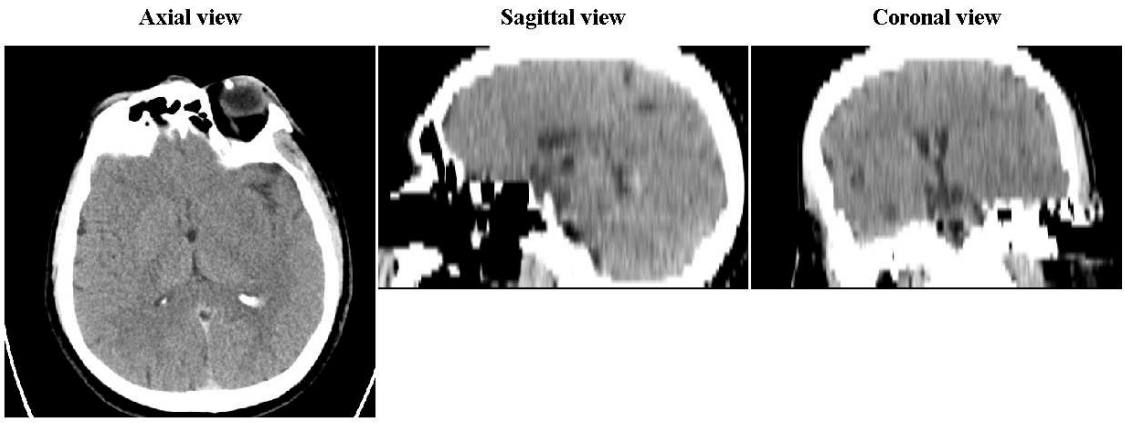

Figure 4.3: Different map views.

Figure 4.4: Axial images according to their z-coordination. From the left z coordiations are: 0, 19, 32, 40.

image of the map. Increasing the z coordination means going up in the map's images towards the top of the head as shown in Figure 4.4.

4.6 PBV and CBV segmentation

PBV and CBV maps are produced by Siemens device which performs segmentation step. At this step only the brain tissue should be preserved and other parts like bones or ears and other objects should be removed. Some other brain structures which are not a brain tissue are segmented in a way that all voxels belonging to these structures are exchanged by value -1024 which is the background value. Further more only in CBV maps there are some anatomical structures replaced by a constant value. Details of mapping between the structures and their constant values were not available. It is available probably in some detailed device documentation which we could not access. On the other hand these constant values are numbers like -500 or -1000 and thus are out of the range of infarction core suspicion. Visualization of the CBV maps device segmentation can be seen in the Figure 4.5.

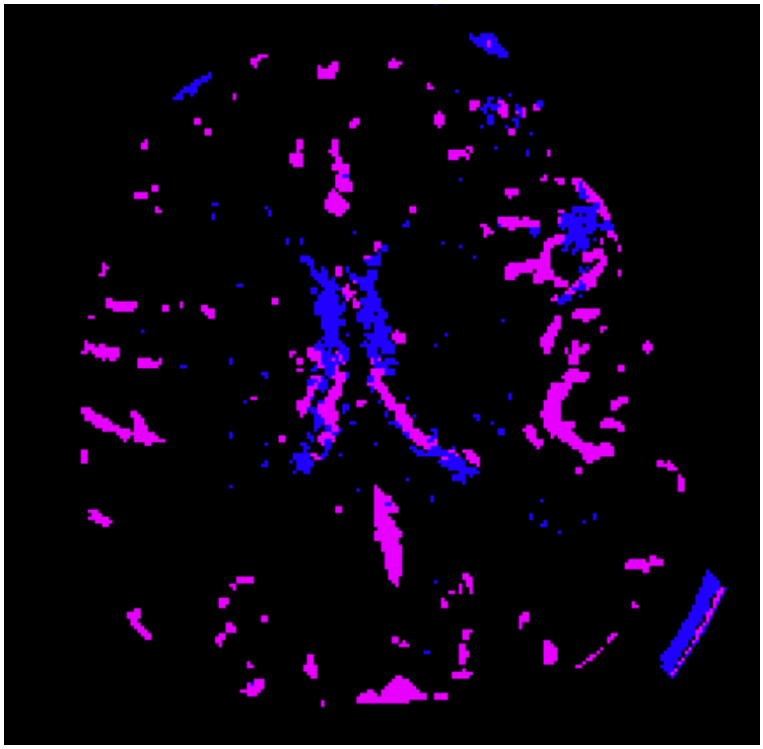

Figure 4.5: Device segmentation in CBV images, blue color corresponds to value -800 and violet color to -1000.

Skull segmentation in PBV images must be considered. PBV images are created by subtraction of NCCT from CTA examination. Mutual registration is performed and then the subtraction on voxel by voxel basis is performed. The borders between brain tissue and skull suffer by partial volume effect and also by fine misalignment of the registration process. This causes subtraction of the voxels with higher density of bones and voxels with lower density of the brain tissue. The difference between these two densities can be significant. The segmentation process does not remove these areas and they are left in the image as shown in the Figure 4.6.

4.7 Typical PBV and CBV histograms

Histogram represents frequencies of values contained in the examination (map). Figure 4.7 shows comparison between the PBV and CBV map histograms. We can see that the PBV histogram is wider than the CBV one. The next observation is that the PBV maps contain negative values while there are no negative values in CBV maps. The only negative values in CBV maps are those used for device segmentation purposes but which are not displayed in the figure since it is out of the used range. Figure 4.8 shows typical CBV histogram focused only to values between 0 and 150 $\mathrm{ml \cdot l^{-1}}$. The CBV map does not contain negative values but the frequency of the value 0 $\mathrm{ml \cdot l^{-1}}$ is considerably increased.

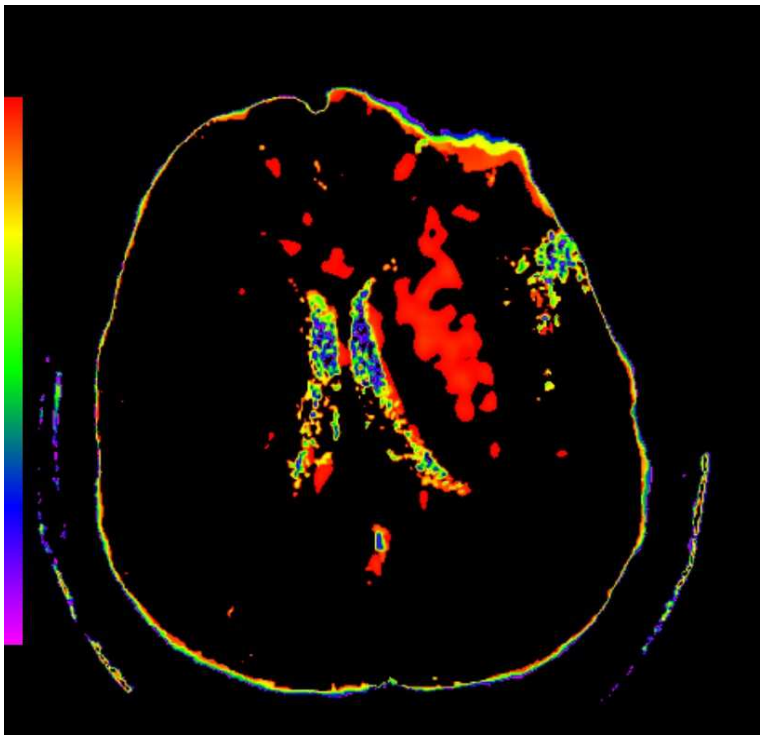

Figure 4.6: Device segmentation in PBV images focused on skull segmentation, depiction of values $[-600; 0]$ in a color scale.

4.8 Infarction core analysis in PBV and CBV images

Figure 4.9 shows the supposed area of infarction in PBV map but only the values in interval from -35 to 0 are shown. The values are in $\mathrm{ml{\cdot}l^{-1}}$ units but at these places it contains negative values. It means that the subtraction process faced to lower density of the CTA examination and higher density of the corresponding voxel in the NCCT image. The negative blood volume is theoretically not possible but the perfused blood volume is influenced also by quantity of the contrast material that reaches the tissue and also by the quality of the registration process and by the influence of the partial volume effect. Here must be considered that the infarction core areas in PBV images may reach also negative values. In the CBV images the lowest stored value corresponds to 0 $\mathrm{ml{\cdot}l^{-1}}$ (excluding the device segmentation constants).

4.9 Maps registration

To simplify methods of future results comparison between different map types, registration process was performed. The registration was performed in the MedInria software using Block Matching Method algorithm [25] with linear interpolation and rigid transformation. Resulting PBV and CBV maps are spatially registered and have common coordination system. Only the registered images were used for the manual tracking by physicians and

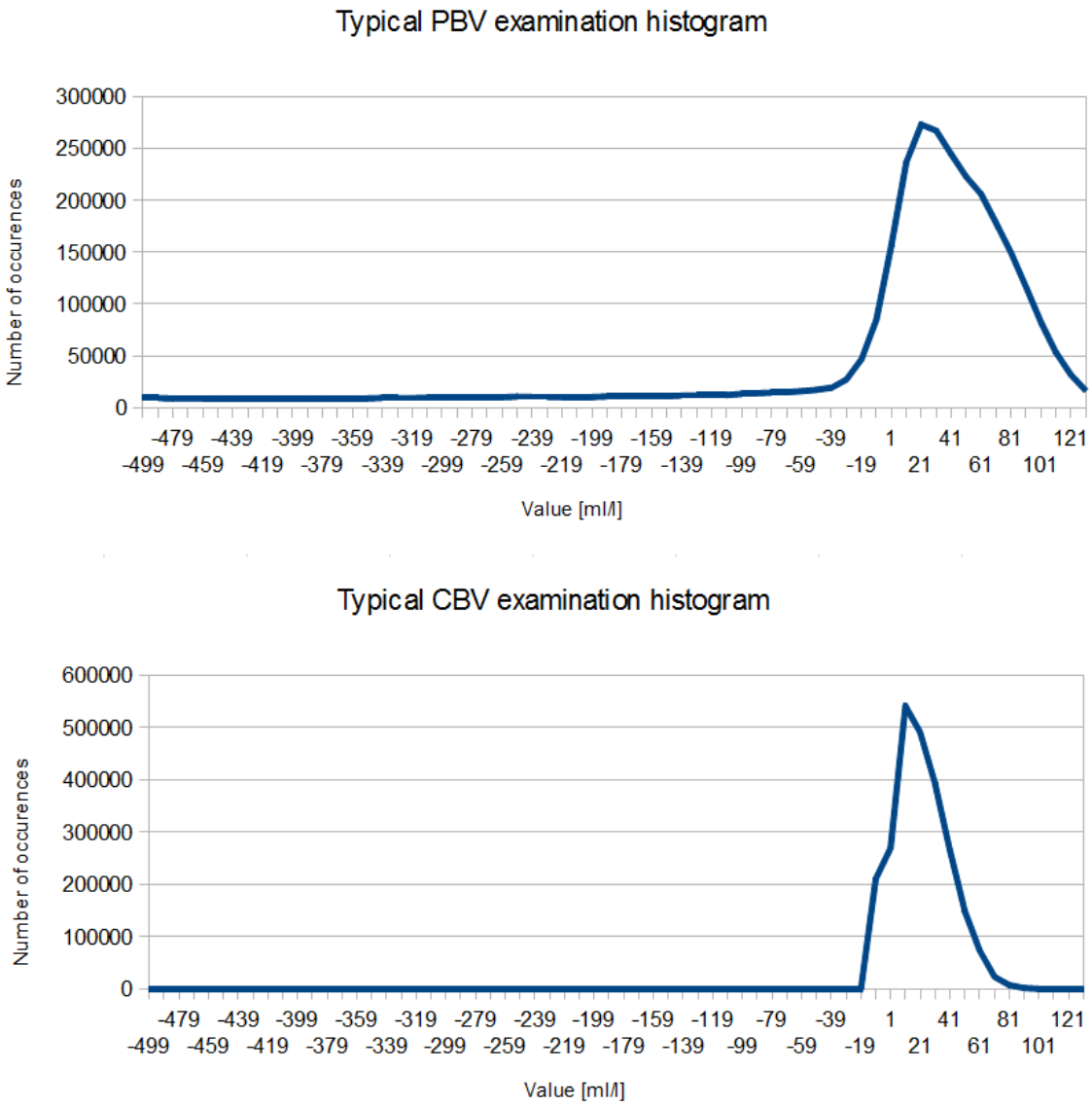

Figure 4.7: Example of typical histograms of PBV (up) and CBV (bottom) maps. Displayed are only values from -499 to 150 $ml \cdot l^{-1}$.

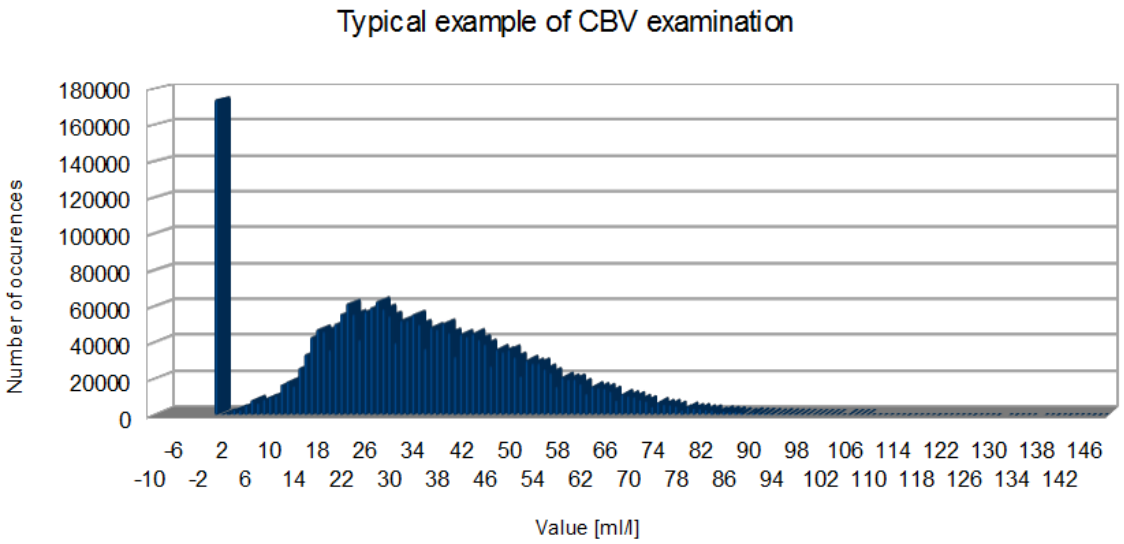

Figure 4.8: Example of typical CBV histogram. Displayed are only values from -10 to 150 $\mathrm{ml \cdot l^{-1}}$.

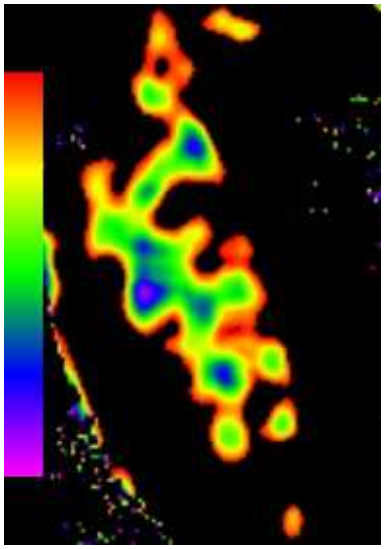

Figure 4.9: Depiction of the supposed area of the infarction core in a PBV image using color scale with values $[-35; 0]$.

also automatically processed by the proposing method. The pixel spacing after registration was in 9 cases 0.3926 mm, in 2 cases 0.3770 mm and in one case 0.4180 mm. Slice thickness was 5 mm with 3 mm image spacing.

4.10 Manual tracking by physicians

As the visual evaluation of the CT examinations depends on experience and can be also subjectively influenced, we decided to ask two physicians for the manual tracking on the same dataset. Thus we have available two individual opinions for each map. The first one "Physician 1" is a radiologist, the second one "Physician 2" is a neurologist. Both were asked by their best opinion to delineate infarction core on the PBV and CBV maps. For the delineating purposes was developed a plugin for Fiji software.

4.10.1 Fiji software

Fiji is an open source image processing project. It is ImageJ software enriched by a set of plugins. It supports a lot of actual formats including DICOM format. Detailed information including download can be found at *http://fiji.sc/*. User can create another plugin which uses the built in image processing functions and also the user can create (or record) macros which automatically process stored commands. The main advantage is that the software is not required to be installed and thus it can be run also on computers with privilege restrictions. The user interface is simple and the main focus is pointed into depiction of the image as you can see in Figure 4.10.

4.10.2 Developed plugin

The developed plugin is placed at the bottom part of the opened examination window. It allows interactive windowing which can be adjusted by mouse or by direct input of the window width and window level settings. The actual mouse position coordinations in the image are displayed in the main window of the Fiji together with the corresponding value of the actual position in the image. For the region of interest selection can be used a brush tool which has a circular shape with adjustable radius. The selection is made by mouse while holding the mouse button. If some selection already exists and the user continues with selecting the selected area can be enlarged or reduced. Moving between all images of the map is made by slider or by mouse wheel. Another possibility of the area selection is based on the windowing technique together with selection of the boundary area where to detect the infarction core. By pressing Delineate the selected area is reduced only to places which have black color so those have the values at the bottom of the current window setting. The described selection is just temporary and must be confirmed.

The button Mark must be pressed to confirm the selected area as necrotic tissue area. It fills the selected area with the values easily detectable by further processing. This

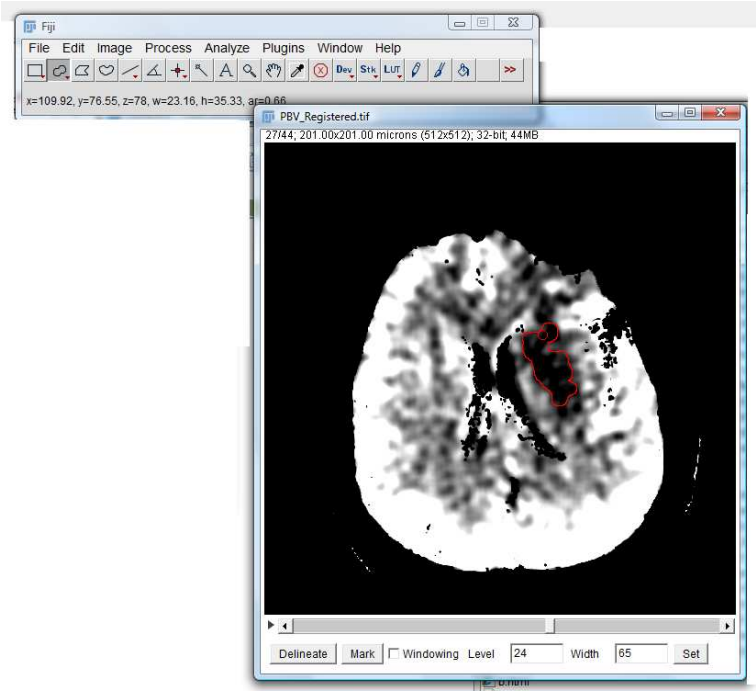

Figure 4.10: Example of manual tracking using the developed Fiji plugin.

filling is made by putting values of +2048 and -2048 which are not present in the original image. These values creates a criss-cross grid of black and white color since it is out of the generally used window and thus are also easily visible for the physicians and are well distinguishable from other tissue. This kind of selection and confirmation must be made on all images containing the infarction core separately while the previous selection is transfered to other images helping to track the intra-image variations.

4.10.3 Mutual comparison between the manual tracking of the physicians

We evaluated match between the two physicians' manual tracking in a Matthews correlation coefficient form. The Matthews correlation coefficient was evaluated for each pair of a map delineations (by Physician1 and Physician2) and finally were these values averaged from all the maps of specific type (CBV, PBV). The physician 2 at one patient did not mark any area meaning no infarction core area in both PBV and CBV maps. This mismatch was not counted into the averaged values and was recorded as a mismatch as shown in Table 4.2.

The example of manual infarction core delineations by both physicians using CBV maps are shown in Figure 4.11 and using PBV maps in figure 4.12.

Map type	**Average Matthews coefficient** [%]	**Mismatch**
PBV	56.90	1/12
CBV	62.09	1/12

Table 4.2: Mutual match evaluation between manual delineations of the infarction core between physicians.

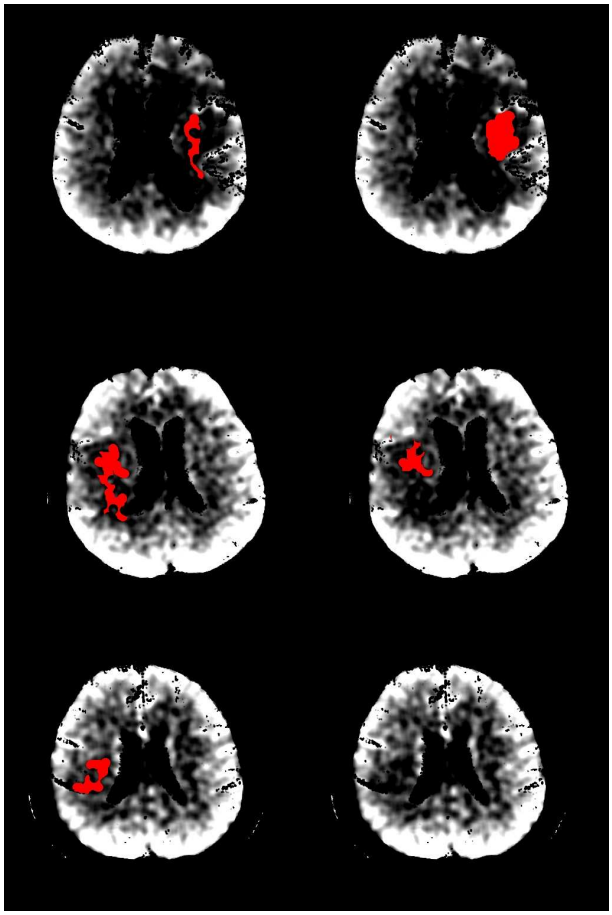

Figure 4.11: Example of different patients' (different rows) manual infarction core delineations (red color) in PBV maps by physician 1 (left column) and physician 2 (right column).

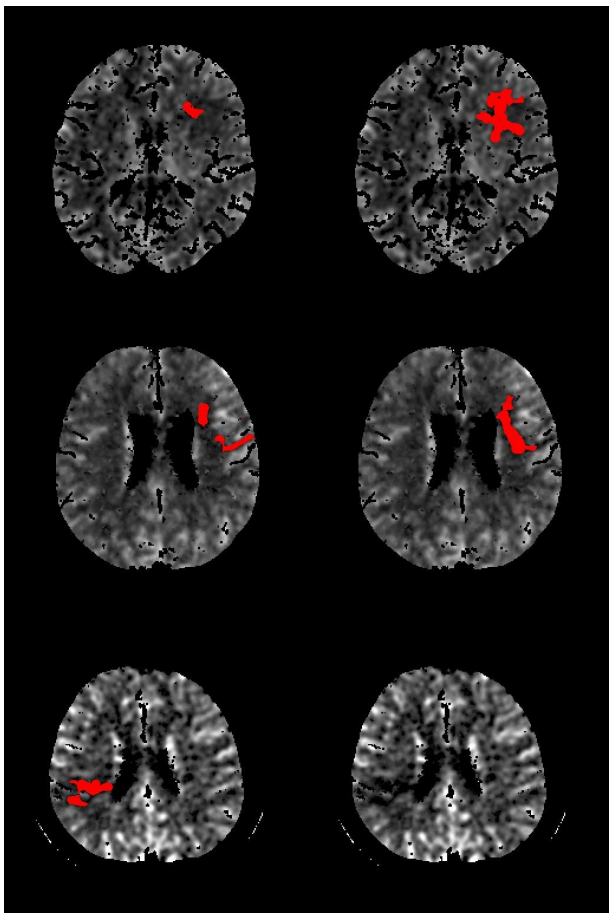

Figure 4.12: Example of different patients' (different rows) manual infarction core delineations (red color) in CBV maps by physician 1 (left column) and physician 2 (right column).

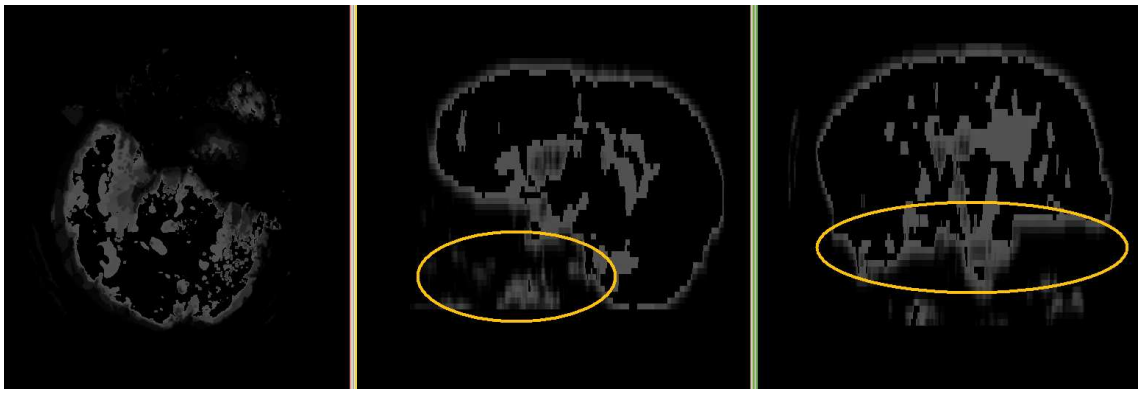

Figure 4.13: Different views of PBV image thresholded by 2 ml·100 g^{-1}. Marked areas show areas with high ratio of false-positive voxels.

4.11 Initial analysis

We used software [21] for material images analysis. One of the presumptions was that the infarction core has very low values. Simple thresholding with the threshold 2 ml·100g^{-1} showed that the CBV and PBV images contain more information than only the infarction core area after the thresholding. We can divide it to:

1. False positive infarction core.
2. Rests of non-ideal segmentation or caused by partial volume effect.

The rests of non-ideal segmentation are well visible in the bottom parts of the maps as shown in Figure 4.13.

Chapter 5

Segmentation Adjustment

5.1 Motivation

This study deals with automated infarction core delineation and uses source images acquired on the CT Somatom Definition instrument. PBV images are provided by the Siemens syngo Neuro PBV software. Despite of the instrument or the software automated segmentation, there still appear non-brain areas which would influence the proposing automated process. Therefore segmentation adjustment step is performed before the infarction core delineation process begins.

5.2 Description

To prepare images for the automated infarction core delineation we process simple but effective segmentation adjustment step. All axial source images are processed one by one and one of them is selected as a divider by Algorithm 5.2.1. Only the images from the top to the divider are further processed and the rest from the divider to the last image are ignored. The example is shown in the Figure 5.1 and the corresponding count of inner voxels C_{in} and count of outter voxels C_{out} of each slice are depicted as a graph with the image index as x-axis and $\frac{C_{in_j}}{C_{out_j}}$ as y-axis. The y-axis is highlighted at position of the divider threshold(for CBV 2.0 and for PBV 1.0). The first image from the left (meaning from the bottom of the head towards the top) with the same or higher value than the divider threshold becomes the divider image. Only the divider image and all the images above it (towards the top of head) are used for the following automated infarction core delineation. The chart for a sample PBV map is shown in Figure 5.2 and for a sample CBV map in Figure 5.3.

Algorithm 5.2.1 Segmentation adjustment

1: **for all** 2D source images S_i of the map X **do**
2: $C_{in_i} \leftarrow$ Count of voxels with value > 0
3: $C_{out_i} \leftarrow$ Count of voxels with value ≤ 0 (ignore outer values -1024).
4: **end for**
5: j $\leftarrow$ 0 - number first image (belonging to the most bottom image)
6: **while** $\frac{C_{in_j}}{C_{out_j}} <$ (2.0 for CBV, 1.0 for PBV) **do**
7: j $\leftarrow$ j + 1 (going up in the direction to the top of the head)
8: **end while**
9: **return** dividerImageIndex $\leftarrow$ j

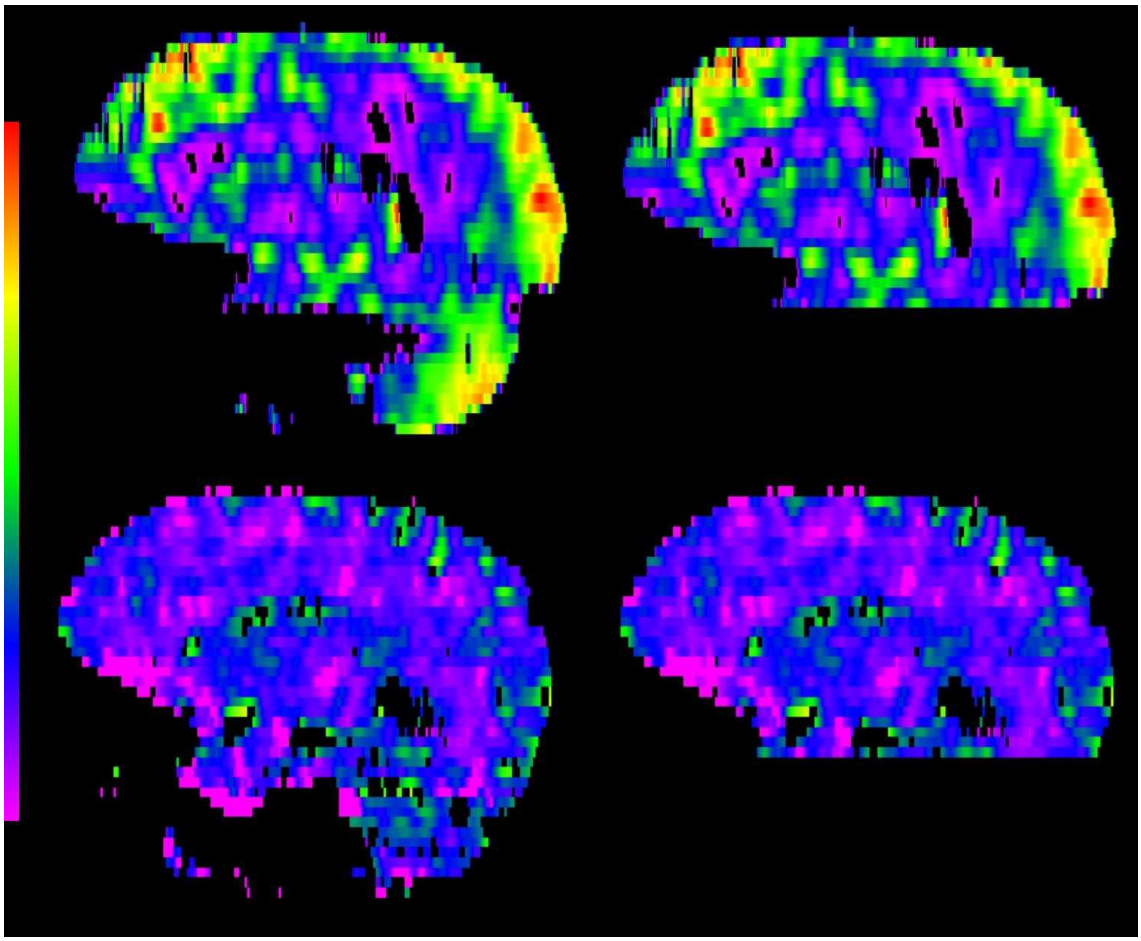

Figure 5.1: Example of PBV (upper image) and CBV (bottom image) segmentation displayed as sagittal views - source images on the left, segmented areas on the right. Only intervals between 0 and 150 ml·l^{-1} are shown using a color scale.

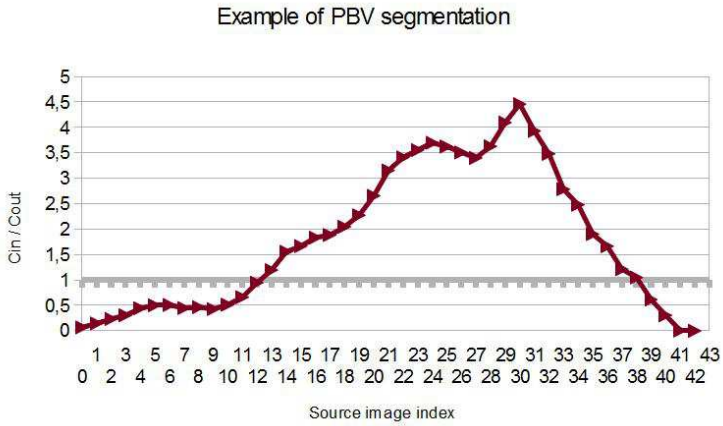

Figure 5.2: PBV segmentation adjustment - values of sample map provided by Algorithm 5.2.1.

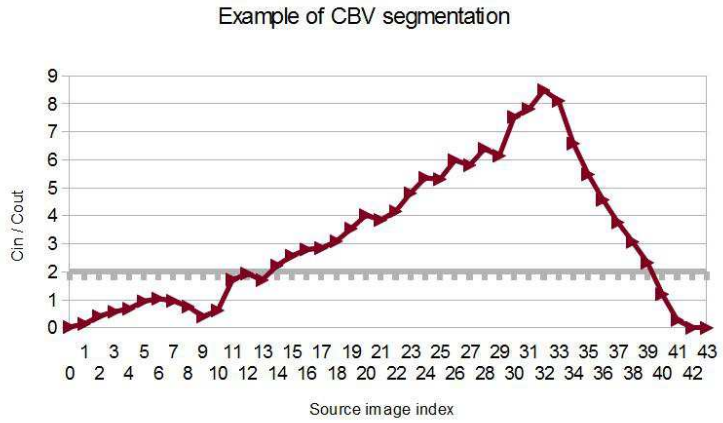

Figure 5.3: CBV segmentation adjustment - values of sample map provided by Algorithm 5.2.1.

Map type	Successful	Percent
PBV	11/12	92%
CBV	12/12	100%

Table 5.1: Successfulness of the segmentation adjustment step in a set of 12 maps per type.

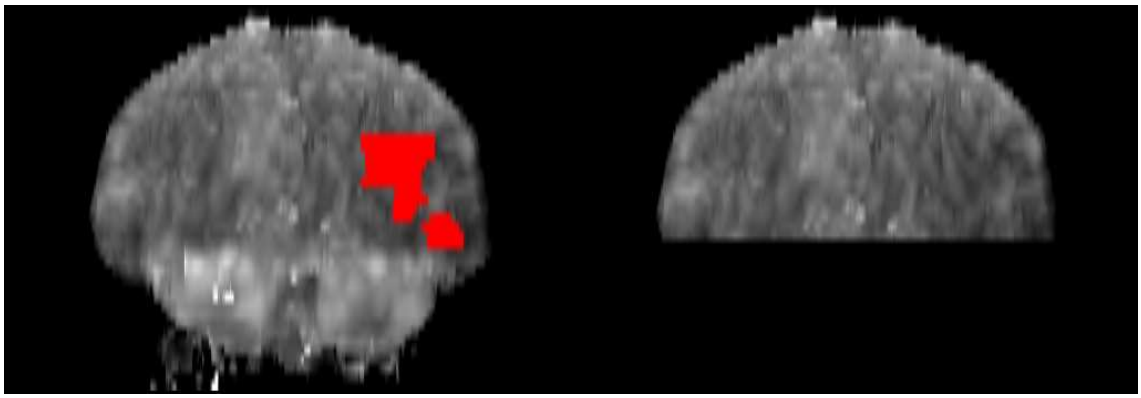

Figure 5.4: Depiction of the one unsuccessful segmentation adjustment clipping also area where the infarction core is present, both PBV maps are presented as maximum intensity projection (MIP) reconstructions, on the left in red color is manually traced infarction core by Physician 2 and on the right is clipped source images used for the automated infarction core detection method.

5.3 Evaluation

We can evaluate segmentation adjustment step according to the physicians' manual infarction core tracking. The source images for the manual tracking are the same as those for the automated detection. We can say that the segmentation adjustment is successful when the whole area of the manually tracked infarction core is not clipped by the adjustment step. It means that we consider the segmentatino adjustment step successful when it leaves enough brain matter to be possible to detect the whole infarction core marked by the physicians. Table 5.1 summarizes the successfulness of the method.

The only one unsuccessful case is in PBV map type and it is shown in Figure 5.4. Here is clipped also one source image which according to Physician 2 also contains infarction core. This one image contains 3.71% of the whole infarction core volume traced by the Physician 2. It means that the proposed automated method, after this one unsuccessful case of the segmentation adjustment step, still can find 96.29% of the supposed infarction core area.

5.4 Discussion

Presented segmentation adjustment step is used in this study. For the wider use it should be more consulted with the physicians whether the clipping process is not too strict limitation of the searched area. In general there can also appear patients with significantly rotated head in the examination which would affect this segmentation adjustment step and thus it would require another pre-processing step dealing with graphical transformation rotating the head into straight position.

The advantage of this segmentation adjustment step is its simplicity and efficiency. For available set of maps it is successful in 23 cases from 24. And the only one unsuccessful case means that the clipped area provides enough brain tissue to find 96.29% of the infarction core voxels manually marked by the physicians. Other cases are large enough to find 100% of the infarction core found by physicians.

Chapter 6

Infarction core detections using the edge preserving smoothing

In this section we will focus to the study [39] where the optimal threshold for infarction core detection was found as 2 ml·100g^{-1}. We will focus to the obtained specificity and we will try to improve the specificity results by our presumptions about the infarction core.

All following methods processes only the area provided by the segmentation adjustment step in order to avoid detections also in bottom parts of the head where the machine segmentation fails and where are present also other non-brain tissue parts and where would be high risk of false indications of the infarction core.

We can try to interpret our presumptions from Section 4.1:

- *The infarction-core is a continuous area* and *there is only one infarction-core area in the brain*: we will look for the largest continuous area satisfying criteria of the thresholding.
- *The values inside the infarction core areas are supposed to be low and it can vary from patient to patient with consideration of the generally accepted threshold 2 ml·100g*$^{-1}$: we will try to find the best thresholds suitable for our material and we can compare it with the supposed value 2 ml·100 g^{-1}.

6.1 Match evaluation

We are about to evaluate matches of different methods according to physicians' manual tracking. But how to evaluate the match? We use labeling of each voxel as TP, FP, TN or FN (see Section 2.7) where the physicians' tracking are taken as a base and each method findings are evaluated according to it. It means when the method voxel is marked as infarction core but the corresponding physician's voxel is not marked as infarction core then the count of FP is increased by 1. If the physician's voxel would be marked also as

infarction core then TP would be increased by 1. Similarly are counted numbers of FN and TN.

6.1.1 Sensitivity, specificity, Matthews correlation coefficient

Using numbers of TP, FP, TN and FN we can evaluate sensitivity (Equation 2.16), specificity (Equation 2.18) and also Matthews correlation coefficient (Equation 2.19). The sensitivity expresses how many percents from all infarction core voxels identified by manual tracking of physician were found by the rated method. The specificity expresses how many percents from all non-infarction core voxels of the manual tracking by physician were correctly marked as non-infarction core by the rated method.

Since the sensitivity and the specificity are two numbers for a quick evaluation of the match there can be used also Matthews correlation coefficient. It can be evaluated by Equation 2.19 and it provides only one number while using all four TP, FP, TN and FN counts.

We want to find the threshold for several methods so we must define how we want to compare different thresholds matches. If we use only the sensitivity we would not be interested in false positives of the rated method. It means that we can reach 100% sensitivity but also in that cases when the method would mark all voxels of the map as infarction core. Such match evaluation would be unusable and this is the reason why the sensitivity itself can not be used for the match evaluation.

Similar case is with the specificity itself. Here we would reach 100% specifity also in cases when the method selects no voxel as infarction core.

The best match evaluation seems to be Matthews correlation coefficient but we must consider FP voxels. Matthews correlation coefficient is such a balance between sensitivity and specificity. But the method application must be considered. False positive voxels can in final increase the detected infarction core volume and thus it can provide information against thrombolytical treatment. The same way low number of TP voxels can lead for underestimation of the real infarction core and thus allowing thrombolytical treatment where it is not desired.

In further results we will present all three values - sensitivity, specificity and Matthews correlation coefficient. Our focus will be tend to specificity since it is the factor having high influence on the detected infarction core volume.

6.1.2 Incorrect detections

We can define incorrect detection (ID) as a no match with the manual tracking. It means the case when the method delineate infarction core area but the physician marked different area with no overlay.

Match type	**Threshold** [$\mathbf{ml \cdot l^{-1}}$]	**Sensitivity** [%]	**Specificity** [%]	**Matthews** [%]	**Incorrect detections**
CBV-Ph1	6	67.28	99.05	30.44	0/12
CBV-Ph1	8	43.50	99.96	57.67	2/12

Table 6.1: Imaginary example of method evaluation records.

6.1.3 Match evaluation model

Our material contains 12 patient having PBV and CBV maps and also for both types we have manual infarction core tracking by 2 physicians. We can label different match types as:

- CBV-Ph1: Automated method on CBV map versus Physician 1.
- CBV-Ph2: Automated method on CBV map versus Physician 2.
- PBV-Ph1: Automated method on PBV map versus Physician 1.
- PBV-Ph2: Automated method on PBV map versus Physician 2.

Each match type can have own best threshold. We used a range of thresholds from which we found the optimal one. Each threshold value was evaluated on all match types separately and always on all 12 patients' maps. We evaluated summary sensitivity, specificity and Matthews correlation coefficient values from the 12 patients as an average values from the 12 sensitivities, 12 specificities and 12 Matthews correlation coefficients. If there was an incorrect detection then the corresponding sensitivity, specificity and Matthews correlation coefficient were not used for the summary averaging and instead of it the count of incorrect detections was increased.

Example of the method evaluation description is shown in Table 6.1.

6.1.4 Specificity expectations

Physicians and also the automated methods have available PBV and CBV maps having dimensions 512x512 containing 44 images. Lets take as an example average size of infarction core by Physician 1 on PBV maps. The average infarction core has 28603 voxels. It means that in average 11505733 voxels are non-infarction core. Specificity is 100% when all of these 11505733 voxels are marked by automated method also as non-infarction core. This would be an ideal case but in real we will face to worse specificity. Lets assumes that the automated method selected 3 times larger infarction core area but fully overlaying the manually marked one. Now the specificity is:

$$\text{specificity} = \frac{TN}{TN + FP} = \frac{512 \cdot 512 \cdot 44 - 3 \cdot 28603}{512 \cdot 512 \cdot 44 - 3 \cdot 28603 + 2 \cdot 28603} = 0.995 \tag{6.1}$$

Specificity corresponds to ability of the automated method to mark non-infarction core as non-infarction according to the manual tracking by physicians. Even if the automated method mark 3 times larger area than the physician, the specificity is still 99.5%. It is because the huge number of the whole map voxels. If the area would not be 3 times larger but only 2 times larger we get the specificity 99.75% and if the area would be only half larger than by physician the specificity would be 99.88%.

At this example we showed that the values of the specificity are supposed to be very high also in bad match cases and that the attention should be focused on a comparison of specificities reaching almost 100%.

6.2 Edge preserving filtering followed by thresholding

Study [39] found the best threshold value at 2 ml·100 g^{-1} (21 ml·l^{-1}). Now we will reproduce the procedure of [39] on our dataset. The difference will be that we use the whole brain coverage while [39] is limited to 4x10 mm. We had available slices of 5 mm thickness with 3 mm image spacing. We used meaning of 3 slices to get an image covering area of 11 mm. Using these slices we performed the edge preserving smoothing. Details of the used edge preserving smoothing in [39] are not described. We used Curvature Anisotropic Diffusion smoothing (Section 2.5.4) with the usually used parameters for 3D medical images from [18]. It means:

- Time step: 0.0625
- Iterations: 5
- Conductance: 3

Using the smoothed images we can perform thresholding to obtain the ROC curves. We will use exactly the same value ranges as in [39]. It means from 0.5 (5.25) to 3.5 (36.75) ml·100 g^{-1} (ml·l^{-1}) with increment 0.3 ml·100 g^{-1} (3.15 ml·l^{-1}).

6.2.1 Results and discussion

This method is an analogy to study [39] and thus we evaluated also the optimal thresholds (Table 6.2.1). We can see that we received almost the same values as presumed 2 ml·100 g^{-1} by [39]. Corresponding specificities (lowest was 94.9389%) were even better than in study [39] where we can assess from the study ROC graph of the group of patients with admission diffusion-weighted imaging (DWI) as 80% with 90% of sensitivity. Our

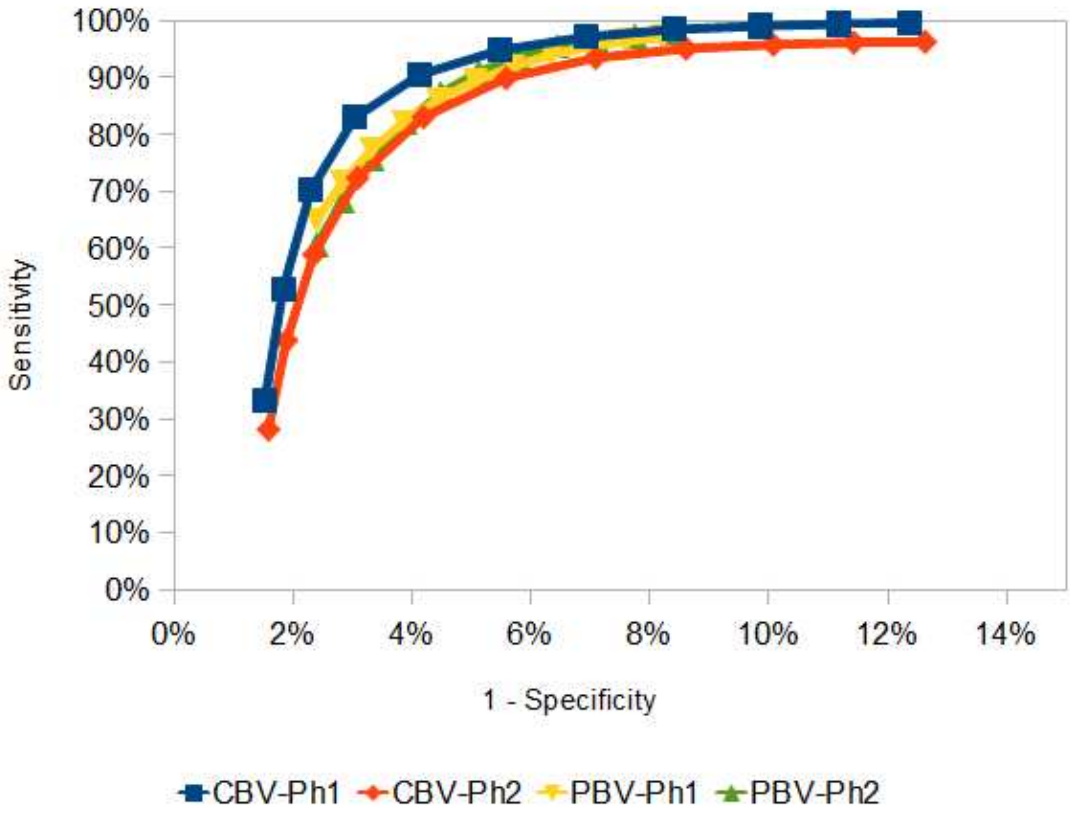

Figure 6.1: ROC curves provided by edge preserving smoothing performed before thresholding method using interval from 0.5 to 3.5 ml·100 g^{-1} with 1 ml·100 g^{-1} (analogy to study [39]).

Type	Threshold [ml·100 g^{-1}] (ml·l^{-1})	Sensit.[%]	Specif.[%]	Matthews [%]
PBV-Ph1	2.0 (21.00)	89.39	94.9389	19.19
PBV-Ph2	1.7 (17.85)	87.20	95.5162	23.22
CBV-Ph1	1.7 (17.85)	90.45	95.8762	20.14
CBV-Ph2	1.7 (17.85)	83.05	95.8020	22.58

Table 6.2: Optimal threshold values for automated infarction core detection by thresholding method with edge preserving smoothing

Type	Threshold [ml·100 g^{-1}] (ml·l^{-1})	Sensit.[%]	Specif.[%]	Matthews [%]
PBV-Ph1	0.5 (5.25)	64.99	97.6009	18.18
PBV-Ph2	0.5 (5.25)	60.54	97.6037	20.07
CBV-Ph1	0.5 (5.25)	33.12	98.4730	14.20
CBV-Ph2	0.5 (5.25)	28.14	98.4081	13.87

Table 6.3: Best specificity threshold values for automated infarction core detection by thresholding method with edge preserving smoothing

higher specificity is provided by the larger coverage and thus by the higher number of true negative voxels.

Our focus is given to the specificity which using the optimal values is still relatively low according to our expectations (Section 6.1.4). The best specificities are reached for the lowest tested threshold values 0.5 ml·100 g^{-1} (5.25 ml·l^{-1}) where the average specificity values according to the both physicians' manual delineations are 97.6023% for PBV and 98.4406% for CBV maps. Figure illustrating behavior of different thresholds can be seen in Figure 6.2.

6.3 Edge preserving filtering followed by thresholding and selection of the largest continuous area

If we apply the presumption that the infarction core is the largest continuous area then we can expect higher specificity because we can discard all detected areas except the largest one leading to lower number of false positives. We will use the same method as in Section 6.2) with the same edge preserving smoothing and the same thresholding using thresholds from 0.5 to 3.5 ml·100 g^{-1} with increment 0.3 ml·100 g^{-1}. The difference is that after the thresholding only the largest continuous area (in the sense of 6-neighborhood) is marked as an infarction core. All other areas are discarded and are supposed to contain normal tissue even it satisfies the threshold criteria.

6.3.1 Results

The best specificity results can be found in Table 6.4 and in all cases the best specificity is reached for the lowest tested threshold value 0.5 ml·100 g^{-1}. We can see that the best PBV specificities (in average to both physicians 98.6709%) are still very low while the CBV best specificities (in average 99.9766%) are already almost ideal. The selection of the largest

continuous area as infarction core brings the risk of possible incorrect detections (Section 6.1.2). If we focus on the count of the incorrect detections and corresponding the highest specificity we get results shown in Table 6.4. We can see that the number of incorrect detections decreases with increasing threshold. It is because the found areas satisfying the threshold grows with the threshold and it can also merge together as you can see also in Figure 6.2.

We can see that PBV results are still not good enough in the specificity but in the case of CBV we can discuss about the optimal threshold for our material. The best specificity (average 99.9766%) may be too strict, it makes also the count of incorrect detections higher. As optimal threshold for CBV could be used in case of CBV-Ph1 threshold 0.8 ml·100 g^{-1} (8.4 ml·l^{-1}) with specificity 99.9148%, sensitivity 54.86% and count of incorrect matches 2/12. In the case of CBV-Ph2 we can choose the same threshold as optimal with specificity 99.9215%, sensitivity 49.38% and count of incorrect detections 3/12.

If we look in detail into two incorrect detections of CBV-Ph1 map with threshold 0.8 ml·100 g^{-1} we can see that the incorrect detections are caused by presence of different larger continuous area which also satisfies the threshold criteria (Figure 6.3). The area marked by the physician would need higher threshold to be more compact but with the higher threshold it would grow also the incorrectly marked area.

6.4 Discussion

Study [39] balances the sensitivity and specificity values only using the thresholding technique. If we focus in study [39] to group of patients with admission diffusion-weighted imaging (DWI) we can see that the optimal threshold was found as 2.0 $ml/100\ g$ (21 ml·l^{-1}). From the study figure containing corresponding ROC graph we can assess the CBV threshold sensitivity as 90% and specificity as 80%. The total number of used voxels was 5911234. Even if we consider the fact that we use the whole brain coverage against 40 mm used by the study, we can see that the specificity 80% is relatively low. We can expect that such specificity is provided because high number of FP voxels which also means that the threshold condition is satisfied for higher number of voxels than marked in the pattern. In other word we can find values satisfying the threshold also in other places (mostly in white brain matter) than only in the real infarction core.

The step of selection as infarction core only the largest continuous area satisfying the threshold criteria improved specificity but only in case of CBV maps we determined optimal threshold as 0.8 ml·100 g^{-1} with corresponding specificity in average to both physicians 99.9182%. With higher thresholds there appear such number of FP voxels that the specificity decreases. The selection of the largest continuous area focuses the detected infarction core only to the place where it was marked also by physicians but with higher thresholds the detected area is larger - floods the neighborhood or connects with other low valued areas which decreases the specificity.

Match type	**Threshold** [**ml·100 g^{-1}**] (**ml·l^{-1}**)	**Sensitivity** [%]	**Specificity** [%]	**Matthews** [%]	**Incorrect detections**
PBV-Ph1	1.10 (11.55)	76.38	98.0196	29.96	0/12
PBV-Ph1	0.80 (8.40)	77.11	98.4279	33.91	1/12
PBV-Ph1	0.50 (5.25)	76.41	98.6447	35.18	3/12
PBV-Ph2	1.10 (11.55)	74.42	98.0206	34.28	1/12
PBV-Ph2	0.80 (8.40)	73.92	98.4366	38.47	2/12
PBV-Ph2	0.50 (5.25)	70.83	98.6970	37.15	3/12
CBV-Ph1	2.00 (21.00)	94.24	96.5523	22.54	0/12
CBV-Ph1	1.70 (17.85)	89.45	97.8927	29.01	1/12
CBV-Ph1	0.80 (8.40)	54.86	99.9148	59.42	2/12
CBV-Ph1	0.50 (5.25)	37.34	99.9771	53.88	3/12
CBV-Ph2	2.00 (21.00)	89.21	96.5185	26.09	1/12
CBV-Ph2	1.70 (17.85)	83.45	97.8117	31.07	2/12
CBV-Ph2	0.80 (8.40)	49.38	99.9216	58.68	3/12
CBV-Ph2	0.50 (5.25)	34.78	99.9760	52.62	4/12

Table 6.4: Results of the edge preserving smoothing with thresholding and selecting the largest continuous area. Each row corresponds to best specificity results corresponding to the numbers of incorrect detections (up to 4 where available). Used thresholds were between 0.5 and 3.5 ml·100 g^{-1} with 0.3 ml·100 g^{-1} increment.

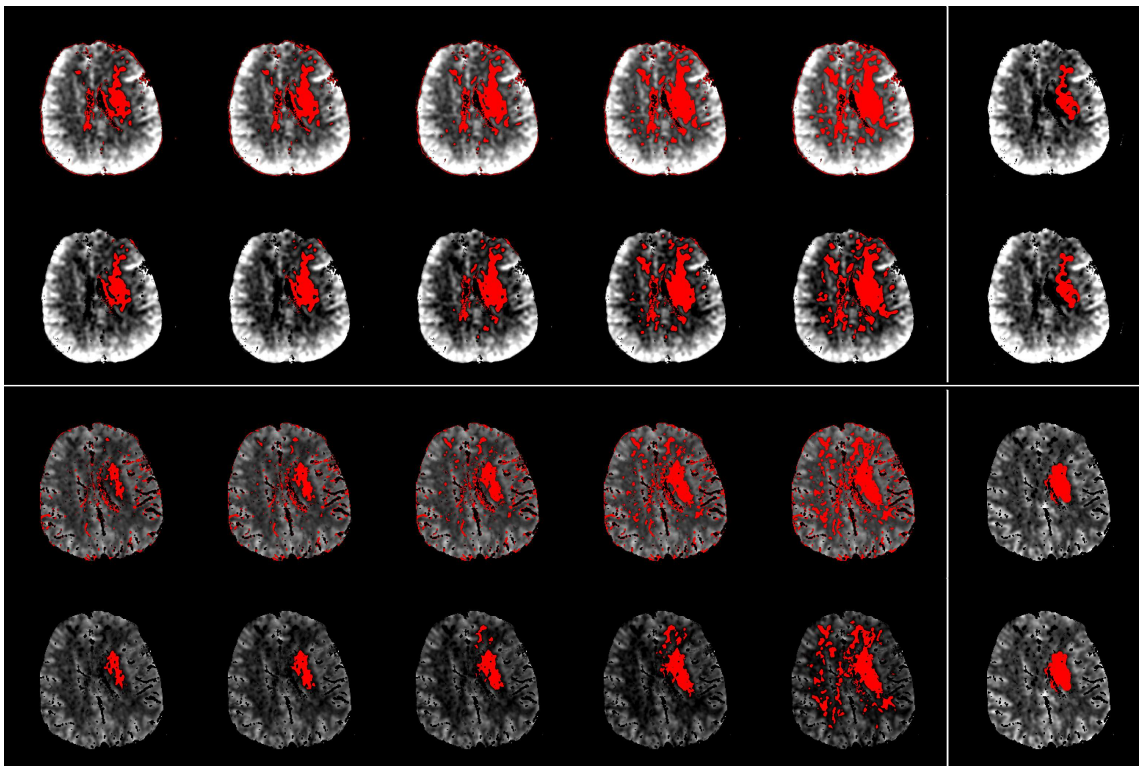

Figure 6.2: Example of infarction core detections (red color) using different threshold values. Upper part shows CBV-Ph1 match and bottom PBV-Ph1 match. In each area the first row means edge preserving smoothing with following thresholding while the second row in additional considers only the largest continuous area as infarction core. Columns express different thresholds. From left 5.25, 8.40, 11.55, 14.70, 17.85 $\mathrm{ml \cdot l^{-1}}$. The last column expresses corresponding manual delineations by physician 1.

Match type	**Threshold** [**ml·100 g^{-1}**] (**ml·l^{-1}**)	**Sensitivity** [%]	**Specificity** [%]	**Matthews** [%]	**Incorrect detections**
CBV-Ph1	0.80 (8.40)	54.86	99.9148	59.42	2/12
CBV-Ph2	0.80 (8.40)	49.38	99.9216	58.68	3/12

Table 6.5: Optimal thresholds for the automated infarction core detection in CBV maps using edge preserving smoothing method with selection of the largest continuous area as infarction core (described in Section 6.3).

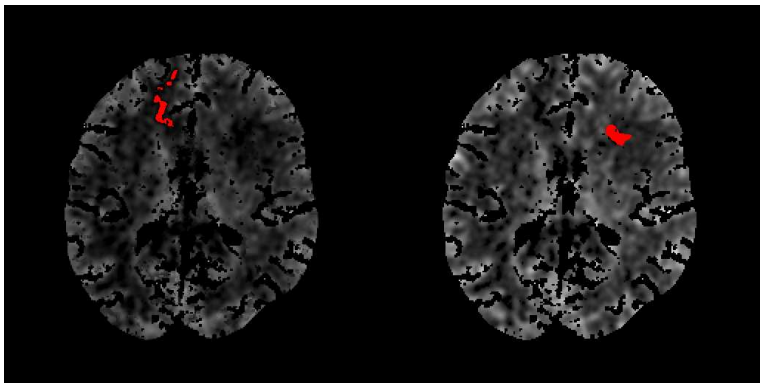

Figure 6.3: Example of incorrect detection of infarction core findings (red color) on CBV map using the edge preserving smoothing with selection of the largest continuous area on the left (details in Section 6.3) and manual delineation by Physician 1 on the right.

In case of PBV we found (in both methods) the best specificity threshold 0.5 ml·l^{-1} which was the lowest tested value in order to reproduce the procedure used by study [39]. These low values could be explained by steep changes in stored values. For example the values inside the infarction core can be negative while the lower limit is not specified. Automated segmentation by instrument was perfect to segment high density values of bones but in case of chambers there still persist values which rapidly changes from positive to high negative values. Such rapid changes are also present at the boundaries between brain tissue and segmented bones. Edge preserving filtering in this case is not able to fully emphasize and separate the infarction core from its neighborhood and it is the reason why following thresholding still face to flooding larger areas or why the largest continuous area is often not the one marked by the physicians.

Chapter 7

Proposed method

7.1 Introduction

We presented that automated infarction core delineation based on edge preserving smoothing and selecting the largest continuous area (as described in Section 6.3) has very good results on CBV maps but results on PBV maps suffer by low specificity. The proposing method is designed to reach higher specificity in PBV maps. From previous sections we can summarize that PBV maps contain steep changes of intensities at borders of brain tissue and tissue of other types (rests of automated segmentation of bones and chambers). Also we noticed that the infarction core values can be also negative and the lowest value is not defined and can vary from patient to patient. Edge preserving smoothing with the traditional settings (details in Section 6.3) does not differentiate enough the infarction core from the neighborhood to use the previously described method and obtain similar specificity as in case of CBV maps.

7.2 Inspiration

If we want to reach higher specificity and higher number of correct matches we must reach better differentiation between the infarction core and its neighborhood. Our approach was inspired by study [36]. This study is concerned in automated infarction core delineation in the NCCT examinations and it is based on an adaptive image by image thresholding. For each image separately is found a threshold value and standard deviations range and all voxels of the current image satisfying these conditions are suspicious to be the infarction core. Finally the reconstruction algorithm connects adjacent groups of suspicious voxel through all images and the largest one is marked as infarction core. The features of the NCCT examinations are different from PBV maps. Values acquired in NCCT examination correspond to real property of the tissue and are measured in Hounsfield's unit. The values in PBV maps are proportional to a subtraction of Hounsfield's units with and without contrast material and are expressed in $\mathrm{ml \cdot l^{-1}}$ units.

7.3 Method description

Our aim is to differentiate the infarction core area enough for its extraction. In opposite of CBV maps the PBV maps seem to be influenced by the partial volume effect caused by usage of different slice thickness of the source NCCT and CTA examinations. Infarction core areas but also some other parts like segmented skull or areas around the cerebral ventricles also contain steep changes of values and overall the PBV values seem to be more patient depended probably because of the CTA examination where the details of the contrast medium application in combination with individual person can influence the acquired values.

We believe that simple meaning corresponding to the nearest neighborhood can provide enough smoothing for local areas. We also believe that this kind of meaning in combination with standard deviations of the nearest neighborhood and adaptive selection of the threshold value can provide enough information for the infarction core extraction.

Proposing method can be described by the flowchart in Figure 7.1.

7.3.1 Mean filtering

Mean filtering is a noise reduction method based on averaging values of the nearest neighborhood. The dimensions of the neighborhood is application depended. This kind of filtering we used in the maps in order to differentiate the infarction core from its neighborhood and the best size of the neighborhood is to be found by optimization process described in Section 8. The used area for the mean filtering has rectangular shape and for the averaging purposes were used only voxels with values higher than -500. This value -500 was chosen to be low enough to cover all infarction core values and high enough for use also in CBV maps where by value -500 are already marked anatomical structures (Section 4.6). The mean filtering is evaluated from source images but only for as many images as provided by the segmentation adjustment step. Meaning is evaluated on a voxel by voxel basis and for one voxel the Equation 7.1 is used where X, Y and Z area dimensions of the used rectangular neighborhood, i, j, k are coordinations of the currently processed voxel. For the summarization are used only voxels with values higher than -500 and their count inside the used neighborhood is used for division as $Count\ of\ used\ voxels$. All resulting values are stored into newly created image (of the same size as input map) called *MeanImage* at coordinations i, j, k.

$$MeanImage_{i,j,k} = \frac{\sum_{x=-X}^{X} \sum_{y=-Y}^{Y} \sum_{z=-Z}^{Z} SourceImage_{i+x,j+y,k+z}^{>-500}}{Count\ of\ used\ voxels} \tag{7.1}$$

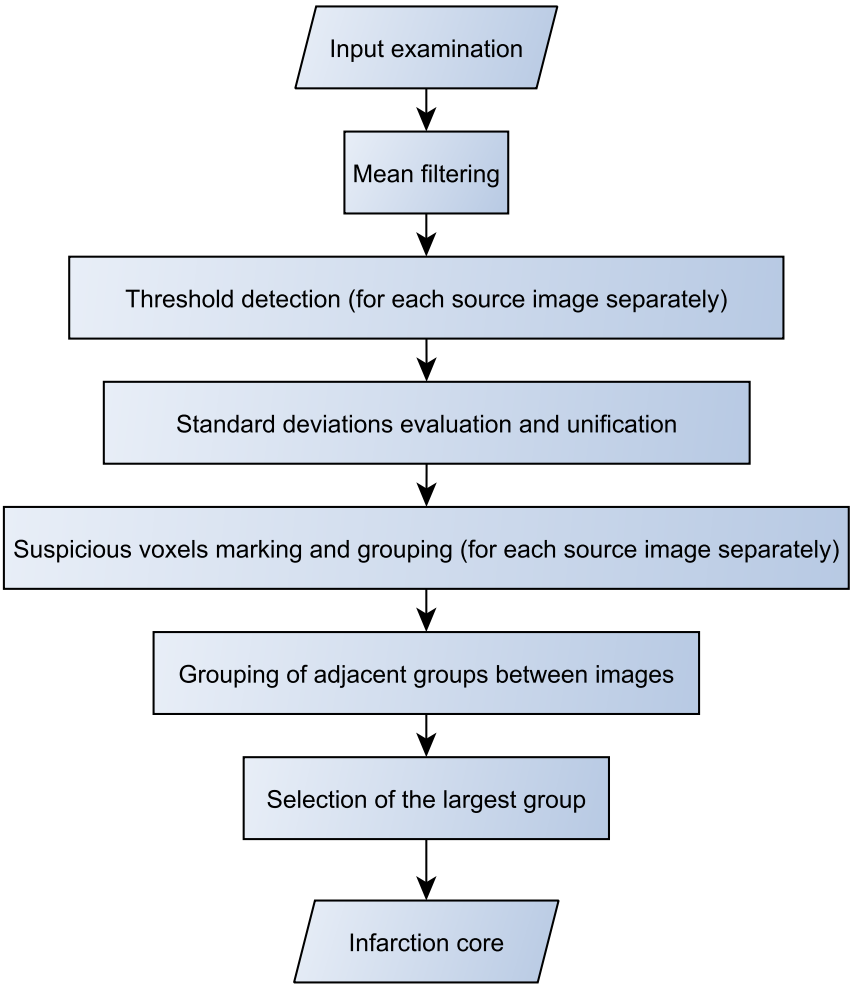

Figure 7.1: Flowchart of the proposed method.

7.3.2 Threshold detection

We believe that the threshold can differ from patient to patient and thus we want to find it from histogram of the image instead of using one global threshold value. We search for the best threshold for each axial image separately and only for as many images as provided by the segmentation adjustment step. For each axial image of *MeanImage* we compute histogram and the value with the maximal frequency V_{max} is localized. We make a distribution function of frequencies for values from -499 to V_{max} referring as $D_{V_{max}}(v)$. It means that $D_{V_{max}}(-499) = 0$ and $D_{V_{max}}(V_{max}) = 1$. The image threshold is computed as $p\%$ quantile of the $D_{V_{max}}$ (with minimum value limitation -20) and lets denote it as $ThRaw_i$. The p is common for whole map and the optimal value is again found by optimization process in Section 8. If the segmentation adjustment step provided $C + 1$ images to be processed then we get thresholds $ThRaw_i$ for i from 0 to C. The last thresholds operation is their approximation by polynomial of k-th degree. The optimal k is again found by the optimization process in Section 8. The threshold detection process results in adjusted values Th_i for i from 0 to C.

7.3.3 Standard deviations evaluation

We have denoised image $MeanImage$ and thresholds for all images Th_k. For further purposes we define $MIThSubtracted$ (Mean Image Threshold Subtracted) which is subtraction of threshold values Th_k from $MeanImage$. Such image contains values which represent differences from the local threshold Th_k.

$$MIThSubtracted_{i,j,k} = MeanImg_{i,j,k} - Th_k \tag{7.2}$$

Now we compute another image $StDev$ which contains the standard deviations of the same neighborhood as used for construction of the $MeanImage$.

$$StDev_{i,j,k} = \sqrt{\frac{\sum_{x=-X}^{X}\sum_{y=-Y}^{Y}\sum_{z=-Z}^{Z}((SourceImg^{>-500}_{i+x,j+y,k+z} - Th_{k+z}) - MIThSubtracted_{i,j,k})^2}{Count\ of\ used\ voxels}} \tag{7.3}$$

When the $Stdev$ for coordinations i, j, k is being computed its neighborhood is processed. Local differences from the i, j, k are symbolized by x, y, z. Every voxel of this neighborhood is taken from the source image and the change from the current image threshold with index $k + z$ is evaluated: $(SourceImg^{>-500}_{i+x,j+y,k+z} - Th_{k+z})$ and the $MIThSubtracted$ (Mean Image Subtracted Threshold) value with coordinations i, j, k is subtracted.

There are again processed only voxels having value above -500 in the source image and their count is remembered for the final division in the Equation 7.3.

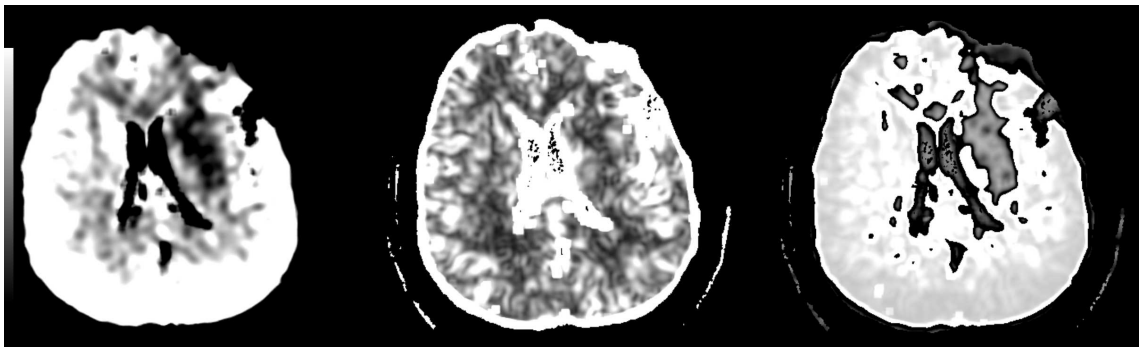

Figure 7.2: Depiction of the $MIThSubtracted$ (left), $StDev$ (middle) and $StDevUnified$ (right) images of the PBV map using neighborhood 4x4x1 threshold 0.6 and the degree 1 for approximating thresholds. Images are displayed using windowing technique with window settings (Center, Width): left (0, 50), middle (10, 20) and right (0, 3).

7.3.4 Standard deviations unification

Previous sections described the process of construction of the $MeanImage$ containing the mean values evaluated from the nearest neighborhood. After finding of the thresholds for each image separately, these thresholds were subtracted from corresponding $MeanImage$ and were stored in $MIThSubtracted$.

Next we measured changes from local image threshold in the nearest neighborhood area of the source image and we evaluated standard deviation according to the mean values stored in $MIThSubtracted$.

The aim is to accept local threshold of each image and evaluate values using the nearest neighborhood and express them in relation to the local image threshold. If we want to describe a voxel in just single number we must use some kind of unification. We have standard deviation and a mean value. If we divide the standard deviation by the mean value (using Equation 7.4) we get the standard deviation connected with the unit value (1 ml·l^{-1}). In the case of possible dividing by zero we just put $StDevUnified_{i,j,k} = 0$.

$$StDevUnified_{i,j,k} = \frac{StDev_{i,j,k}}{MIThSubtracted_{i,j,k}} \tag{7.4}$$

Due to the expressing standard deviations and the mean values as a relation to the local thresholds the resulting value $StDevUnified_{i,j,k}$ preserves the relation to the local image threshold. If the value $StDevUnified_{i,j,k}$ is negative then the $MeanImage_{i,j,k}$ is also below the local image threshold. The positive value of Equation 7.4 also means higher value than the local image threshold. The amplitude (or the absolute value) expresses the ratio of the value changes in the nearest neighborhood. We can expect that very steep changes will have very high values and also little changes will be characterized by low values.

7.3.5 Suspicious voxels marking

Voxels which satisfy certain condition are marked as suspicious. All adjacent suspicious voxels are grouped and finally the largest group is considered to be an infarction core group containing voxels of the infarction core. The suspicious voxels are suspicious to be an infarction core.

The conditions which voxel with index i, j, k must satisfy to be considered as suspicious are:

- -1.0 $\leq StDevUnified_{i,j,k} \leq 0$
- $StDev_{i,j,k} < 50$

These values were found by analysis of the corresponding images $StDevUnified_{i,j,k}$ and $StDev_{i,j,k}$. The unified values of the $StDevUnified_{i,j,k}$ corresponding to the infarction core must be negative (or zero) in order to be below the threshold. The -1.0 value is satisfied when the local standard deviation is maximally the same as the mean value. It means the linear dependency between the standard deviation value ($StDev$) and the mean value $MIThSubtracted$. The second condition just expresses that the standard deviation is not allowed to be too high. values above the 50 are present in the areas of the cerebral ventricles in the PBV maps and also at the borders of brain tissue and segmented bones.

7.3.6 Suspicious voxels grouping

All axial images of one map are processed separately. Once the suspicious voxel is found then new group is created and the voxel is added. The 4-nearest neighborhood (we process the 2D axial image) of the voxel is browsed for finding another suspicious voxel which would be added also into the same group. We continue recursively this way since no other new voxel in the 4-nearest neighborhood is found.

For each group G are evaluated following values:

- $G^{Average}$ - Average value [ml·l^{-1}] of source image voxels evaluated from all voxels in the group.
- G^{Size} - Dimensions of the group. G_X^{Size} = number of voxels between the most left and the most right voxel and G_Y^{Size} = the number of voxels between the most top voxel and the most bottom voxel of the group.
- G^{Center} - Center of the group. The x and y average coordination of all group voxels (G_X^{Center}, G_Y^{Center}).

Example of the grouping is shown in Figure 7.3.

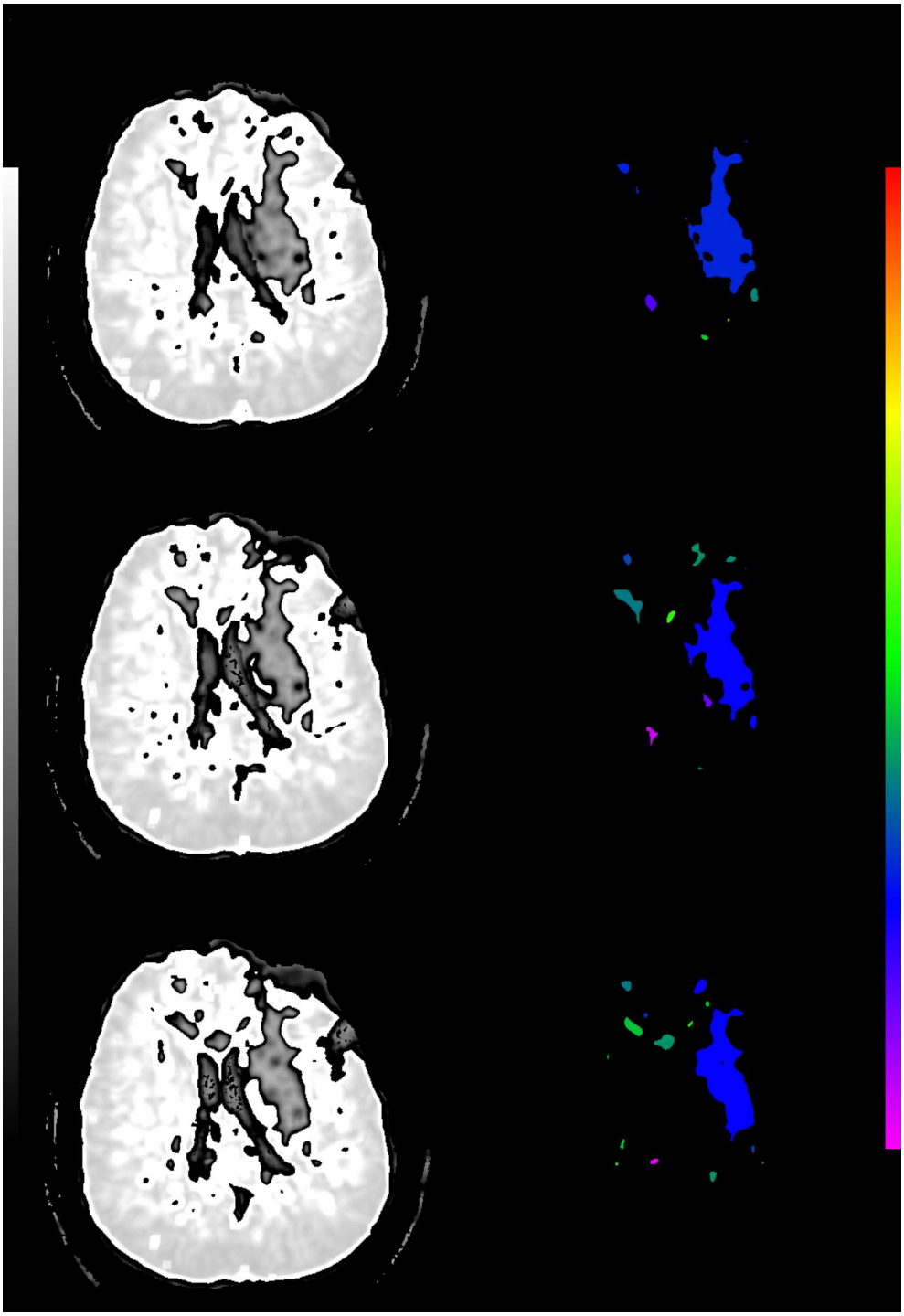

Figure 7.3: Example of suspicious voxels grouping. Unified standard deviations on the left displayed using the windowing technique with window level and center (0, 3). On the right suspicious groups. Each group color corresponds to average voxel values of the group in the source image, displayed in a color scale with range from -15 to 20 $ml \cdot l^{-1}$. Rows correspond to different locations in the map.

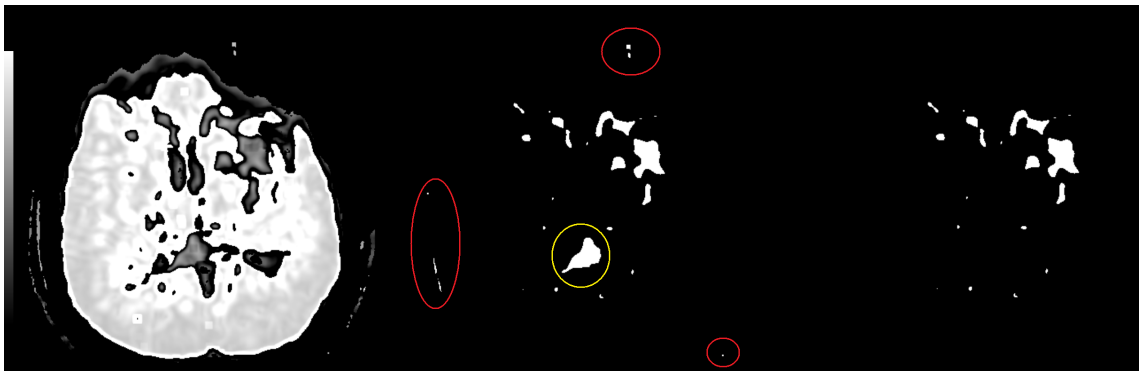

Figure 7.4: Example of discarding criteria use on PBV map. Unified standard deviations on the left displayed using the windowing technique with window level and center (0, 3). Middle image shows suspicious groups (white color). Red marking shows groups discarding by criteria 1 and yellow marked group shows the application of the criteria 2. Image on the right show suspicious groups (white color) after application of the Discarding criteria.

7.3.7 Discarding criteria

The processed maps consist of images where the suspicious groups were found. We can browse all the groups (of all the images) and discard some of them from further processing. A group is discarded when one of the following conditions is satisfied.

1. $(G_X^{Center}$ - $Image_X^{Center})$ / $G_X^{Size} < 0.2$
2. $G^{Average} \leq -50.0$

The first condition discards group of suspicious voxels when the group lies in both hemispheres. Such groups are often false positives groups formed by voxels persisted by non ideal segmentation of cerebral ventricles or using the threshold which flooded large areas enough to spill to both hemispheres. This criteria is satisfied when the distance between the center of the group and the center of the image is lower than 20% of the group size. This limitates the discarded groups to have enough portion in both hemispheres which reduces the influence of not precisely centered head in the image or possible rotation of the head from the straight position.

The second condition discards groups which average value is below or equal to -50.0 ml·l^{-1}. Such groups can be found at borders of brain tissue and segmented objects like bones or cerebral ventricles. Infarction core groups can contain voxels with negative values but the average value of such areas is always above -50 ml·l^{-1}.

The example of discarding criteria use is shown in Figure 7.4.

7.3.8 Grouping of the adjacent groups between images

Grouping of the adjacent groups between images is based on processing of pairs of adjacent images. The first pair of images is formed by image I_0 and I_1, the second pair by I_1 and I_2 and the last pair by images I_{Max-1} and I_{Max}. Two groups are joined into one group when (both conditions must be satisfied):

1. It has at least one voxel with the same xy-coordination (overlaying).
2. The difference between average values is lower or equal to 10.0 ml·l^{-1}.

The first condition means that two group of the adjacent images can be joined only when at least one voxel of the two considered groups has the same xy-coordinations. It means that the groups at least partially overlay each other. The second criteria expresses that two groups which overlay each other must be also similar in the average value. It aims that they should cover tissue with similar features. The similarity is here expressed as the maximal difference between the average group values of 10.0 ml·l^{-1} which we found to be a suitable threshold.

For each group of the image with index i we find all adjacent groups in image with index $i + 1$ satisfying the joining condition. From these groups we select the largest one (L) and all others including the parent group in the image i we join together. The new resulting group average value is set to the average value of the largest group L. All other features of the joined group are recalculated - size and the center position. The used average value of the largest group preservers smooth joining of the adjacent image groups where the average value can slightly differ between adjacent images but the average value difference would get higher with the distance between images.

7.3.9 Selection of the largest group

The final step of the proposed method is descending sorting of the groups according to the count of voxels belonging to a group. The largest group is selected to be the one corresponding to the necrotic tissue area.

Chapter 8

Optimization, results, comparison

8.1 Optimization

Lets recapitulate the proposed method. The source map is processed in order to denoise it by meaning filtering as described in Section 7.3.1. For this purposes we must choose the size of the nearest neighborhood. We process volumetric maps which have 3 dimensions so the size of the nearest neighborhood must have also 3 dimensions. We can denote the dimensions of the nearest neighborhood as D_X, D_Y, D_Z. If the D_X would be for example 1 than it means that the nearest neighborhood in the x direction would contain 3 voxels (1 per each direction and 1 for the current voxel which the neighborhood is considered to).

When the meaning is finished the thresholds are found for each image separately as described in Section 7.3.2. The thresholds are found using a common parameter p which is used for computing the $p\%$ quantile of the image which becomes the image threshold. When all these local thresholds are found then they are approximated by a polynomial of the k-th degree for a smoothing purposes.

All other steps are described without need for other parameters. If we summarize the required parameters we get the following list:

- Nearest neighborhood dimensions: D_X, D_Y, D_Z
- Parameter for the threshold detection: p
- Degree of the polynomial used for approximation of the thresholds: k

The way how to find the best parameters is comparing results according to the manual infarction core by the physicians. Two physicians marked their findings on all of the PBV and CBV maps. The proposed method was aimed to provide better specificity than other methods described in Section 6 using PBV maps. We try to find the best parameters for the PBV maps but also for the CBV maps. Since the findings of the physicians are not

the same for the PBV and CBV maps, we will look for the best parameters individually for the following combinations:

- PBV-Ph1
- PBV-Ph2
- CBV-Ph1
- CBV-Ph2

In the used material, one voxel size in the direction of the x-axis is the same as the voxel size in the y-axis direction. We can reduce parameters to be optimized by considering D_X as the same value as D_Y and thus we can replace two parameters D_X and D_Y by only one parameter D_{XY} and interpret it like D_X=D_{XY} and D_Y=D_{XY}.

8.1.1 PBV optimization

For the PBV maps we evaluated matches using parameter ranges described in Table 8.1.

Parameter	**From**	**To**	**Step**
D_{XY}	0	11	1
D_Z	0	2	1
p	0.4	1	0.1
k	0	3	1

Table 8.1: Range of parameters used for the proposed method optimization in PBV maps.

8.1.2 CBV optimization

For the CBV maps we evaluated matches using parameter ranges described in Table 8.2.

Parameter	**From**	**To**	**Step**
D_{XY}	0	11	1
D_Z	0	2	1
p	0.1	0.6	0.1
k	0	3	1

Table 8.2: Range of parameters used for the proposed method optimization in CBV maps.

8.2 Results

Using the optimization range of parameters we received a lot of match records. By analyzing these records we can get following results.

8.2.1 Best specificity results

For each combination of the parameters was evaluated a match as described in Section 6.1. Table 8.3 shows the best specificity results for PBV and CBV maps having 0-2 numbers of the incorrect detections.

We can see that the obtained specificities are relatively high with the low number of the incorrect detections. The best specificity for PBV maps was 99.9999% with 4 incorrect detections and for CBV maps 99.9982% again with 4 incorrect detections. In both cases there was used large neighborhood area D_{XY}=10 and D_Z=2. The larger the neighborhood is the more are removed the steeper changes and the more are preserved only the infarction core areas which we suppose are the largest continuous areas with the low values. The large neighborhood in combinations with relatively low threshold value p provide small sensitivities (for PBV 2.13%, for CBV 16.52%). The larger neighborhood also limits flooding of the infarction core detections to the surrounding areas which supports the higher specificity (especially in PBV maps).

8.2.2 Optimal parameters for the used material

Previous section and the best specificity results (Table 8.3) show that the proposed method can reach high specificities (around 99.99%) in both PBV and CBV maps. Focusing only to the best specificity we can get low sensitivity. In this section we will try to find the best balance between the sensitivity and the specificity. Optimization process resulted in a huge amount of evaluated matches. We chose low number of incorrect detections, relatively high specificity and high sensitivity as a criteria for the optimal parameters.

From all of the PBV-Ph1 matches we can find only one parameters combination that can reach 0 incorrect detections but with specificity 99.8376%. We considered this specificity as too low and thus we will search for the best parameters from a group of evaluated matches which reached 1 incorrect detection. CBV-Ph2 does not contain any record with lower than 2 incorrect detections. The optimal parameters will be searched only from those match evaluated records corresponding to the number of incorrect matches defined in Table 8.4.

For the optimal parameters selection is often used ROC analysis where the best parameters correspond to the point which is nearest to the upper-left corner or in other words the point which balances the sensitivity and specificity. The ROC curve is used for tuning classifiers where the parameter is a kind of threshold value. Adjusting this threshold we always get two sets where the one is correctly classified while the second is not. The count

Match type	**Parameters** D_{XY}**x**D_Z (k) p	**Sensitivity** [%]	**Specificity** [%]	**Matthews** [%]	**Incorrect detections**
PBV-Ph1	11x1 (2) 0.8	53.52	99.8376	47.21	0/12
PBV-Ph1	7x2 (1) 0.7	33.19	99.9660	44.33	1/12
PBV-Ph1	11x2 (1) 0.7	24.52	99.9772	37.99	2/12
PBV-Ph1	4x2 (1) 0.5	7.62	99.9991	23.21	3/12
PBV-Ph1	7x2 (0) 0.5	3.75	99.9998	15.03	4/12
PBV-Ph2	10x1 (1) 0.7	30.50	99.9711	44.16	1/12
PBV-Ph2	7x2 (1) 0.7	29.77	99.9730	43.47	2/12
PBV-Ph2	8x1 (1) 0.6	23.08	99.9952	41.30	3/12
PBV-Ph2	10x2 (1) 0.5	2.13	99.9999	10.43	4/12
CBV-Ph1	6x1 (0) 0.2	24.33	99.9939	43.31	1/12
CBV-Ph1	7x1 (0) 0.2	21.87	99.9963	42.05	2/12
CBV-Ph1	7x1 (1) 0.2	26.06	99.9958	47.48	3/12
CBV-Ph1	5x1 (2) 0.2	29.39	99.9951	50.21	4/12
CBV-Ph2	8x1 (0) 0.2	18.73	99.9980	38.12	2/12
CBV-Ph2	10x2 (1) 0.2	15.91	99.9977	35.17	3/12
CBV-Ph2	10x2 (0) 0.2	16.52	99.9982	35.85	4/12

Table 8.3: Proposed method best specificity results with 0-4 incorrect detections (where available) from a set of parameters defined in Section 8.

Match type	**Incorrect detections**	**Count of records**
PBV-Ph1	1	33/980
PBV-Ph2	1	37/980
CBV-Ph1	1	35/840
CBV-Ph2	2	47/840

Table 8.4: Optimal parameters features reducing the searched set of parameters defined in Section 8.

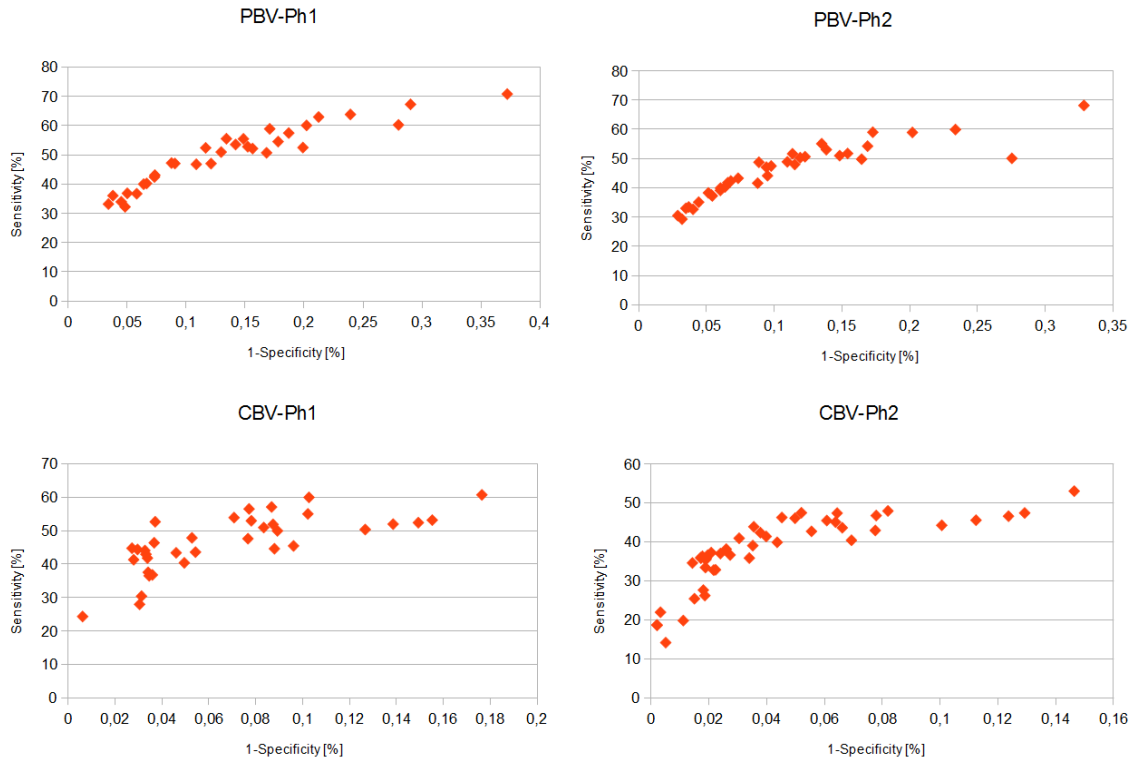

Figure 8.1: ROC depiction of the evaluated match records with features defined in Table 8.4.

of member of both sets changes continuously with the threshold which preserves the ROC curve to be monotonicity function coming out from the lower-left corner and going to the upper-right corner.

This kind of curve can not be constructed from the evaluated match records because the method uses the criteria of the selection of the large continuous area. This step influences the sensitivity and specificity and can provide discontinuity of the ROC curve or breaking the monotonicity rule.

We used depiction only of points obtained by evaluated match records for each match type separately (Figure 8.1). Choosing of optimal parameters is not clear since there is no clear balancing point. Instead of arbitrary choosing the optimal parameters we decided to use another criteria.

Stability criteria

If we suppose the method to be used on a larger set of maps we can focus to select as optimal such parameters combination which would preserve similar results also on other maps than only the total 24 of the used material. Such parameters combination could be named as stable. As we have no more maps available we can just suppose that the most stable parameters should be low sensitive for little changes of parameters leading only to

Type	D_{XY}	D_Z	k	p	Sensit.	Specif.	Matthews	Incorrect detections
PBV-Ph1	10	2	1	0.8	40.0%	99.94%	48.4%	1/12
PBV-Ph2	9	1	1	0.7	33.0%	99.97%	45.9%	1/12
CBV-Ph1	7	1	0	0.3	43.0%	99.97%	53.1%	1/12
CBV-Ph2	7	1	0	0.3	36.6%	99.98%	51.1%	2/12

Table 8.5: Optimal parameters for the proposed method.

small changes in results and preserve the low number of incorrect detections. For this purpose we defined what are the little changes in parameters. We selected following:

- D_{XY} - the change of ± 1
- p - the change of ± 0.1

These changes express the nearest members of the D_{XY} and p in a set of evaluated matches generated by optimization process (Section 8). The other parameters D_Z and k are not considered for the stability purposes because their little change means different behavior of the method (k parameter) or the rapid growing of the considered neighborhood area (D_Z) parameters.

To evaluate the most stable parameters we found for each parameters combination all adjacent parameters combinations (according to the D_{XY} and p) including the base (central) combinations and we summarized up the numbers of incorrect detections and we also evaluated the average sensitivity and specificity. The total number of the used match evaluation records was 9 for 1 tested combination of the parameters. Finally we sorted the results by the number of the incorrect matches of the base parameters combination, next by the number of the total incorrect matches using the parameters neighborhood and third by the specificity. Results are shown in Table 8.5 and performance in the 9-neighborhood is shown in Table 8.6.

8.2.3 Inaccuracies visualization

We can compare manual delineation by a physician with with the best findings of the proposed method. The proposed method is actually based on evaluation of the mean values and corresponding standard deviations. Now we want to show the manual infarction core delineation in a form of 2D histogram where the y-axis is a mean value and the x-axis is a standard deviation. We will use the best found parameters and we will use the corresponding neighborhood settings. For the mean value and standard deviation calculations we will use standard equations (Equation 8.1 and Equation 8.2).

Type	Sensit.	Specif.	Matthews	Incorrect detections
PBV-Ph1	40.5%	99.92%	45.9%	14/108
PBV-Ph2	37.1%	99.94%	47.0%	16/108
CBV-Ph1	41.4%	99.95%	50.4%	14/108
CBV-Ph2	35.8%	99.97%	49.3%	21/108

Table 8.6: Performance of the optimal parameters using the parameters 9-neighborhood of the stability criteria (Section 8.2.2).

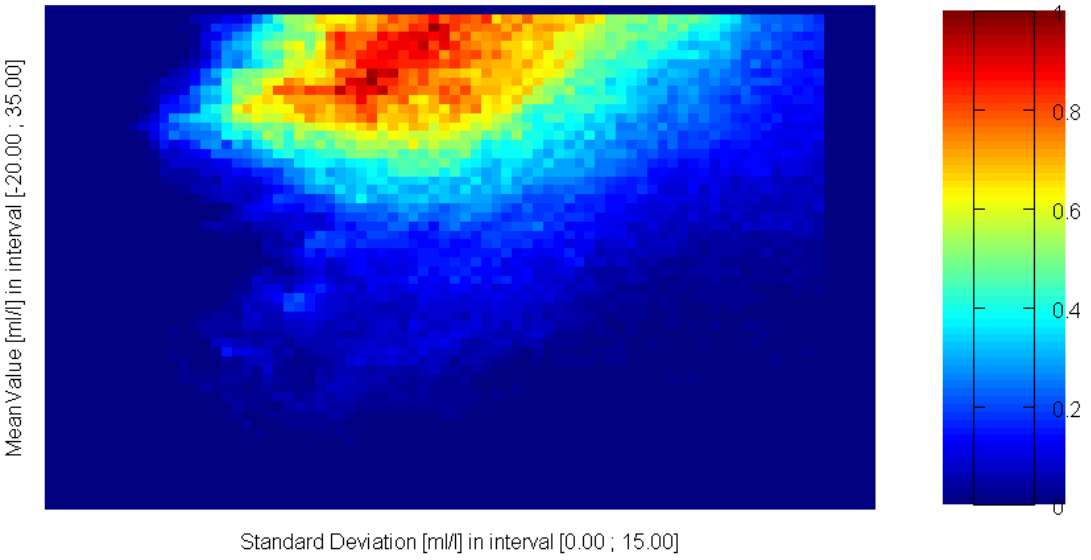

Figure 8.2: Example of frequency histogram of combination of mean values and standard deviations in PBV map using neighborhood 9x9x1. The color frequency scale is from 0 to the highest value 624.

$$MeanValue_{i,j,k} = \frac{\sum_{x=-X}^{X} \sum_{y=-Y}^{Y} \sum_{z=-Z}^{Z} SourceImage_{i+x,j+y,k+z}^{>-500}}{Count\ of\ used\ voxels} \tag{8.1}$$

$$StDev_{i,j,k} = \sqrt{\frac{\sum_{x=-X}^{X} \sum_{y=-Y}^{Y} \sum_{z=-Z}^{Z} ((SourceImg_{i+x,j+y,k+z}^{>-500}) - MeanValue_{i,j,k})^2}{Count\ of\ used\ voxels}} \tag{8.2}$$

If we summarize the counts of the voxels corresponding to the mean value and standard deviation pairs in the whole map limited by the segmentation adjustment step (Section 5) we get the histogram like in Figure 8.2.

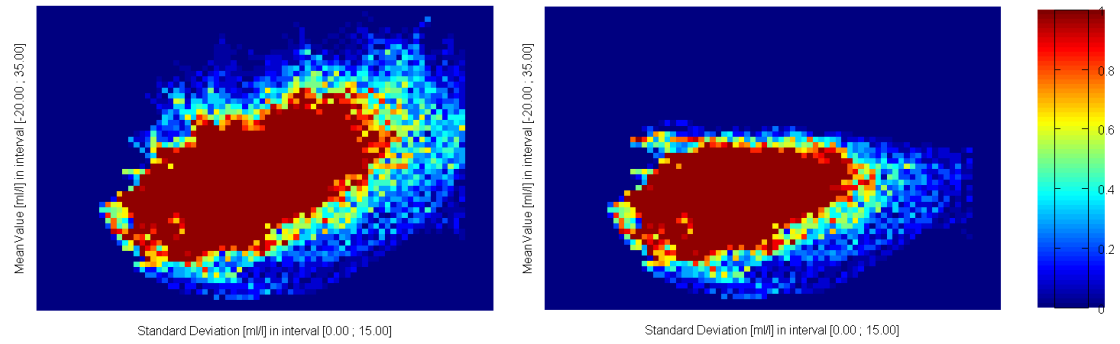

Figure 8.3: Comparison of infarction core features delineated by Physician 2 (on the left) and the proposed method (on the right) using PBV map with the best sensitivity using optimal parameters for PBV-Ph2. The frequency scale is from 0 to the limited maximal value 20.

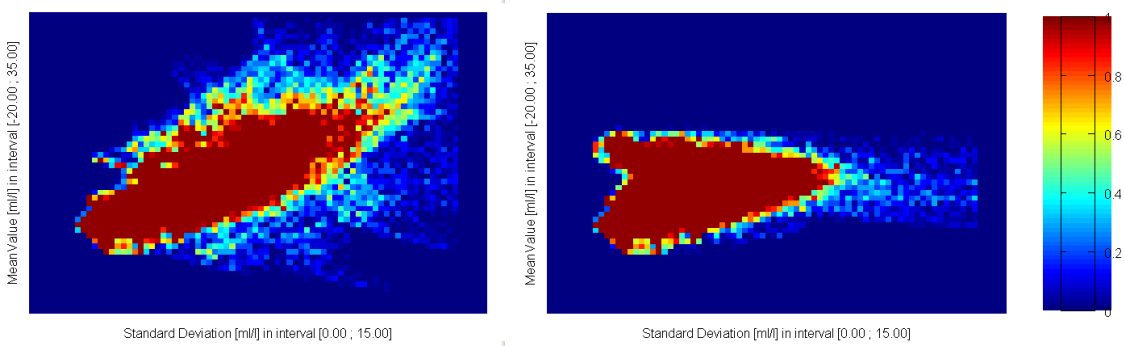

Figure 8.4: Comparison of infarction core features delineated by Physician 2 (on the left) and the proposed method findings (on the right) using PBV map with the worst specificity using optimal parameters for PBV-Ph2. The frequency scale is from 0 to the limited maximal value 20.

Lets consider the optimal parameters for Physician 2 and calculate such histograms. The comparison between manual delineation by Physician 2 and the proposed method can be seen in Figure 8.3.

We can see that the proposed method results in lower number of detected infarction core voxels and the detected ones mutually correspond. This reflects the high specificity and confirms the sensitivity values. The figure shows an example of a map where was reached the highest sensitivity 62.04%, specificity 99.9841% and Matthews correlation coefficient 76, 19%. Now lets have a look to the case of the worst specificity map using the same method parameters. The comparison is depicted in Figure 8.4 and corresponding specificity is 99.8714%, sensitivity is 55.56% and the Matthews correlation coefficient is 59.47%. The last example is shown in Figure 8.5 and it is for a map with the lowest sensitivity which is only 6.89% but with the specificity 99.9999% and the corresponding Matthews coefficient 26.13%.

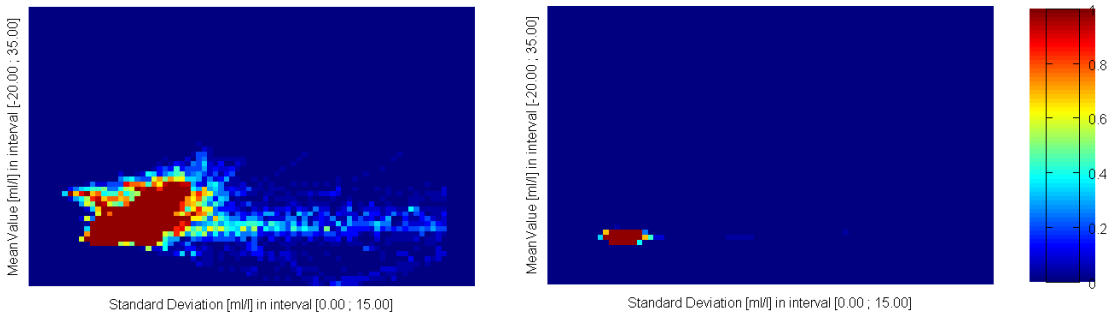

Figure 8.5: Comparison of infarction core features delineated by Physician 2 (on the left) and the proposed method findings (on the right) using PBV map with the worst sensitivity using the optimal parameters for PBV-Ph2. The frequency scale is from 0 to the limited maximal value 20.

These figures does not differentiate between map's images separately and are displayed one for the whole map. We can see that the proposed method tends to delineation of smaller areas and those parts with the higher mean value and higher standard deviations (upper right areas of the physician's manual delineations) are not delineated at all. The reason is in the used criteria:

$-1.0 \leq StDevUnified_{i,j,k} \leq 0$

This equation provides the clipping and causes the missing parts of the delineations with the higher mean values and higher standard deviations. But on the other hand these higher mean values with the higher standard deviations are in the maps more frequent also at places which should not be considered as infarction core area and thus it can provide higher risk of the worse specificity or the higher number of the incorrect detections. Table 8.7 shows results comparison between different lower limits of the criteria using the optimal parameters. It supports the choice of the proposed method lower limitation -1.0 which has the best results according to the Table 8.7. We can find samples of individual maps which provide better match while using different lower limitation than -1.0 but the overall match is the best for the value -1.

8.2.4 Memory and processing time requirements

Required processing time for the proposed method depends on the used examination features. One of the biggest influence has the dimensions of the input map. In our case, all the processed maps had dimensions 512x512x44. Linear increase of the dimensions will cause a linear increase of required processing time.

In details, the highest portion of processing time is spent by providing mean filtering with standard deviations calculation. This time is dependent on the used neighborhood size. If we denote the total number of examination voxels as N and the total number of voxels in the neighborhood area as M, then we get M*N as a number of voxels required to

Match type	**Lower limit [-]**	**Average sensitivity** [%]	**Average specificity** [%]	**Average Matthews** [%]	**Incorrect detections**
PBV-Ph1	-1.0	40.10	99.9361	48.41	1/12
PBV-Ph1	-1.5	54.79	99.8659	52.39	2/12
PBV-Ph1	-0.5	14.47	99.9930	30.28	4/12
PBV-Ph2	-1.0	32.98	99.9652	45.89	1/12
PBV-Ph2	-1.5	47.63	99.9103	52.82	1/12
PBV-Ph2	-0.5	24.61	88.8871	23.74	3/12
CBV-Ph1	-1.0	42.95	99.9669	53.12	1/12
CBV-Ph1	-1.5	61.13	99.9165	58.58	2/12
CBV-Ph1	-0.5	19.66	99.9965	38.08	4/12
CBV-Ph2	-1.0	36.60	99.9804	51.13	2/12
CBV-Ph2	-1.5	52.46	99.9411	60.09	3/12
CBV-Ph2	-0.5	19.45	99.9982	39.54	5/12

Table 8.7: Different lower limitation results for the optimal parameters ordered by number of incorrect detections and the highest specificity

be accessed when considering the mean filtering. The same it is for the standard deviations calculation. All other steps like identifying suspicious groups or their grouping, are less time expensive. Just one passage of N voxels is required for suspicious groups identification or in case of grouping between images, only two adjacent slices are considered at a time.

If we look on the memory requirements, we can see that the method proposes to create temporary images to store the mean values, standard deviations and unified values. All of these images have the same dimensions as the original map. If we calculate the map itself and one more image, where the final image with highlighted infarction core is delineated, we get that the required memory is 5 times larger than the original map (which has about 25 MB).

We can conclude that the processing time is almost constant for the fixed dimensions of the input map and fixed parameters of the method. The memory requirements are close to 5x of the input map size. On a computer with Intel Xeon 1.86 GHz CPU (2 processors) and 10 GB of installed memory, the required processing time was 2 minutes an 5 seconds for a sample of CBV map using the optimal parameters. We must also mention that our implementation did not use any parallel operations which would be beneficial and easy to use especially with the mean filtering and standard deviations evaluation.

8.3 Methods comparison

In this study we reproduced procedure of [39] on our dataset. This procedure is based on edge preserving smoothing with following thresholding (Method 1). We found optimal values but corresponding specificities were too low for the further infarction core volume evaluation. Next was described the same procedure enriched by the final selection of the largest continuous area considered as infarction core (Method 2). This method already provided satisfactory results but only for case of CBV maps. The proposed method provides satisfactory results despite of the map type. All these three methods we will compare using different kind of statistics.

For simple comparison between different methods we chose the optimal parameters and only results using these parameters are compared. The optimal parameters were not determined only for the Method 2 for case of PBV maps. In this case we will use the best specificity settings, it means thresholds 0.5 ml·100 g^{-1} (5.25 ml·l^{-1}).

The comparison is presented in Table 8.8 for PBV maps and in Table 8.9 for CBV maps. The volume error is evaluated as an absolute value (Equation 8.3) and as a percentage value (Equation 8.4). The *pattern* in equations means the manual delineations by physicians while *method* is one of the Method 1, Method 2 and Proposed method.

$$Volume\ error\ [cm^3] = Volume\ of\ pattern - Volume\ of\ method \tag{8.3}$$

$$Volume\ error\ [\%]\ =\ \frac{Volume\ of\ pattern\ -\ Volume\ of\ method}{Volume\ of\ pattern}\cdot 100 \tag{8.4}$$

If we browse the results we can see that the Method 1 - the process reproduced by [39] reaches the best sensitivity and the worst specificity. The specificity even if it reaches in average to both physicians 95.2276% for PBV maps and 95.8391% for CBV maps suffer by the highest volume error from all the tested methods. The average volume error for Method 1 was found for PBV maps in average -2660% and for CBV maps -3221.78%. The negative value expresses that the detected area by Method 1 is larger than the pattern by physicians and also expresses that it is in average 26.6x and 32.2x larger than the pattern.

Method 2 should be considered separately for PBV and CBV maps. In case of PBV maps we could not find such settings which would provide better specificity. Because of this reason we used the settings corresponding to the highest specificity. The specificity is higher than in the Method 1 but still produces relatively large volume error (in average -806.94% meaning 8x larger detections). In case of CBV we selected the optimal parameters also in order to reach low number of incorrect detections while preserving high precision with average relative volume error 24.64% meaning that the average detected area is only 0.25x smaller than the manual delineations which is the lowest volume error from all the tested methods.

The last method is the Proposed method. We can see that in case of CBV maps we received better specificity in average 99.9737% than in using the Method 2 but the corresponding volume error is in average 41.71%. Using the PBV maps we can see the highest benefit of the proposed method because the specificity reaches 99.9507% which is the highest from all the methods and corresponding volume error is 39.38% expressing that the proposed method results in average in 0.4x smaller area according to manual delineations.

If we compare the number of incorrect detections we see that the Method 1 has the lowest numbers (1/24 for CBV maps and 1/24 for PBV maps), the second place gets the proposed method with 3/24 for CBV maps and 2/24 for PBV maps and at the last place is for Method 2 with 4/24 for CBV and 6/24 for PBV maps.

8.3.1 Delineated infarction core areas features

As it was already described in Section 8.2.3 the proposed method's drawback is that it does not mark voxels having higher values. We can see this feature in the Table 8.10. In this table we measured the average maximal values (and corresponding standard deviations) present in the delineated areas. For the manual delineations we used 95% quantile because of presence of some very high values on borders marked probably by mistake connected with limited precision of mouse selection with a brush tool.

		Method 1		Method 2		Proposed method	
		PBV-Ph1	PBV-Ph2	PBV-Ph1	PBV-Ph2	PBV-Ph1	PBV-Ph2
Sensitivity [%]	Mean	89.39	87.20	76.41	70.83	40.01	32.98
	St. dev.	13.63	12.87	18.75	17.74	20.56	21.60
	Min.	51.82	51.71	39.63	44.11	6.71	6.89
	Max.	100.00	96.32	99.35	95.57	64.62	62.04
Specificity [%]	Mean	94.9389	95.5162	98.6447	98.6970	99.9361	99.9652
	St. dev.	2.3713	2.2316	1.1125	1.1142	0.0657	0.0417
	Min.	89.6871	90.8134	96.6436	96.6497	99.7645	99.8714
	Max.	98.1537	98.4134	99.8121	99.8519	99.9996	100.0000
Matthews [%]	Mean	19.19	23.22	35.18	37.15	48.41	45.89
	St. dev.	6.70	9.08	14.86	13.53	12.17	17.13
	Min.	10.90	11.02	17.69	17.80	25.59	22.62
	Max.	30.80	37.60	61.33	60.51	65.05	76.19
Volume error $[cm^3]$	Mean	-266.69	-235.05	-66.54	-60.82	5.13	10.54
	St. dev.	124.89	116.70	59.50	60.69	7.32	10.43
	Min.	-549.06	-488.75	-164.81	-164.24	-7.99	-3.49
	Max.	-96.87	-83.37	0.73	0.66	15.98	30.58
Volume error [%]	Mean	-3150.05	-2170.11	-931.58	-682.30	29.13	49.63
	St. dev.	2662.31	2024.74	1106.15	913.13	53.41	45.88
	Min.	-8304.81	-6783.51	-3048.38	-2749.36	-70.78	-67.79
	Max.	-822.25	-499.83	3.22	3.13	93.16	93.06
Incorrect detections							
		0/12	1/12	3/12	3/12	1/12	1/12

Table 8.8: Comparison of performance between different methods using PBV maps

		Method 1		Method 2		Proposed method	
		CBV-Ph1	CBV-Ph2	CBV-Ph1	CBV-Ph2	CBV-Ph1	CBV-Ph2
Sensitivity [%]	Mean	90.46	83.05	54.86	49.38	42.95	36.60
	St. dev.	6.64	15.28	21.17	20.64	18.43	21.23
	Min.	78.47	46.26	10.92	4.34	8.51	2.86
	Max.	98.98	96.35	77.52	75.10	69.31	68.00
Specificity [%]	Mean	95.8762	95.8020	99.9148	99.9216	99.9669	99.9804
	St. dev.	0.8901	0.7756	0.1172	0.1086	0.0267	0.0159
	Min.	93.6712	93.8270	99.5784	99.6303	99.9167	99.9537
	Max.	97.2482	96.6611	99.9947	99.9967	99.9996	99.9997
Matthews [%]	Mean	20.14	22.58	59.42	58.68	53.12	51.13
	St. dev.	9.93	9.85	17.15	18.88	16.12	20.51
	Min.	6.77	10.01	26.70	18.40	28.43	16.54
	Max.	36.15	36.34	83.76	81.51	80.91	80.29
Volume error $[cm^3]$	Mean	-218.18	-220.62	2.24	6.28	7.09	12.00
	St. dev.	51.27	44.89	6.02	4.74	9.60	10.08
	Min.	-331.60	-320.09	-6.32	0.34	-0.88	-0.20
	Max.	-146.17	-156.44	16.33	14.89	27.99	36.32
Volume error [%]	Mean	-4412.33	-2031.23	15.57	33.71	32.35	51.07
	St. dev.	5253.37	1892.32	38.14	27.13	34.57	31.56
	Min.	-19969.59	-7262.94	-50.88	3.52	-19.73	-6.74
	Max.	-8304.81	-564.51	83.29	94.45	91.04	97.03
Incorrect detections							
		0/12	1/12	1/12	3/12	1/12	2/12

Table 8.9: Comparison of performance between different methods using CBV maps

	PBV-Ph1	PBV-Ph2	CBV-Ph1	CBV-Ph2
Proposed method	12.57±9.64	8.61±9.04	12.54±2.60	12.01±2.10
Manual delineations	20.35±14.33	18.53±10.45	20.02±3.76	20.53±2.08

Table 8.10: Comparison of maximal values in detected infarction core areas (values in $ml \cdot l^{-1}$)

We can see that the manual delineations by physicians reach almost the threshold 2 $ml \cdot 100\ g^{-1}$ (21 $ml \cdot l^{-1}$) found by study [39]. The proposed method reaches lower values and thus the delineated area is smaller. The another observation is that the manual delineations maximal values are almost the same for all CBV maps - average standard deviation is 2.92 while using the PBV maps the average standard deviation is 24.78 $ml \cdot l^{-1}$. This also supports possibility of using a constant threshold for infarction core detection in CBV maps but in case of PBV maps there should be the threshold found individually for a patient. The proposed method searches such threshold from the map histogram and this is probably the reason why it reaches the best results on PBV maps from the tested methods.

8.4 Discussion

In this chapter we described the process of finding optimal parameters for the proposed method. Next we mutually compared the results of different automated methods. We can see that the proposed method is usable with both PBV and also with CBV maps. If we consider only the CBV maps then the proposed method results are competitive to the Method 2 (the edge preserving smoothing followed by thresholding and selection of the largest continuous area as infarction core). For usage with PBV maps the proposed method reaches the best results from all the tested method.

Analysis of the features of the delineated infarction core areas showed that the proposed method does not mark infarction core voxels with higher mean values and higher standard deviations as can be seen in Figures 8.3, 8.4, 8.5. This behavior is a method feature which is not depended on the selection of the parameters and it causes also the lower maximal values of the delineated areas and the lower volumes. Using the higher threshold value (the higher p parameter) would lead to covering the higher mean values but together with accepting the corresponding low standard deviations which would decrease the match. It seems that better results could be obtained probably by adjustment of the proposed method where for the higher mean values would be considered as infarction core only voxels with higher standard deviations.

Chapter 9

Conclusion

This work proposed a method for automated infarction core delineation using the PBV maps and showed that it can be used also with CBV maps. Detected infarction core volumes are lower than the volumes manually delineated by physicians. The relative volume error is 39.38% for PBV maps and 41.71% for CBV maps. The volume error compares just the volume but the overlaying of the automated detections with the manual detections is expressed by the sensitivity and specificity or also by the Matthews correlation coefficient. Especially the specificity has high influence to the precision of the infarction core delineation. The proposed method reached the highest average specificity from the tested methods. The average specificity (to both physicians) is 99.9507% for PBV maps and 99.9737% for CBV maps and thus the delineated infarction core areas have the lowest number of false positive voxels. The proposed method with this high specificity preserves sensitivity 36.5% for PBV maps and 39.8% for CBV maps. The proposed method has also relatively low number of incorrect detections 2/24 (8.3%) for PBV maps and 3/24 (12.5%) for CBV maps.

From the manual delineations marked for our material by two independent physicians we can confirm supposed infarction core threshold 2.0 $ml \cdot 100g^{-1}$ (21 $ml \cdot l^{-1}$) [39] in the way that the maximal values present in the delineated areas have similar values (19.44 for PBV maps and 20.28 $ml \cdot l^{-1}$ for CBV maps). We also reproduced the same procedure as presented in [39] (with modifications for the whole brain usage) and we found the optimal values close to the supposed threshold 2.0 $ml \cdot 100g^{-1}$. We must mention that the [39] does not describe details of the used edge preserving smoothing so it can differ from the edge preserving smoothing method used in our study. The thresholds reach very high sensitivities (88.30% for PBV and 86.78% for CBV) but the specificities 95.2276% for PBV maps and 95.8391% for CBV maps are too low for automated infarction core volume detections since it provides high number of false positive voxels. It also means that voxels equal or lower the infarction core thresholds are present also at places where the infarction core was not marked by physicians. This can explain that the threshold from [39] is in different studies used only in connection with region of interests delineated by humans or

with some kind of additional information provided by follow-up examinations where the final infarction core area is superimposed to the admission images (like in studies [7], [23], [17]).

The proposed method is unique. It is a fully automated method delineating the infarction core while minimizing the number of false positive voxels. We did not find any similar method with comparable results in available literature dealing with automated infarction core delineation in PBV maps. This automated method could be used by physicians like a first information about the extent and location of the infarction. The method tend to delineate smaller infarction core areas according to the manual delineations by physicians with previously mentioned volume error. Physicians can use this volume information as another factor helping them with the thrombolytical treatment indication decision.

9.1 Advantages of the proposed method

The used mean filtering is beneficial for processing PBV maps. It smooths the values in the map enough for further infarction core thresholding purposes. The standard deviations are also used for segmentation of the cerebral ventricles. The used selection of the largest continuous area from all the thresholded voxels supports the high specificity of the proposed method and focuses the delineated area to the same location as marked by physicians and thus the measured volume is not influenced by false positive areas of different regions. The overall match evaluation of the proposed method to the manual delineations (the average Matthews coefficient for PBV maps is 47.15% and for CBV maps 53.13%) is relatively close to the mutual match between both physicians (Matthews coefficient is 56.90% for PBV maps and 62.09% for CBV maps).

The proposed method can serve as another tool for physicians which can provide information about the location and volume of the infarction. The used algorithm can be easy parallelized and provide results in a short time. Since the method tends to mark smaller infarction core areas than by the physicians, the evaluated volume could be considered as the lowest infarction core volume estimation.

9.2 Disadvantages of the proposed method

Many of the mentioned advantages can be also considered in a way as disadvantages. The using of the mean filtering smooths the local neighborhood and it can theoretically smooth out also the little infarctions or to reduce or larger the area of the detected infarctions. The selection of the largest continuous area satisfying the infarction core threshold can cause also the incorrect detection - the discarding of the real infarction core area while accepting larger false-positive one. This criteria has also disadvantage in possible presence of more than one continuous area of the infarction core in the map which happened 5x in total of 48 (10.4%) manual delineations by physicians.

The proposed method also requires the segmentation adjustment step (Section 5) which in the general use should reflect the rotation of the head and before using of the proposed method the rotation adjustment should be made.

As the infarction core area is selected the largest continuous area but even if there would be no infarction core area the method would still select one. This corresponds to the presence of false positive voxels also in non-infarction core areas.

The used material contains only 12 patients and it would be desirable to prove the proposed method on a larger set of maps to provide more reliable results.

We can discuss also about the mutual match between physicians which is only 56.90% for the PBV maps and 62.09% for the CBV maps. It would be desirable to evaluate match according to some more stable pattern. May be the use of the magnetic resonance follow-up examinations would provide such pattern but it would also require to use only recanalised patients.

9.3 Future works proposals

As a future work we can propose to verify the method using the larger set of patients and as the pattern to use the magnetic resonance follow-up examinations. The another possibility of the future work is considering the symmetry plane axis and using also information from the opposite hemisphere.

Another point for the future works can be the fact that the manual delineations made by the physicians can contain more than one continuous area. The proposed method was designed according to presumption that there is only one continuous infarction core area. The future work could handle this situation which would lead to better precision. Another point could be handling of cases with no infarction core at all. We can see possible improvement of the method by using atlases which can provide additional information about the area location and probability whether it is some kind of artifact or not.

Bibliography

[1] J. B. Antoine Maintz, Max A. Viergever: *A survey of medical image registration*, Oxford University Press volume 2, pp 1-36, 1997.

[2] P. Baldi, S. Brunak, Y. Chauvin et al. *Assessing the accuracy of prediction algorithms for classification: an overview*, Bioinformatics 2000, 16, 412–424.

[3] I. N. Bankman: *Handbook of Medical Imaging*, Academic Press, ISBN 0-12-077790-8, 2000.

[4] G. Borgefors: *Hierarchical Chamfer Matching: A Parametric Edge Matching Algoritm*, IEEE Transaction on Pattern Analysis and Machine Intelligence, Vol. 10, No. 6, 1988.

[5] E. C. S. Camargo, K. L. Fuire, A. B. Singhal et al., *Acute Brain Infarct: Detection and Delineation with CT Angiographic Source Images versus Nonenhanced CT Scans*, Radiology 2007: Volume 244: Number 2.

[6] F. Charvát, B. Markalous a kol., *Zobrazení hlavy, metodika vyšetřování, anatomie, patologie, klinika. (2. upravené a rozšířené vydání)*, TRITON Praha/Kroměříž, ISBN 80-7254-904-9, 2006.

[7] M.A. Ezzeddine, M.H. Lev, C.T. McDonald, G. Rordorf, et al. *CT angiography with whole brain perfused blood volume imaging: added clinical value in the assessment of acute stroke.*, Stroke. 2002; 33: 959–966.

[8] S. Chokchaitam, S. Feueanggan, S. Muengtaweepongsa, *Stroke-Analysis Program for Searching Infarct/Penumbra Area from CT-Scan Images via Digital Image Processing Technique*, Proceedings of the International MultiConference of Engineers and Computer Scientists, 2011 Vol I, IMECS 2011, ISBN: 978-988-18210-3-4.

[9] T. Fawcett, *An Introduction to ROC Analysis*, Pattern Recognition Letters, vol. 27, no. 8, pp. 861-874, 2006.

[10] J. Ferda, *CT Angiografie*, Galén, ISBN 80-7262-281-1, 2004.

[11] S. Fueanggan, S. Chokchaitam, S. Muengtaweepongsa, *Simulation Program of Specifying Ischemic Stroke Area from CT Perfusion images Based on Digital Image Processing Techniques*, 8th International Conference on Electrical Engineering/Electronics, Computer, Telecommunications and Information Technology (ECTICON), 2011, 1031 - 1034.

[12] R. Gasparotti, M. Grassi, D. Mardighian, et al., *Perfusion CT in Patients with Acute Ischemic Stroke Treated with Intra-Arterial Thrombolysis: Predictive Value of Infarct Core Size on Clinical Outcome*, AJNR Am J Neuroradiol 2009,; 30:722-27.

[13] D. Grigaitis,*An Optimization of System for Autoamtic Recognition of Ischemic Stroke Areas in Computed Tomography Images*, Informatica, 2007, Vol. 18, No. 4, 603-614.

[14] D. Grigaitis, M. Meilunas, *Automatic extraction of symmetry plane from Falx cerebi areas in CT slices*, In Proceedings of Bildverarbeitung für die Medizin. 2007, 267-271.

[15] L.M. Hamberg, G.J. Hunter, D. Kierstead, E.H. et al., *Measurement of cerebral blood volume with subtraction three-dimensional functional CT*, AJNR Am J Neuroradiol. 1996; 17: 1861–1869

[16] M. Horák, *MR Diagnostika, Radiodiagnostická klinika FN Na Bulovce v Praze*, [cit. 2012-03-01]. Available from: URL: http://portal.lf1.cuni.cz/clanek-577-zaklady-mr-diagnostiky.

[17] G. J. Hunter, H. M. Silvennoinen, L. M. Hamberg et al., *Whole-Brain CT Perfusion Measurement of Perfused Cerebral Blood Volume in Acute Ischemic Stroke: Probability Curve for Regional Infarction*, Radiology 2003; 227:725-730.

[18] L. Ibanez L., W. Schroeder, L. Ng, J.Cates, *The ITK Software Guide*, Kitware, Inc. ISBN 1-930934-10-6, [cit. 2012-04-18]. Available from: URL: http://www.itk.org/ItkSoftwareGuide.pdf, 2003.

[19] E. M. de Lucas, E. Sánchez, A. Gutiérrez, et al., *CT Protocol for Acute Stroke: Tips and Trics for General Radiologists*, RadioGraphics 2008;28:1673-1687.

[20] D. Mattes, D.R. Haynor, H. Vesselle, T.K. Lewellen, W. Eubank, *PET-CT image registration in the chest using free-form deformations*, Medical Imaging, IEEE Transactions on , vol.22, no.1, pp.120-128, Jan. 2003. doi: 10.1109/TMI.2003.809072.

[21] P. Maule, J. Klečková, *Volumetric Data Subtraction Analyser*, 2010 [cit. 2012-03-01]. Available from: URL:
http://www.kiv.zcu.cz/cz/vyzkum/software/produkt-detail.html?produkt_id=81

[22] Ministry of Health of the Czech Republic, *DASTA - Datový standard MZ ČR - verze 4*. [cit. 2012-03-01]. Available from: URL: http://ciselniky.dasta.mzcr.cz

[23] B. D. Murphy, A. J. Fox, D. H. Lee, et al., *Identification of Penumbra and Infarct in Acute Ischemic Stroke Using Computed Tomography Perfusion-Derived Blood Flow and Blood Volume Measurements*, Stroke 2006;37;1771-1777.

[24] National Electrical Manufacturers Association, *The DICOM Standard*. [cit. 2012-03-01]. Available from: URL: http://dicom.nema.org

[25] S. Ourselin, A. Roche, S. Prima et al., *Block Matching: A General Framework to Improve Robustness of Rigid Registration of Medical Images.*, Third International Conference on Medical Robotics, Imaging And Computer Assisted Surgery, volume 1935 of Lectures Notes in Computer Science, pages 557-566, 2000.

[26] P. Perona, J. Malik, *Scale-space and edge detection using anisotropic diffusion.*, Pattern Analysis and Machine Intelligence, IEEE Transactions on, vol.12, no.7, pp.629-639, Jul 1990, doi: 10.1109/34.56205.

[27] M. J. D. Powell, *An efficient method for finding the minimum of a function of several variables without calculating derivatives*, Computer J., vol.7, pp.155-162, July 1964.

[28] B. Preim, S. Oeltze, M. Mlejnek, E. Groeller, A. Hennemuth, S. Behrens, *Survey of the Visual Exploration and Analysis of Perfusion Data*, Visualization and Computer Graphics, IEEE Transactions on , vol.15, no.2, pp.205-220, March-April 2009, doi: 10.1109/TVCG.2008.95.

[29] P. A Puech, L. Boussel, S. Belfkih, et al., *DicomWorks: software for reviewing DICOM studies and promoting low-cost teleradiology.*, Journal of digital imaging the official journal of the Society for Computer Applications in Radiology (2007), Volume: 20, Issue: 2, Publisher: Springer-Verlag, Pages: 122-130. DOI 10.1007/s10278-007-9018-7.

[30] V. Rohan, *Určení jádra mozkového infarktu pomocí zdrojových řezů výpočetní tomografie u pacientů s akutní ischemickou mozkovou příhodou*, Disertační práce v oboru Chirurgie, LF UK Plzeň 2011.

[31] U. Sabatini, P. Celsis, G. Viallard, A. Rascol, J. Marc-Vergnes, *Quantitative assessment of cerebral blood volume by single-photon emission computed tomography*, Stroke (1991), Volume: 22, Issue: 3, Pages:324–330. DOI 10.1161/01.STR.22.3.324.

[32] B. P. Soares, J. W. Dankbaar, J. Bredno et al., *Automated versus manual post-processing of perfusion-CT data in patients with acute cerebral ischemia: influence on interobserver variability*, Neuroradiology, 2009; 51:445-451.

[33] A. Srinivasan, M. Goyal, F. A. Azri et al., *State-of-the-Art Imaging of Acute Stroke*, RadioGraphics 2006; 26:S75-S95.

[34] K. Suzuki, S. Morita, A. Masukawa et al., *Utility of CT perfusion with 64-row multidetector CT for acute ischemic brain stroke*, Emerg Radiol 2011; 18:95-101.

[35] The European Stroke Organisation (ESO) Executive Committee and the ESO Writing Committee: *Guidelines for Management of Ischaemic Stroke and Transient Ischaemic Attack 2008.* Cerebrovasc Dis 2008;25:457-507.

[36] A. Ušinskas, D. Navakauskas, *Segmentation of Ischemic Stroke in CT Images of Human Brain*, 3rd International Symposium, Image and Signal Processing and Analysis, 2003.

[37] X.-C. Wang, P.-Y. Gao, J. Xue, et al., *Identification of Infarct Core and penumbra in Acute Stroke Using CT Perfusion Source Images*, AJNR Am J Neuroradiol 2010; 31:34-39.

[38] W. M. Wells III, P. Viola, H. Atsumi, S. Nakajima, and R. Kikinis, *Multi-modal volume registration by maximization of mutual information*, Med. Imag. Anal., vol 1, pp. 35-51, 1996.

[39] M. Wintermark, A. E. Flanders, B. Velthuis, et al., *Perfusion-CT Assessment of Infarct Core and Penumbra: Receiver Operating Characteristic Curve Analysis in 130 Patients Suspected of Acute Hemispheric Stroke*, Stroke 2006;37;979-985.

[40] G. Wittkamp, Buerke B., Dziewas R., Ditt H.,Seidensticker P., et al., *Whole Brain Perfused Blood Volume CT: Visualization of Infarcted Tissue Compared to Quantitative Perfusion CT*, Academic radiology 1, vol. 17 issue 4, pp. 427-432, 2010.

[41] J. Zvárová, *Základy statistiky pro biomedicínské obory*, Karolinum, ISBN 80-7184-786-0, Praha, 1998.

[42] J. Žára, et al. *Moderní počítačová grafika.* 2. vyd. Brno : Computer Press, 2004. ISBN 80-251-0454-0.

[43] Anonymous, *Guidelines subcommittee World Health Organization—International Society of Hypertension Guidelines for the Management of Hypertension*, Journal of Hypertension. 1999;17:151–183.

Appendix A

Delineated infarction core areas features

Following tables express the features of the delineated infarction cores using the found optimal parameters. The records with no value (-) means incorrect detection or in the case of the physicians' manual tracking it means no infarction core area found. The methods are:

- Method 1 - reproduction of method [39], edge preserving smoothing followed by thresholding
- Method 2 - same like Method 1 but after thresholding there was selected the largest continuous area and only this area was considered to be the infarction core
- Proposed method

The optimal parameters for the methods are presented in Table A.1 and in following table are presented detailed match information where each row expresses the match of one patient's map with the corresponding manual delineation by physician. The tables are 4 for one method reflecting different match type (PBV-Ph1, PBV-Ph2, CBV-Ph1, CBV-Ph2). The patients are identified by anonymous ID called PID.

Details about the optimal parameters description or the volume error evaluation can be found in Section 8 and Section 8.3.

Type	**Method 1** $ml \cdot 100g^{-1}$ $(ml \cdot l^{-1})$	**Method 2** $ml \cdot 100g^{-1}$ $(ml \cdot l^{-1})$	**Proposed method** D_{XY}xD_Z (k) p
PBV-Ph1	2.0 (21.00)	0.5 (5.25)	10x2 (1) 0.8
PBV-Ph2	1.7 (17.85)	0.5 (5.25)	9x1 (1) 0.7
CBV-Ph1	1.7 (17.85)	0.8 (8.40)	7x1 (0) 0.3
CBV-Ph2	1.7 (17.85)	0.8 (8.40)	7x1 (0) 0.3

Table A.1: Optimal parameters for different methods

PID	**Sensit.** [%]	**Specif.** [%]	**Matthews** [%]	**Max. value** $[ml \cdot l^{-1}]$	**Volume** $[cm^3]$	**Volume error** [%]	**Volume error** $[cm^3]$
2	6.71	99.9996	25.59	17.41	1.17	93.16	15.98
3	27.91	99.9063	41.31	18.10	13.00	54.81	15.77
6	46.41	99.9604	62.43	15.35	12.46	45.04	10.21
9	16.30	99.9968	37.17	-5.96	1.04	80.80	4.37
13	59.55	99.9356	65.05	22.60	11.94	16.51	2.36
15	49.01	99.9452	62.57	11.64	16.76	38.99	10.71
16	59.76	99.7645	45.61	13.58	19.28	-70.78	-7.99
21	-	-	-	-	-	-	-
23	13.16	99.9990	35.23	-1.70	1.00	86.07	6.20
24	32.93	99.9824	48.72	25.10	3.37	54.40	4.02
25	64.62	99.9188	52.79	2.41	7.62	-49.56	-2.52
41	63.73	99.8883	56.02	19.71	11.75	-29.06	-2.65

Table A.2: Detailed results of PBV-Ph1 by proposed method

PID	**Sensit.** [%]	**Specif.** [%]	**Matthews** [%]	**Max. value** $[ml \cdot l^{-1}]$	**Volume** $[cm^3]$	**Volume error** [%]	**Volume error** $[cm^3]$
2	7.00	100.0000	26.39	13.28	0.81	92.98	10.68
3	9.13	99.9553	22.62	13.65	5.50	83.95	28.77
6	55.56	99.8714	59.47	14.55	17.52	13.26	2.68
9	6.89	99.9999	26.13	-8.83	0.41	93.06	5.56
13	62.04	99.9841	76.19	14.74	13.99	33.96	7.20
15	25.84	99.9993	50.56	5.29	10.71	74.06	30.58
16	38.88	99.9811	59.77	10.20	13.34	57.96	18.40
21	-	-	-	-	-	-	-
23	7.07	99.9989	25.39	-4.08	0.70	92.26	8.30
24	44.93	99.9774	55.32	23.09	3.79	34.13	1.96
25	43.48	99.9517	55.16	0.04	8.63	38.11	5.31
41	62.00	99.8977	47.81	12.81	8.65	-67.79	-3.49

Table A.3: Detailed results of PBV-Ph2 by proposed method

PID	**Sensit.** [%]	**Specif.** [%]	**Matthews** [%]	**Max. value** $[ml \cdot l^{-1}]$	**Volume** $[cm^3]$	**Volume error** [%]	**Volume error** $[cm^3]$
2	68.83	99.9796	80.91	10.78	25.56	28.13	10.00
3	32.16	99.9730	53.49	10.18	13.87	64.15	24.82
6	69.31	99.9377	76.69	15.80	20.80	18.78	4.81
9	8.51	99.9996	28.43	10.45	0.40	91.04	4.09
13	53.65	99.9855	68.78	13.09	6.63	39.30	4.30
15	45.78	99.9167	50.68	12.17	11.51	18.76	2.66
16	19.45	99.9954	43.18	8.30	7.07	79.85	27.99
21	34.96	99.9521	35.33	17.76	3.97	2.31	0.09
23	41.09	99.9618	37.52	14.07	3.10	-19.73	-0.51
24	38.34	99.9968	52.84	13.77	0.64	47.38	0.57
25	-	-	-	-	-	-	-
41	60.42	99.9373	56.51	11.53	7.10	-14.09	-0.88

Table A.4: Detailed results of CBV-Ph1 by proposed method

PID	**Sensit.** [%]	**Specif.** [%]	**Matthews** [%]	**Max. value** $[ml \cdot l^{-1}]$	**Volume** $[cm^3]$	**Volume error** [%]	**Volume error** $[cm^3]$
2	68.00	99.9781	80.29	10.78	25.56	28.77	10.32
3	26.40	99.9882	49.96	10.18	13.87	72.36	36.32
6	64.28	99.9607	76.14	15.80	20.80	29.18	8.57
9	2.86	99.9997	16.54	10.45	0.40	97.03	13.13
13	55.89	99.9846	69.93	13.09	6.63	36.25	3.77
15	34.17	99.9929	57.20	12.17	11.51	64.52	20.92
16	27.88	99.9872	50.06	8.30	7.07	69.14	15.83
21	-	-	-	-	-	-	-
23	32.62	99.9596	31.54	14.07	3.10	-6.74	-0.20
24	6.26	99.9990	23.94	13.77	0.64	93.17	8.67
25	-	-	-	-	-	-	-
41	47.64	99.9537	55.70	11.53	7.10	27.05	2.63

Table A.5: Detailed results of CBV-Ph2 by proposed method

PID	**Sensit.** [%]	**Specif.** [%]	**Matthews** [%]	**Max. value** $[ml \cdot l^{-1}]$	**Volume** $[cm^3]$	**Volume error** [%]	**Volume error** $[cm^3]$
2	-	-	-	-	-	-	-
3	39.63	99.0748	26.87	5.25	60.47	-110.19	-31.70
6	55.86	99.8105	56.56	5.25	21.93	3.22	0.73
9	99.35	96.6436	17.69	5.25	170.22	-3048.38	-164.81
13	73.60	99.8121	61.33	5.25	20.52	-43.46	-6.22
15	72.67	98.8285	39.78	5.25	90.46	-229.26	-62.99
16	73.49	99.2506	35.44	5.25	48.18	-326.75	-36.89
21	-	-	-	-	-	-	-
23	94.84	96.9364	19.48	5.25	169.99	-2259.97	-162.79
24	-	-	-	-	-	-	-
25	98.33	98.0534	21.27	5.25	108.72	-2033.83	-103.63
41	79.93	99.3920	38.21	5.25	39.65	-335.57	-30.54

Table A.6: Detailed results of PBV-Ph1 by Method 2

PID	**Sensit.** [%]	**Specif.** [%]	**Matthews** [%]	**Max. value** $[ml \cdot l^{-1}]$	**Volume** $[cm^3]$	**Volume error** [%]	**Volume error** $[cm^3]$
2	-	-	-	-	-	-	-
3	44.11	99.1440	32.74	5.25	60.47	-76.47	-26.21
6	54.08	99.7752	51.69	5.25	21.93	-8.60	-1.74
9	95.23	96.6497	17.80	5.25	170.22	-2749.36	-164.24
13	59.74	99.8519	60.51	5.25	20.52	3.13	0.66
15	61.21	98.9142	40.93	5.25	90.46	-119.07	-49.17
16	60.93	99.4560	49.14	5.25	48.18	-51.80	-16.44
21	-	-	-	-	-	-	-
23	95.57	96.9686	21.94	5.25	169.99	-1789.51	-160.99
24	-	-	-	-	-	-	-
25	85.14	98.1792	30.35	5.25	108.72	-679.72	-94.78
41	81.41	99.3346	29.29	5.25	39.65	-669.33	-34.49

Table A.7: Detailed results of PBV-Ph2 by Method 2

PID	**Sensit.** [%]	**Specif.** [%]	**Matthews** [%]	**Max. value** $[ml \cdot l^{-1}]$	**Volume** $[cm^3]$	**Volume error** [%]	**Volume error** $[cm^3]$
2	77.52	99.9495	83.76	8.40	30.24	14.96	5.32
3	58.65	99.5784	54.02	8.40	45.01	-16.34	-6.32
6	73.76	99.9762	83.13	8.40	20.06	21.68	5.55
9	10.92	99.9947	26.70	8.40	0.75	83.29	3.74
13	61.87	99.9785	72.67	8.40	7.90	27.68	3.03
15	75.76	99.8871	67.98	8.40	17.54	-23.81	-3.37
16	42.16	99.9255	57.43	8.40	18.73	46.58	16.33
21	45.10	99.9566	44.61	8.40	4.15	-2.01	-0.08
23	30.21	99.9926	44.78	8.40	1.18	54.54	1.41
24	-	-	-	-	-	-	-
25	-	-	-	-	-	-	-
41	72.68	99.9086	59.12	8.40	9.39	-50.88	-3.17

Table A.8: Detailed results of CBV-Ph1 by Method 2

PID	**Sensit.** [%]	**Specif.** [%]	**Matthews** [%]	**Max. value** $[ml \cdot l^{-1}]$	**Volume** $[cm^3]$	**Volume error** [%]	**Volume error** $[cm^3]$
2	75.10	99.9378	81.51	8.40	30.24	15.72	5.64
3	50.76	99.6303	53.16	8.40	45.01	10.33	5.18
6	65.97	99.9861	79.58	8.40	20.06	31.71	9.31
9	4.34	99.9967	18.40	8.40	0.75	94.45	12.78
13	63.64	99.9759	72.94	8.40	7.90	24.05	2.50
15	47.62	99.9652	64.55	8.40	17.54	45.93	14.89
16	54.75	99.8833	60.34	8.40	18.73	18.20	4.17
21	-	-	-	-	-	-	-
23	25.39	99.9917	39.86	8.40	1.18	59.47	1.73
24	-	-	-	-	-	-	-
25	-	-	-	-	-	-	-
41	56.86	99.9275	57.81	8.40	9.39	3.52	0.34

Table A.9: Detailed results of CBV-Ph2 by Method 2

PID	**Sensit.** [%]	**Specif.** [%]	**Matthews** [%]	**Max. value** $[ml \cdot l^{-1}]$	**Volume** $[cm^3]$	**Volume error** [%]	**Volume error** $[cm^3]$
2	51.82	94.9512	12.23	21.00	277.27	-1516.55	-260.12
3	74.86	95.4036	24.18	21.00	265.34	-822.25	-236.57
6	94.04	96.1601	30.80	21.00	209.24	-823.34	-186.58
9	100.00	90.8581	10.90	21.00	454.41	-8304.81	-449.00
13	96.79	96.6847	26.48	21.00	190.17	-1229.37	-175.87
15	96.38	93.7769	25.11	21.00	400.96	-1359.34	-373.49
16	96.42	96.1600	22.03	21.00	215.24	-1806.55	-203.95
21	87.65	96.3963	11.99	21.00	195.29	-5183.80	-191.60
23	97.48	89.6871	11.05	21.00	556.26	-7622.61	-549.06
24	80.32	98.1537	21.28	21.00	104.27	-1309.54	-96.87
25	99.92	94.3958	12.94	21.00	303.67	-5860.05	-298.58
41	97.00	96.6397	21.32	21.00	187.72	-1962.38	-178.62

Table A.10: Detailed results of PBV-Ph1 by Method 1

PID	**Sensit.** [%]	**Specif.** [%]	**Matthews** [%]	**Max. value** $[ml \cdot l^{-1}]$	**Volume** $[cm^3]$	**Volume error** [%]	**Volume error** $[cm^3]$
2	51.71	95.7568	11.02	17.85	231.74	-1917.85	-220.25
3	76.39	95.9880	28.47	17.85	238.76	-596.75	-204.49
6	91.16	96.8035	30.81	17.85	174.93	-766.20	-154.74
9	95.53	91.7427	11.46	17.85	411.21	-6783.51	-405.24
13	92.02	97.3271	33.18	17.85	161.47	-662.22	-140.29
15	91.85	94.8583	31.44	17.85	346.63	-739.41	-305.34
16	92.61	96.9633	37.60	17.85	190.38	-499.83	-158.64
21	-	-	-	-	-	-	-
23	96.24	90.8134	12.88	17.85	497.75	-5432.72	-488.75
24	79.92	98.4134	20.22	17.85	89.12	-1448.61	-83.37
25	96.32	95.0549	21.56	17.85	276.46	-1882.70	-262.52
41	95.47	96.9571	16.74	17.85	167.04	-3141.40	-161.89

Table A.11: Detailed results of PBV-Ph2 by Method 1

PID	**Sensit.** [%]	**Specif.** [%]	**Matthews** [%]	**Max. value** $[ml \cdot l^{-1}]$	**Volume** $[cm^3]$	**Volume error** [%]	**Volume error** $[cm^3]$
2	97.19	95.8445	36.15	17.85	254.70	-616.21	-219.13
3	91.05	93.6712	29.12	17.85	370.29	-857.06	-331.60
6	94.36	96.5034	34.01	17.85	195.20	-662.07	-169.58
9	78.47	96.6116	12.63	17.85	169.98	-3683.87	-165.48
13	92.57	96.0229	20.46	17.85	221.78	-1929.18	-210.85
15	97.44	95.4696	21.59	17.85	287.02	-1926.49	-272.86
16	79.98	96.5169	32.08	17.85	212.57	-506.32	-177.51
21	88.26	97.2482	14.46	17.85	150.23	-3593.24	-146.17
23	86.80	96.0270	9.49	17.85	214.03	-8158.84	-211.44
24	96.13	95.4776	6.77	17.85	242.28	-19969.59	-241.07
25	84.24	96.2125	10.15	17.85	204.41	-6690.02	-201.39
41	98.98	94.9089	14.81	17.85	277.35	-4355.01	-271.12

Table A.12: Detailed results of CBV-Ph1 by Method 1

PID	**Sensit.** [%]	**Specif.** [%]	**Matthews** [%]	**Max. value** $[ml \cdot l^{-1}]$	**Volume** $[cm^3]$	**Volume error** [%]	**Volume error** $[cm^3]$
2	96.35	95.8444	35.98	17.85	254.70	-609.84	-218.81
3	88.03	93.8270	31.96	17.85	370.29	-637.70	-320.09
6	94.18	96.5722	36.34	17.85	195.20	-564.51	-165.82
9	46.26	96.6611	12.51	17.85	169.98	-1155.93	-156.44
13	93.74	96.0165	20.23	17.85	221.78	-2031.05	-211.37
15	91.19	95.7182	30.43	17.85	287.02	-785.05	-254.59
16	88.64	96.3790	28.89	17.85	212.57	-828.41	-189.67
21	-	-	-	-	-	-	-
23	86.51	96.0317	10.01	17.85	214.03	-7262.94	-211.12
24	72.51	95.5757	13.95	17.85	242.28	-2504.85	-232.98
25	62.21	96.2347	10.54	17.85	204.41	-3214.58	-198.24
41	93.99	94.9617	17.53	17.85	277.35	-2748.64	-267.61

Table A.13: Detailed results of CBV-Ph2 by Method 1

Appendix B

Depiction of the individual delineations

Following figures show comparison of different methods automatically delineating the infarction core. There are presented matches for each patient of the used material individually. Each figure is divided into 4 areas. The upper-left area corresponds to PBV-Ph1, upper-right to PBV-Ph2, lower-left to CBV-Ph1 and lower-right to CBV-Ph2. In each area the first row corresponds to manual delineation by physician, second row to the proposed method, third row to Method 2 and the fourth row to Method 1. Columns corresponds to different location in the map. Detected infarction cores are marked by red color. For the maps depiction is used windowing method with settings of the window center to value 50 and window width to 100 $ml \cdot l^{-1}$.

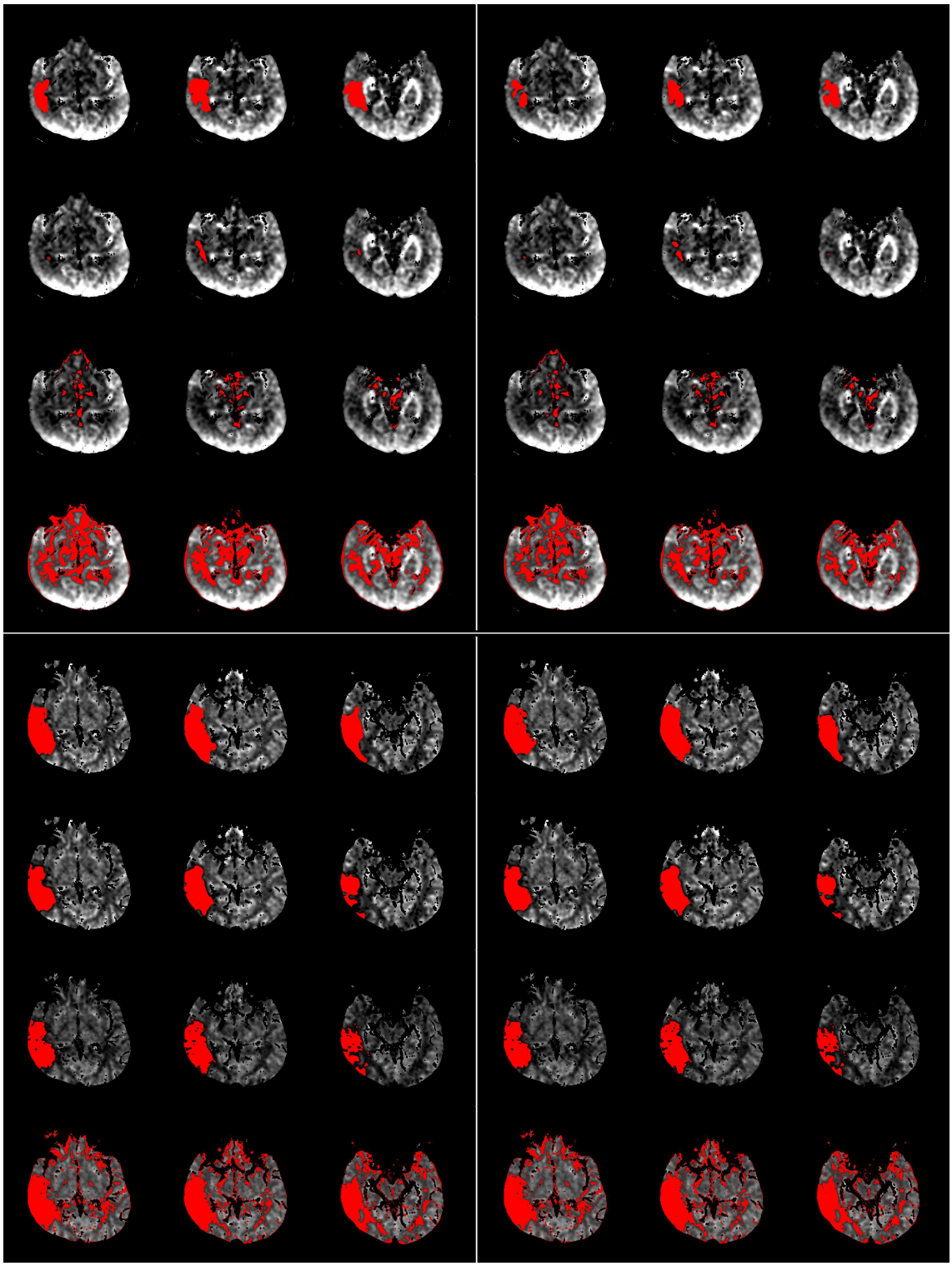

Figure B.1: Patient 2 - Comparison of different automated methods for infarction core detection (red color). Upper-left area corresponds to PBV-Ph1, upper-right to PBV-Ph2, lower-left to CBV-Ph1 and lower-right to CBV-Ph2. In each area the 1. row corresponds to manual delineation by physician, 2. row to the proposed method, 3. row to Method 2 and 4. row to Method 1. Columns corresponds to different location in the map.

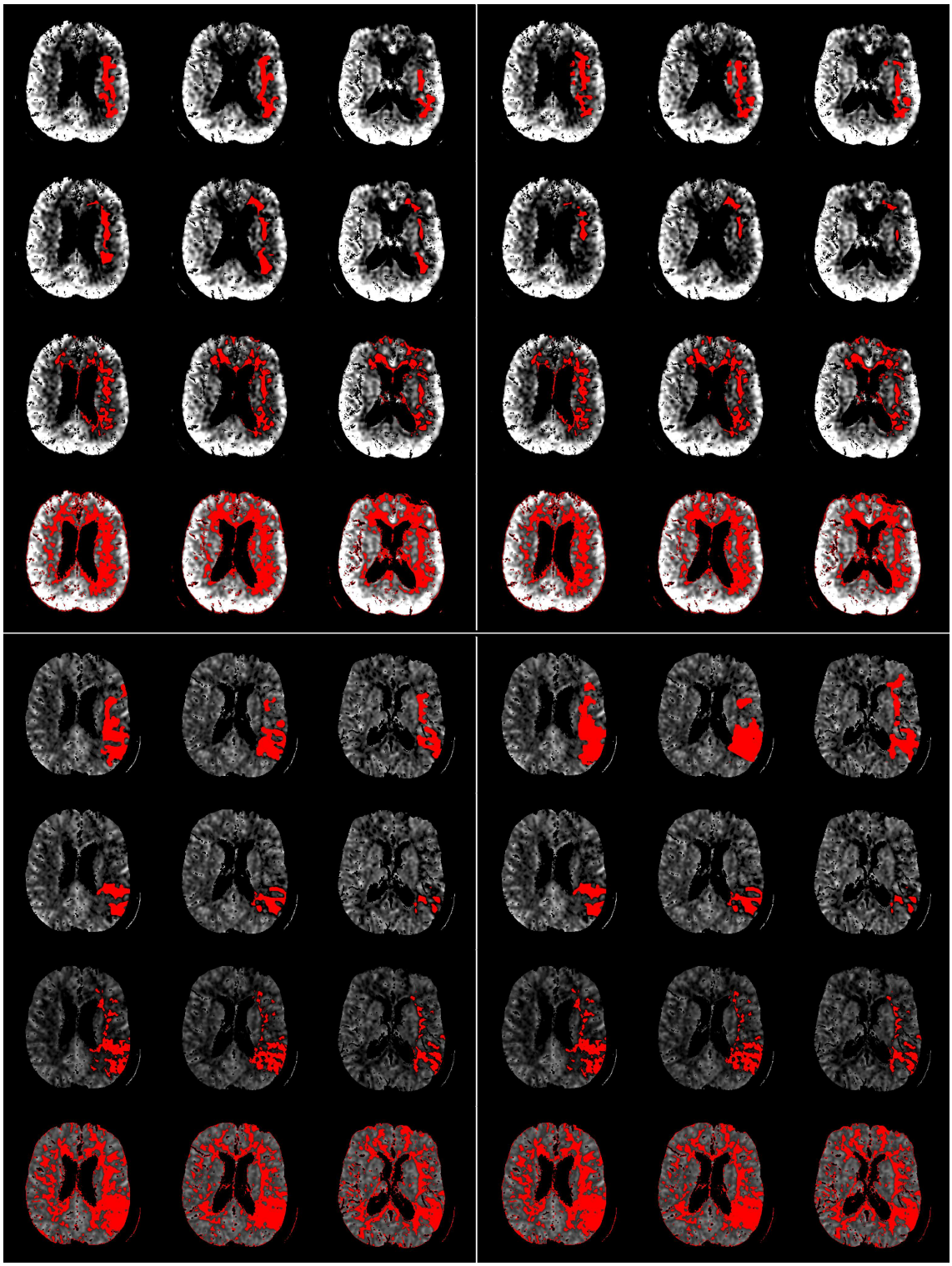

Figure B.2: Patient 3 - Comparison of different automated methods for infarction core detection (red color). Upper-left area corresponds to PBV-Ph1, upper-right to PBV-Ph2, lower-left to CBV-Ph1 and lower-right to CBV-Ph2. In each area the 1. row corresponds to manual delineation by physician, 2. row to the proposed method, 3. row to Method 2 and 4. row to Method 1. Columns corresponds to different location in the map.

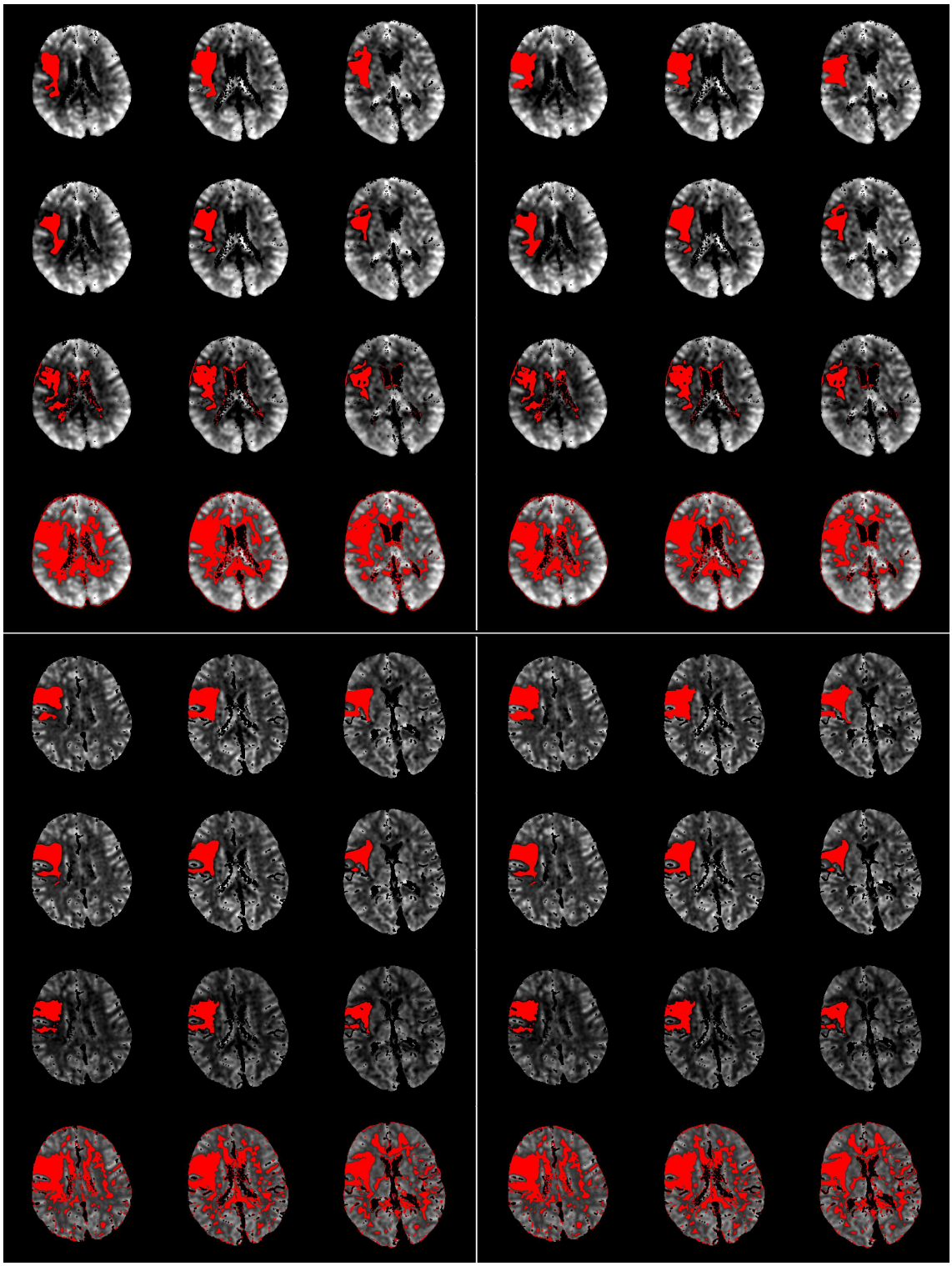

Figure B.3: Patient 6 - Comparison of different automated methods for infarction core detection (red color). Upper-left area corresponds to PBV-Ph1, upper-right to PBV-Ph2, lower-left to CBV-Ph1 and lower-right to CBV-Ph2. In each area the 1. row corresponds to manual delineation by physician, 2. row to the proposed method, 3. row to Method 2 and 4. row to Method 1. Columns corresponds to different location in the map.

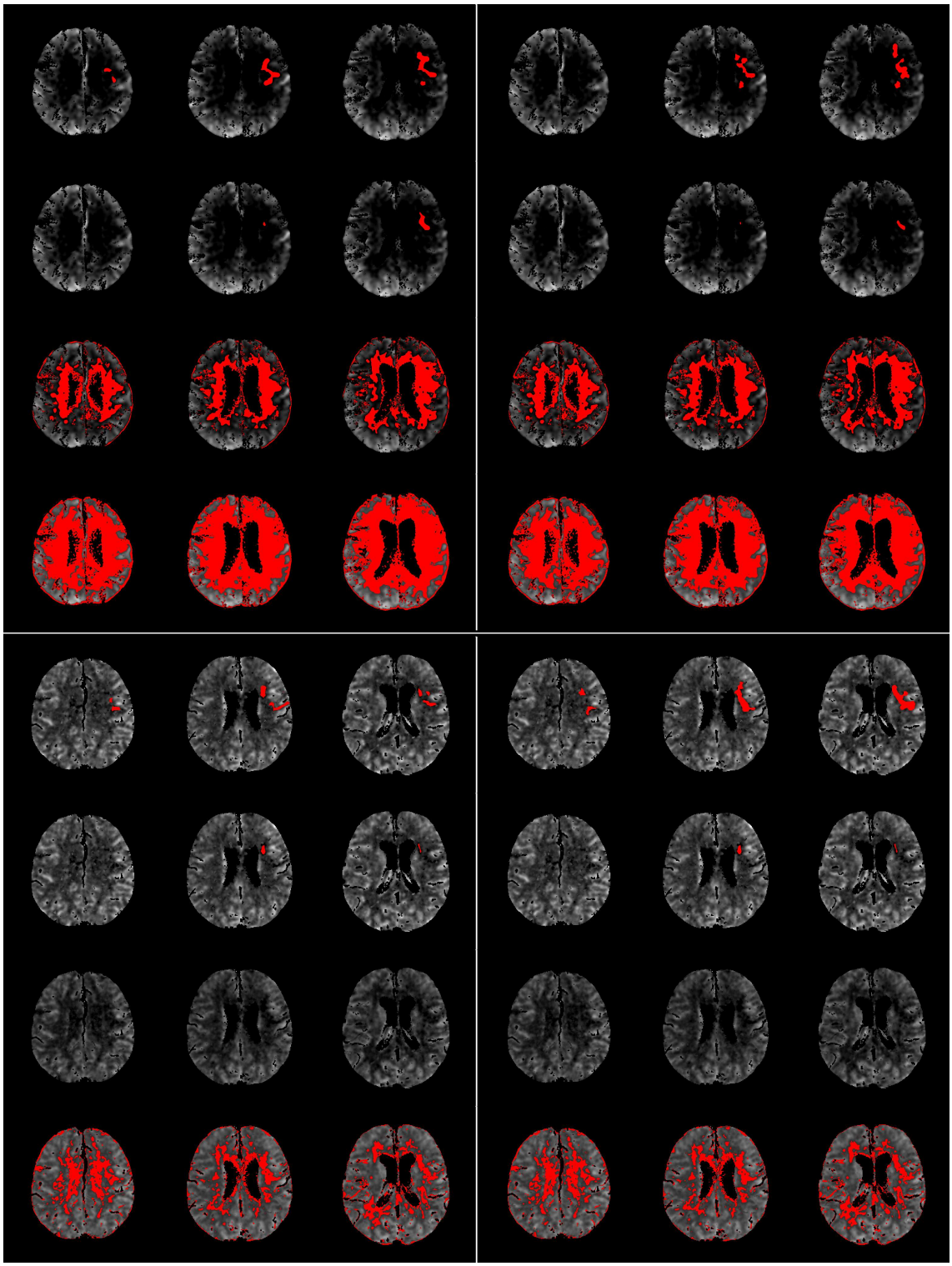

Figure B.4: Patient 9 - Comparison of different automated methods for infarction core detection (red color). Upper-left area corresponds to PBV-Ph1, upper-right to PBV-Ph2, lower-left to CBV-Ph1 and lower-right to CBV-Ph2. In each area the 1. row corresponds to manual delineation by physician, 2. row to the proposed method, 3. row to Method 2 and 4. row to Method 1. Columns corresponds to different location in the map.

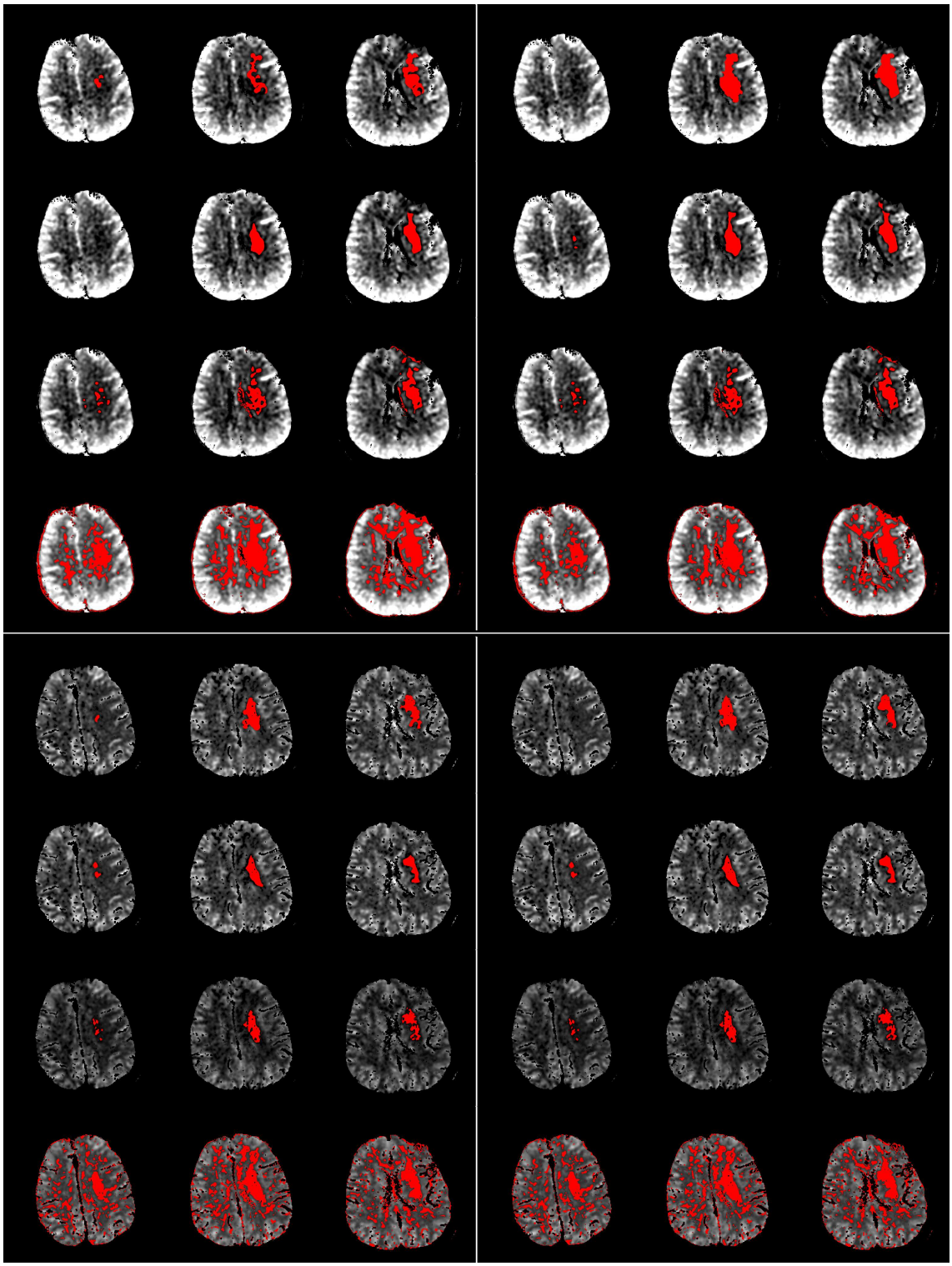

Figure B.5: Patient 13 - Comparison of different automated methods for infarction core detection (red color). Upper-left area corresponds to PBV-Ph1, upper-right to PBV-Ph2, lower-left to CBV-Ph1 and lower-right to CBV-Ph2. In each area the 1. row corresponds to manual delineation by physician, 2. row to the proposed method, 3. row to Method 2 and 4. row to Method 1. Columns corresponds to different location in the map.

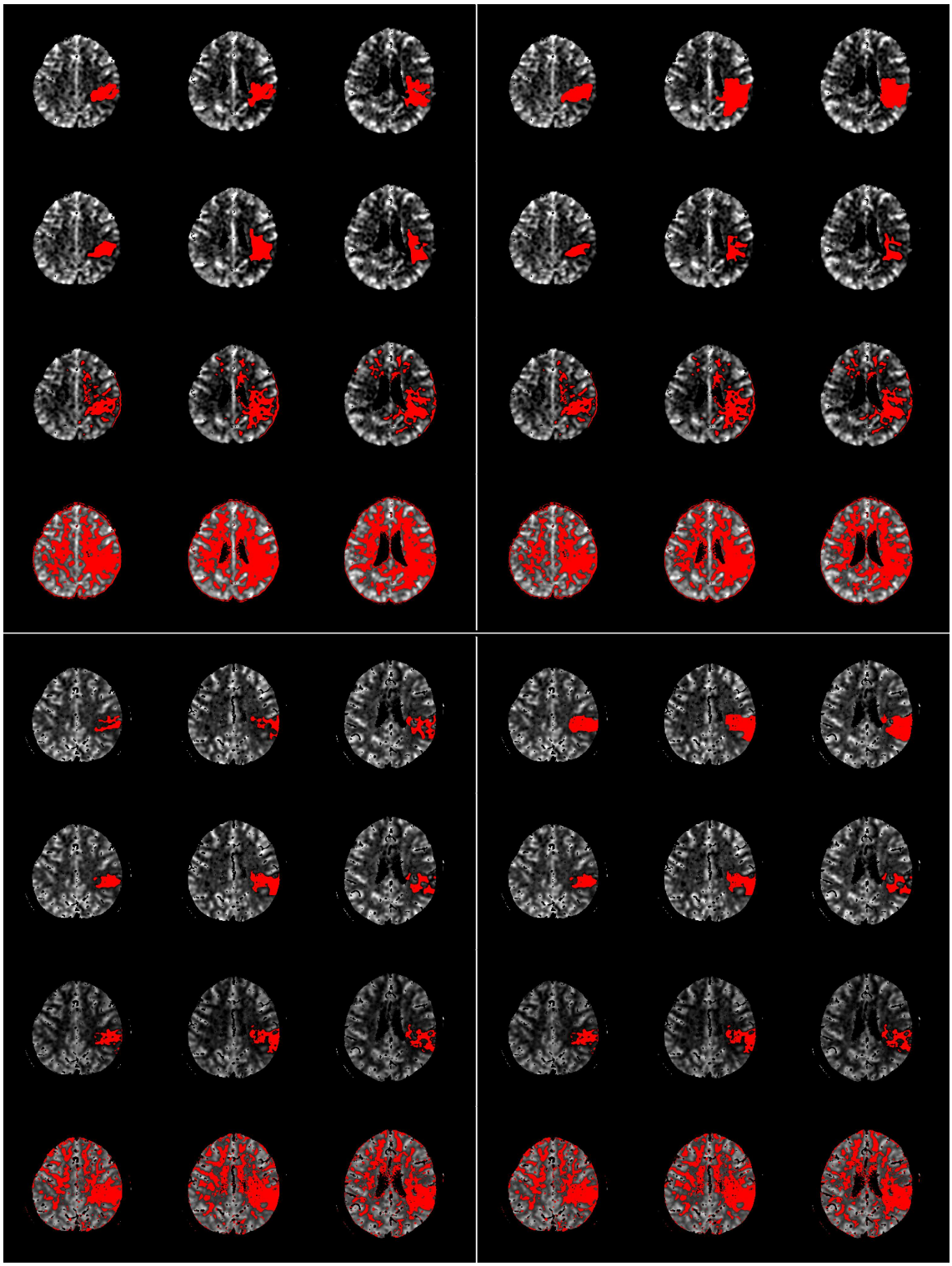

Figure B.6: Patient 15 - Comparison of different automated methods for infarction core detection (red color). Upper-left area corresponds to PBV-Ph1, upper-right to PBV-Ph2, lower-left to CBV-Ph1 and lower-right to CBV-Ph2. In each area the 1. row corresponds to manual delineation by physician, 2. row to the proposed method, 3. row to Method 2 and 4. row to Method 1. Columns corresponds to different location in the map.

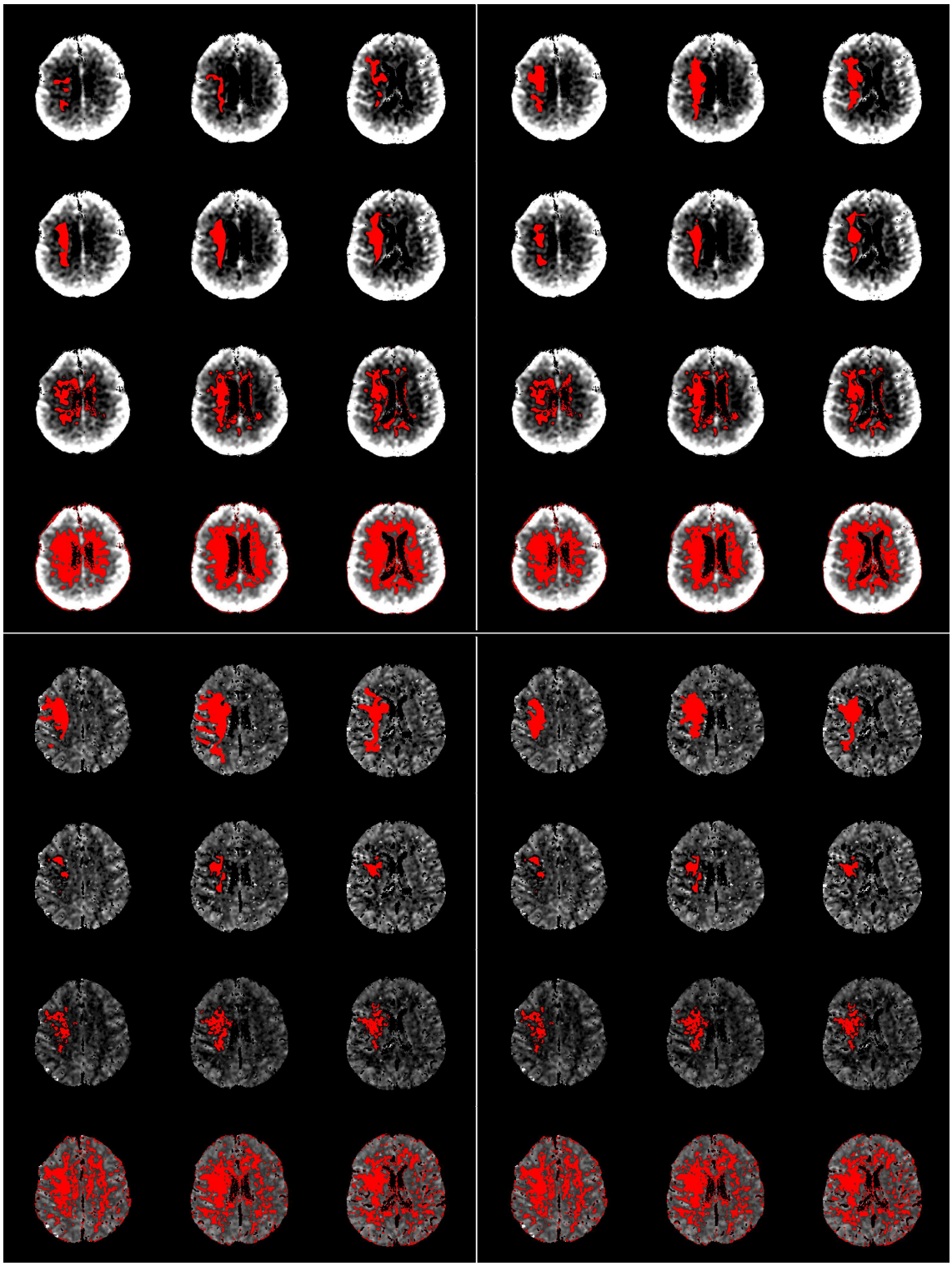

Figure B.7: Patient 16 - Comparison of different automated methods for infarction core detection (red color). Upper-left area corresponds to PBV-Ph1, upper-right to PBV-Ph2, lower-left to CBV-Ph1 and lower-right to CBV-Ph2. In each area the 1. row corresponds to manual delineation by physician, 2. row to the proposed method, 3. row to Method 2 and 4. row to Method 1. Columns corresponds to different location in the map.

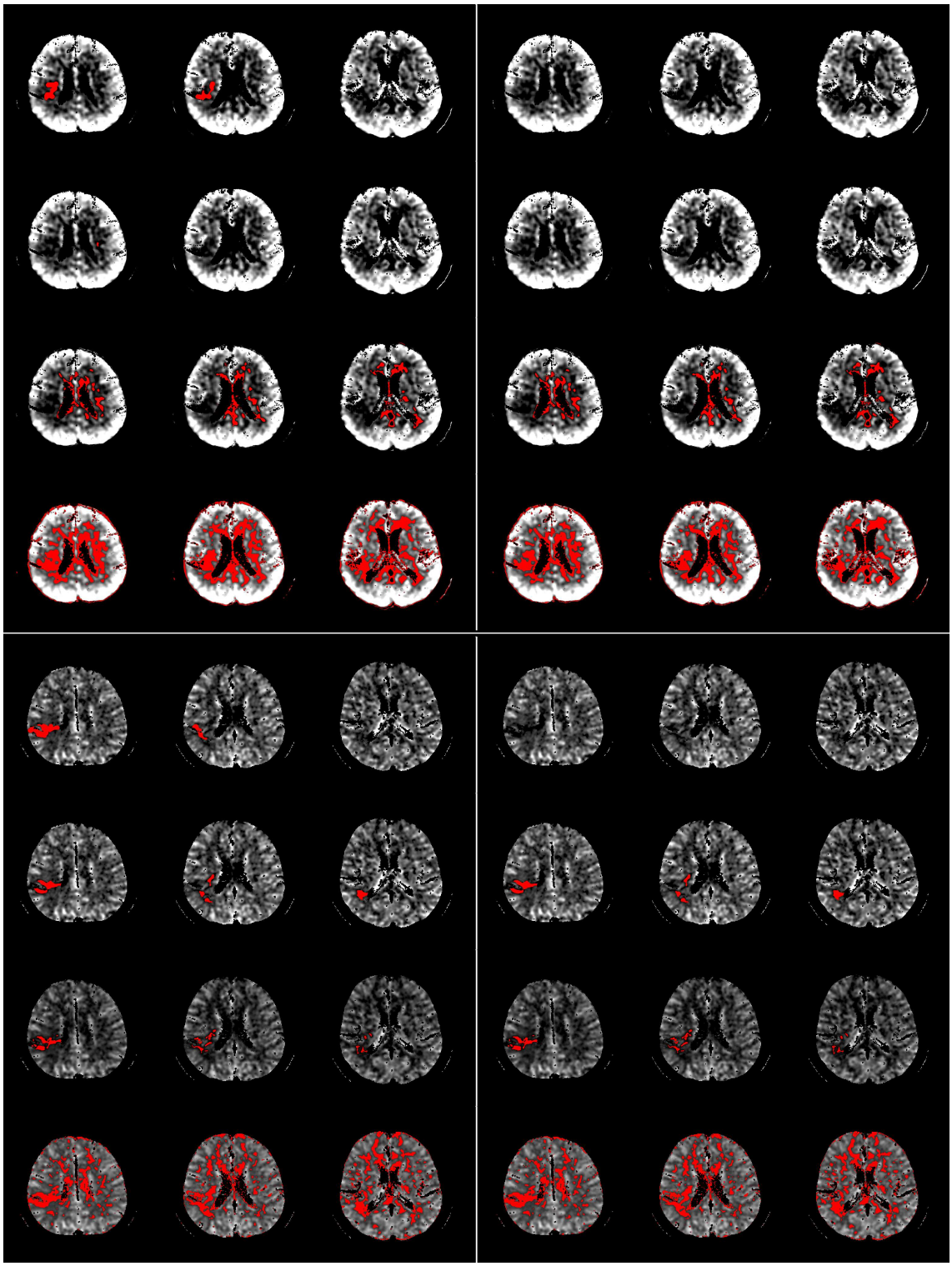

Figure B.8: Patient 21 - Comparison of different automated methods for infarction core detection (red color). Upper-left area corresponds to PBV-Ph1, upper-right to PBV-Ph2, lower-left to CBV-Ph1 and lower-right to CBV-Ph2. In each area the 1. row corresponds to manual delineation by physician, 2. row to the proposed method, 3. row to Method 2 and 4. row to Method 1. Columns corresponds to different location in the map.

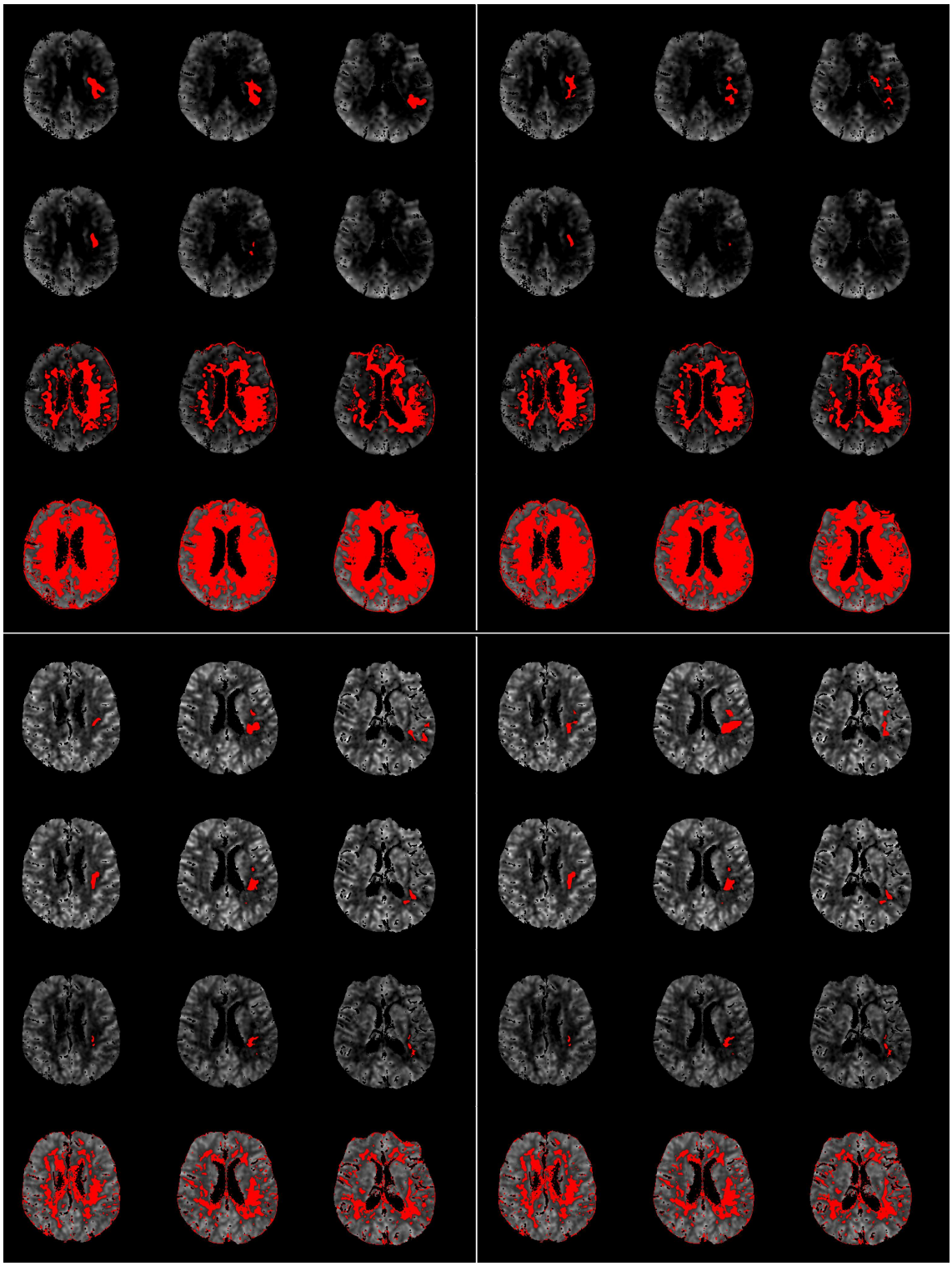

Figure B.9: Patient 23 - Comparison of different automated methods for infarction core detection (red color). Upper-left area corresponds to PBV-Ph1, upper-right to PBV-Ph2, lower-left to CBV-Ph1 and lower-right to CBV-Ph2. In each area the 1. row corresponds to manual delineation by physician, 2. row to the proposed method, 3. row to Method 2 and 4. row to Method 1. Columns corresponds to different location in the map.

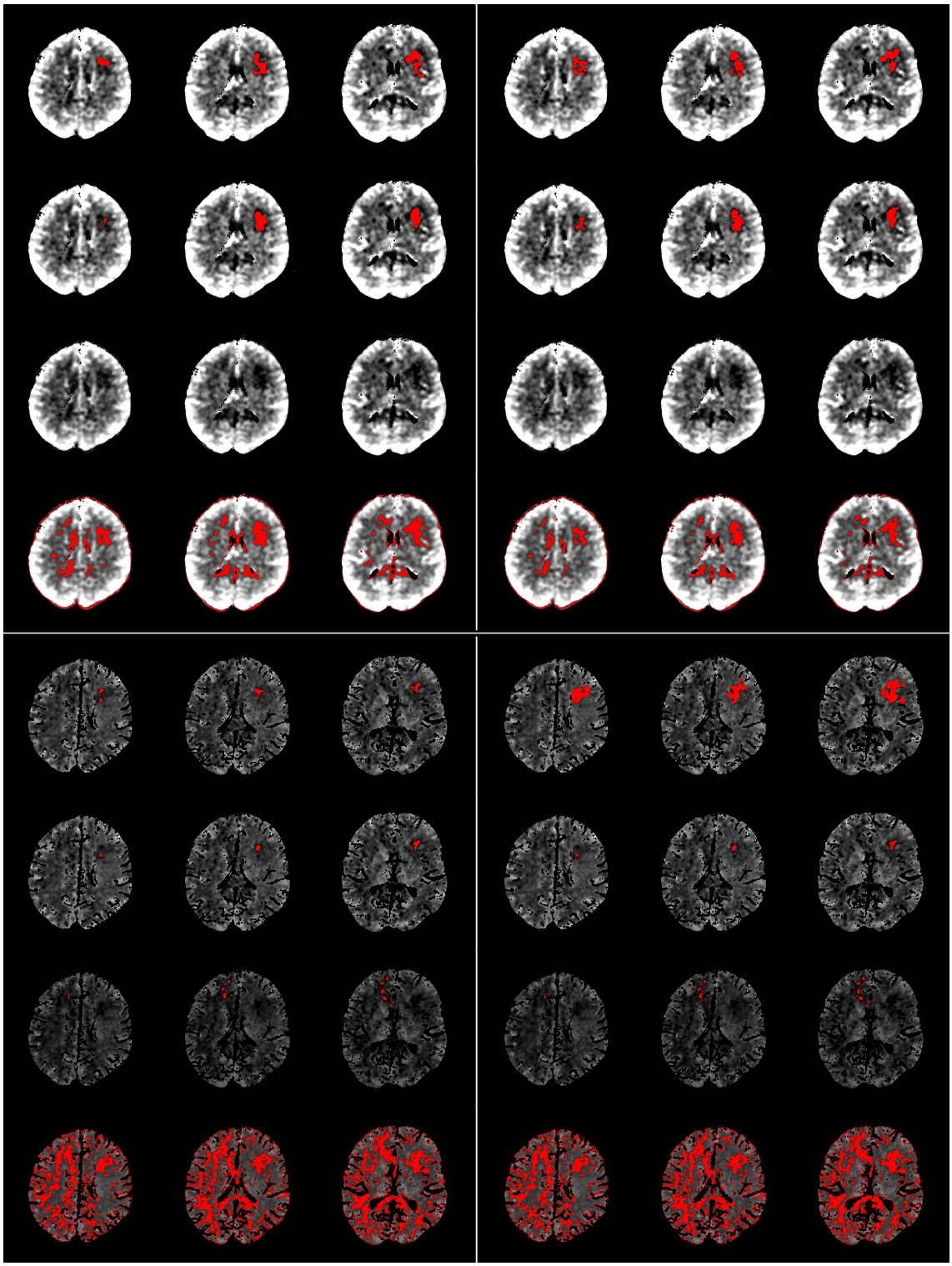

Figure B.10: Patient 24 - Comparison of different automated methods for infarction core detection (red color). Upper-left area corresponds to PBV-Ph1, upper-right to PBV-Ph2, lower-left to CBV-Ph1 and lower-right to CBV-Ph2. In each area the 1. row corresponds to manual delineation by physician, 2. row to the proposed method, 3. row to Method 2 and 4. row to Method 1. Columns corresponds to different location in the map.

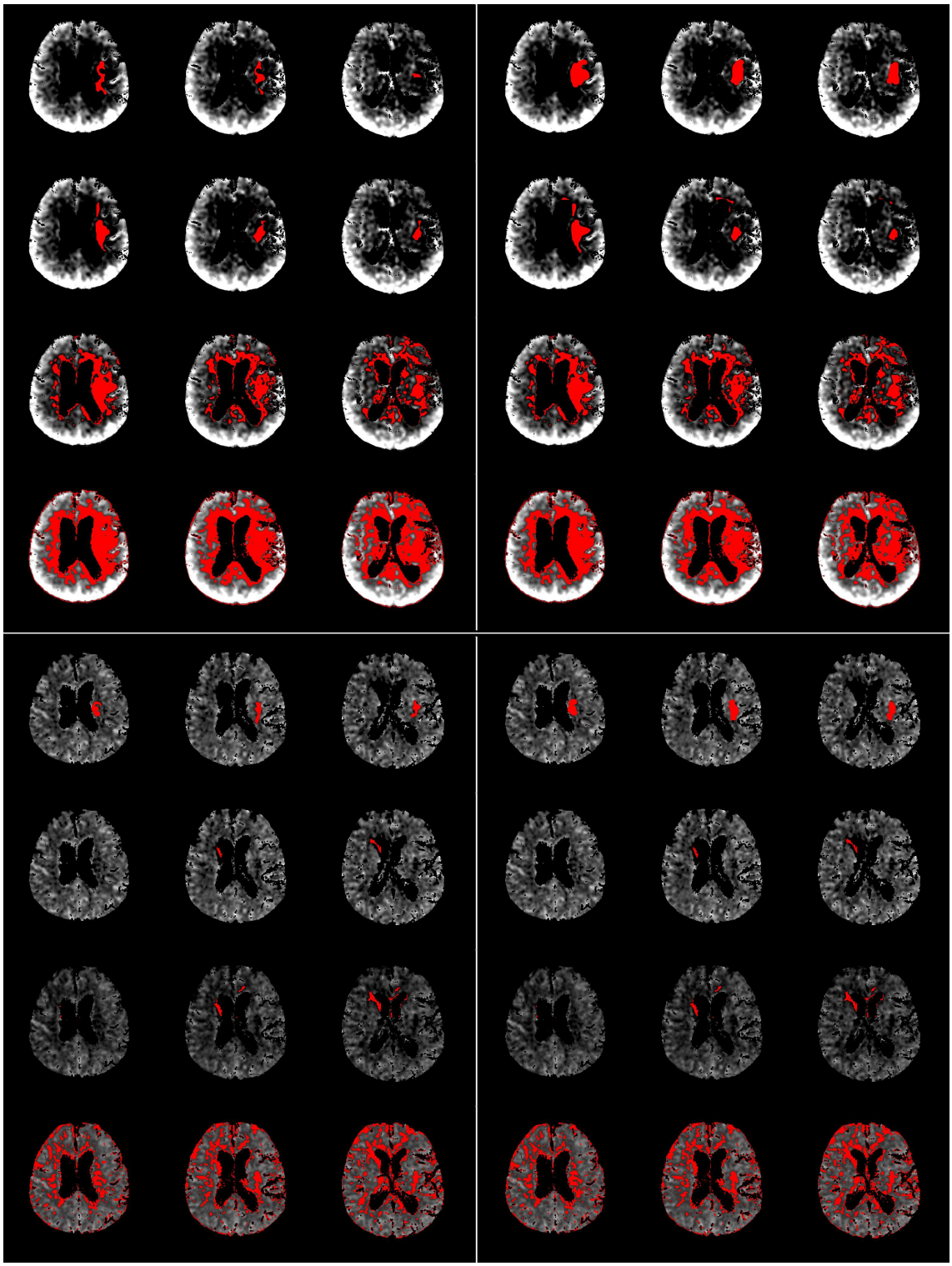

Figure B.11: Patient 25 - Comparison of different automated methods for infarction core detection (red color). Upper-left area corresponds to PBV-Ph1, upper-right to PBV-Ph2, lower-left to CBV-Ph1 and lower-right to CBV-Ph2. In each area the 1. row corresponds to manual delineation by physician, 2. row to the proposed method, 3. row to Method 2 and 4. row to Method 1. Columns corresponds to different location in the map.

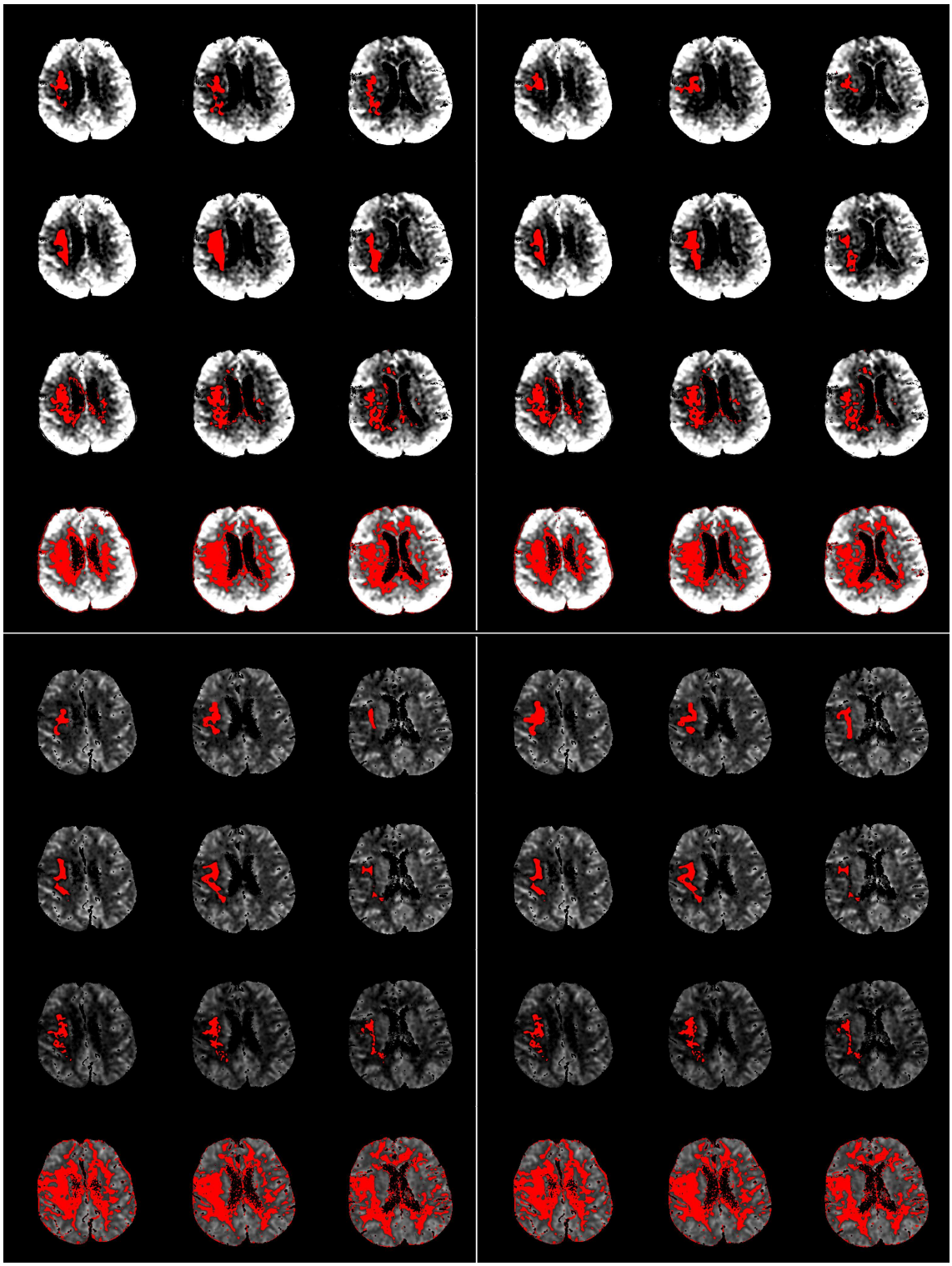

Figure B.12: Patient 41 - Comparison of different automated methods for infarction core detection (red color). Upper-left area corresponds to PBV-Ph1, upper-right to PBV-Ph2, lower-left to CBV-Ph1 and lower-right to CBV-Ph2. In each area the 1. row corresponds to manual delineation by physician, 2. row to the proposed method, 3. row to Method 2 and 4. row to Method 1. Columns corresponds to different location in the map.

Appendix C

Author's Activities

C.1 Publications related to the doctoral thesis

Publications in conference proceedings:

1. Maule, P., Klečková, J., Rohan, V. *Whole Brain CT Perfusion Maps*, In ICONS 2009. New York: IEEE, 2009. pp. 247-250. ISBN: 978-1-4244-3469-5.

2. Klečková, J., Maule, P., Polívka, J., Rohan, V. *Experimental system for neurological case studies*, In Models and Analysis of Vocal Emissions for Biomedical Applications. Firenze: Firenze University Press, 2009. pp. 149-150. ISBN: 978-88-6453-094-9.

3. Maule, P., Rohan, V., Klečková, J. *Intuitive approach for necrotic tissue detection*, Front. Neur. Conference Abstract: Neuroinformatics 2009. doi: 10.3389/conf.neuro.11.2009.08.093.

4. Včelák, P., Polívka, J., Maule, P., Kratochvíl, P., Klečková, J. *Experimental database system for the vascular brain diseases research*, Front. Neur. Conference Abstract: Neuroinformatics 2009. doi: 10.3389/conf.neuro.11.2009.08.002.

5. Maule, P., Polívka, J., Klečková, J. *Vascular Network Semi-Automatic Segmentation Using Computed Tomography Angiography*, In ICSOFT 2010, Vol. 1. Setúbal: SciTe Press, 2010. pp. 323-326. ISBN: 978-989-8425-22-5.

6. Maule, P., Polívka, J., Klečková, J. *Experimental database medical system: Data Acquisition Background and Features*, In BIOSTEC 2010. Setúbal: INSTICC, 2010. pp. 402-405. ISBN: 978-989-674-016-0.

7. Polívka, J., Maule, P., Klečková, J. *Experimental medical research database system and its examples of use*, In Annals of DAAAM for 2010 & Proceedings of the 21st International DAAAM Symposium. Vienna: DAAAM International Vienna, 2010. pp. 1343-1344. ISBN: 978-3-901509-73-5.

8. Maule, P., Klečková, J., Rohan, V. *Automated approach for whole brain infarction core delineation*, In Proceedings of the International Conference on Knowledge Discovery and Information Retrieval. Setúbal: SciTePress, 2011. pp. 433-437. ISBN: 978-989-8425-79-9.

9. Maule, P., Klečková, J., Rohan, V., Tupý, R. *Automated Infarction Core Delineation*, In The Seventh International Multi-Conference on Computing in the Global Information Technology, in press.

Publications in scientific journals:

1. Maule, P., Klečková J., Rohan V., Tupý R. *Automated Infarction Core Delineation*, Neuroinformatics, in approval process.

C.2 Published software

1. Maule, P., Klečková, J. *Volumetric Data Subtraction Analyser*, 2010 [cit. 2012-04-25]. Available from: URL: http://www.kiv.zcu.cz/vyzkum/software/2010/subtraction-analyser

2. Maule, P., Klečková, J. *Volumetric Infarction Core Delineator*, in approval process.

C.3 Teaching activities

1. 2007 - 2009: KIV/ZIHB - Fundamentals of Informatics for History Studies

C.4 Participation in projects

1. Microstructure oriented hierarchical modeling of brain perfusion for CT based cerebral blood flow evaluation, Grant Agency of the Czech Republic no. 106/09/0740.

2. Teaching Laboratory of Experimental Surgery - Introduction of experimental surgery teaching in 2009, Faculty of Medicine in Pilsen.